

University of Alberta

**Fundamental Understanding of the Flocculation of
Mineral Tailings in High Salinity Water**

by

Yaguan Ji

A thesis submitted to the Faculty of Graduate Studies and Research
in partial fulfillment of the requirements for the degree of

Master of Science

in

Materials Engineering

Department of Chemical and Materials Engineering

©Yaguan Ji

Spring 2013

Edmonton, Alberta

Permission is hereby granted to the University of Alberta Libraries to reproduce single copies of this thesis and to lend or sell such copies for private, scholarly or scientific research purposes only. Where the thesis is converted to, or otherwise made available in digital form, the University of Alberta will advise potential users of the thesis of these terms.

The author reserves all other publication and other rights in association with the copyright in the thesis and, except as herein before provided, neither the thesis nor any substantial portion thereof may be printed or otherwise reproduced in any material form whatsoever without the author's prior written permission.

Abstract

In this study, the effect of three polymer flocculants, polyacrylamide (PAM), Magnafloc 1011 (MF) and Al(OH)₃-polyacrylamide (Al-PAM), on the settling of mineral freshwater and saline tailings was investigated. The settling of tailings significantly depends on solution salinity, polymer flocculant type and dosage. MF was identified as the most efficient flocculant among the three polymers to enhance the settling of freshwater and saline tailings. The flocculation mechanism of MF was further studied through model clay (i.e. kaolinite) under controlled solution conditions. The maximum initial settling rate (ISR) of kaolinite was found to increase with the addition of NaCl and CaCl₂ at the cost of higher MF consumption. Using multiple advanced techniques, the interaction between MF molecules and clay particles were probed. The results indicate that the different settling behaviors of MF treated tailings of various salinities were mainly due to the change of polymer conformations and polymer-particle interactions in the suspensions.

Acknowledgement

I would like to give my sincere gratitude to my supervisors, Dr. Qingxia (Chad) Liu and Dr. Hongbo Zeng for their kindness guidance, support and encourage throughout my MSc study.

It was Dr. Zeng who gave me valuable suggestions when I encountered challenges in experiment design and results interpretation. I clearly remember he showed me sentence by sentence how to write a report or paper. Many discussions as we had had, I still learned a lot after every discussion with him. His encourage and tolerance of my mistakes helped me go through the most difficult stage of my study.

Dr. Liu is a professor with both profound research and industry experience from whom I benefited a lot. Not only did he give me insightful ideas in tailings treatment but precious opportunities to deal with industrial sponsors. His critical thinking and precise attitude towards research has been and will always be a criterion for myself.

I'm also very grateful to the postdoctoral fellow, Qingye Lu, for her training in using the surface forces apparatus (SFA) and valuable discussions. Many thanks to other members in my group including Yuanchun Hu, Ling Zhang, Fucheng Teng, and also thanks Mr. Jim Skwarok, Mrs. Jie Ru in Dr. Xu's group, for their kind help and training me on some instruments.

The financial support from Teck Metals Ltd and Collaborative Research and Development (CRD) Grant of the NSERC is acknowledged. The authors also thank the research fellows in the Applied Research and Technology Center of Teck for the helpful discussions.

Finally, I would like to thank my parents and my wife Xi Luo who accompany me all the time. Without their support and comfort, I could not go this far.

Table of Content

Chapter 1 Introduction	1
1.1 Mineral processing in seawater and challenges in saline tailings treatment	1
1.2 Stability of colloidal system: coagulation and flocculation	3
1.3 Review of the effect of salt on tailings treatment using flocculants	4
1.4 Intermolecular and surface forces	5
1.4.1 van der Waals forces	6
1.4.2 Electrostatic double layer (EDL) force	7
1.4.3 Steric repulsion and bridging force	10
1.5 References	11
Chapter 2 Experimental Techniques	15
2.1 Surface forces apparatus (SFA)	15
2.1.1 Development of SFA	15
2.1.2 SFA 2000	16
2.1.3 Multiple beam interference (MBI)	18
2.1.4 Normal and adhesive force measurements	19
2.2 Quartz crystal microbalance with dissipation monitoring (QCM-D)	21
2.2.1 Development of QCM-D	21
2.2.2 Working mechanism	22
2.3 Other techniques	23
2.3.1 Inductively coupled plasma mass spectrometry (ICP-MS)	24
2.3.2 Dynamic light scattering (DLS)	24
2.3.3 Mastersizer 2000	25
2.4 References	25

Chapter 3 Effect of Solution Salinity on Settling of Mineral Tailings by Polymer Flocculants	28
3.1 Introduction.....	28
3.2 Materials and methods	31
3.2.1 Tailings	31
3.2.2 Polymer flocculants	31
3.2.3 Settling test	32
3.2.4 Molecular conformations of polymer flocculants.....	33
3.2.5 Simplified model for polymer-particle interaction	34
3.3 Results and discussion	37
3.3.1 Characterization of tailings.....	37
3.3.2 Settling test	38
3.3.3 Conformation of the flocculants in bulk solution	42
3.3.4 Interaction mechanism between polymers and solid particles under different solution conditions.....	43
3.4 Conclusion	50
3.5 References.....	50
Chapter 4 Molecular and Surface Interactions between Polymer Flocculants and Clay Particles: Effect of Salinity	55
4.1 Introduction.....	55
4.2 Experimental	58
4.2.1 Materials	58
4.2.2 Settling test	59
4.2.3 Surface force measurement.....	60
4.2.4 Measurement of hydrodynamic radii of polymer flocculants	63

4.2.5 Measurement of adsorption of MF on model clay surfaces using quartz crystal microbalance with dissipation monitoring (QCM-D).....	63
4.3 Results and discussion	64
4.3.1 Effect of NaCl and CaCl ₂ on the settling of kaolinite.....	64
4.3.2 Mica-mica interaction in polymer solution with salt	69
4.3.3 Conformation of MF molecules in solution of different salt concentrations ...	78
4.3.4 Adsorption of MF molecules on model clay surfaces.....	79
4.3.5 Interaction between MF and clay particles surfaces	87
4.4 Conclusions.....	91
4.5 References.....	92
Chapter 5 Conclusions and Future Work.....	96
5.1 Major conclusions	96
5.2 Contributions to the original knowledge.....	98
5.3 Future work.....	98
5.3.1 Enhancement of settling.....	98
5.3.2 Flocculation mechanism	99

List of Tables

Table 1.1. Composition of natural seawater (modified from [14]).	2
Table 3.1. Properties of the flocculants used for enhancing tailings settling.	32
Table 3.2. Parameters and constants used in equation (3.1) to (3.3).	35
Table 3.3. Ion concentrations (ppm) of saline and freshwater tailings.	38
Table 4.1. Properties of MF 1011.	58
Table 4.2. Key parameters in force measurement.	69
Table 4.3. Fitting parameters for measured force-distance profiles shown in Figure 4.14.	75
Table 4.4. Hydrodynamic radii of MF in solution of different salt concentration.	78

List of Figures

Figure 1.1. Schematic of electrical double layer structure on a positively charged particle surface.....	9
Figure 2.1. Schematic drawing of SFA 2000 [8].	16
Figure 2.2. Schematic of SFA setup [8].	17
Figure 2.3. FECO fringes for two contacted mica surfaces in air.	18
Figure 2.4. Schematic of normal and adhesive force measurement.	20
Figure 2.5. Quartz crystal microbalance with dissipation monitoring	22
Figure 2.6. Principle of frequency and dissipation measurement: (a) sensor vibrates when an AC voltage is applied (b) slow decay-small dissipation-rigid layer (c) fast decay-large dissipation-loose layer.	23
Figure 2.7. Schematic of the layer structure of silica and alumina sensors.	23
Figure 2.8. Scattering of light from small and large particles.	25
Figure 3.1. Schematic of ISR calculation based on the settling results of mudline height vs. settling time	33
Figure 3.2 Schematic of interaction energy calculation.....	34
Figure 3.3. Characterization of the saline tailings: (a) XRD pattern of the solids, and (b) particle size distribution measured by Mastersizer.	37
Figure 3.4. The impact of flocculant type and dosage on the initial setting rate (ISR) of tailings: (a) freshwater tailings treated by MF (black, 0- 25 ppm), PAM (blue, 0-100 ppm), and Al-PAM (red, 0-100 ppm), and; (b) saline tailings treated by MF (black, 0-100 ppm), PAM (blue, 0-100 ppm), and Al-PAM (red, 0-100 ppm).	39
Figure 3.5. The impact of flocculant type and dosage on the supernatant turbidity of tailings: (a) freshwater tailings treated by MF (black, 0- 50 ppm), PAM (blue,	

0-100 ppm), and Al-PAM (red, 0-100 ppm); (b) saline tailings treated by PAM (0-100 ppm), Al-PAM (0-100 ppm) and MF (0- 100 ppm).	40
Figure 3.6. The impact of flocculant type and dosage on the supernatant zeta potential of tailings: (a) freshwater tailings treated by MF (black, 0- 50 ppm), PAM (blue, 0-100 ppm), and Al-PAM (red, 0-100 ppm); (b) saline tailings treated by MF (black, 0-100 ppm), PAM (blue, 0-100 ppm), and Al-PAM (red, 0-100 ppm).	41
Figure 3.7. The impact of salt type and concentration on the distribution of hydrodynamic radii R_H of the flocculants: (a) 50 ppm MF, (b) PAM, and (c) Al-PAM in mili-Q water (black), 1 M NaCl solution (red), and 1 M $CaCl_2$ solution (blue).	42
Figure 3.8. Schematic of the impact of ionic strength on the conformation and adsorption of flocculants on negatively-charged particle surfaces: (a) MF, (b) PAM and Al-PAM.	43
Figure 3.9. Theoretical interaction energy vs. distance profiles between two silica particles in MF treated tailings: (a) freshwater, and (b) saline tailings.....	46
Figure 3.10. Images of the flocs after 4 mins of settling tests for: (a) freshwater tailings treated by 25 ppm MF (b) saline tailings treated by 25 ppm MF (c) gel-like suspension of freshwater tailings treated by 100 ppm MF (d) saline tailings treated by 100 ppm MF.....	48
Figure 3.11. Theoretical interaction energy vs distance profiles between two silica particles in PAM and Al-PAM treated tailings: (a) freshwater tailings, and (b) saline tailings.	49
Figure 3.12. Images of the flocs after 4 mins of settling tests for: (a) freshwater tailings treated by 75 ppm PAM, and (b) saline tailings treated by 75 ppm PAM.	49
Figure 4.1. Schematic of settling test procedure.	60

Figure 4.2. Schematic of ISR calculation	60
Figure 4.3. Schematic of the SFA experimental setup for measuring the interactions between two mica surfaces in MF solutions of different salt concentration. .	62
Figure 4.4. The initial settling rate of 5 wt% solid kaolinite suspension versus MF dosage at pH 7.5 in mili-Q (▼) and in the presence of 0.01 M (■), 0.1 M (●) and 1 M (▲) Na (I) ions.	65
Figure 4.5. The initial settling rate of 5 wt% solid kaolinite suspension versus MF dosage at pH 7.5 in mili-Q (▼) and in the presence of 0.01 M (■), 0.1 M (●) and 1 M (▲) Ca (II) ions.	65
Figure 4.6. The supernatant turbidity values of 5 wt% solid kaolinite suspension after 18 hours settling versus MF dosage at pH 7.5 in mili-Q (not shown) and in the presence of 0.01 M (■), 0.1 M (●) and 1 M (▲) Na (I) ions.	67
Figure 4.7. The supernatant turbidity values of 5 wt% solid kaolinite suspension after 18 hours settling versus MF dosage at pH 7.5 in mili-Q (not shown) and in the presence of 0.01 M (■), 0.1 M (●) and 1 M (▲) Ca (II) ions.	67
Figure 4.8. The zeta potential values of kaolinite particles in the supernatant of 5 wt% solid kaolinite suspension after 18 hours settling at pH 7.5 in the presence of 0.01 M (■), 0.1 M (●) and 1 M (▲) Na (I) ions.	68
Figure 4.9. The zeta potential values of kaolinite particles in the supernatant of 5 wt% solid kaolinite suspension after 18 hours settling at pH 7.5 in the presence of 0.01 M (■), 0.1 M (●) and 1 M (▲) Ca (II) ions.	69
Figure 4.10. Interaction forces between two mica surfaces in 5 ppm MF solution without salt at 30 mins incubation.	70

Figure 4.11. Interaction forces between two mica surfaces in 5 ppm MF solution of different NaCl concentrations: (a) 0.01M, (b) 0.1 M and (c) 1 M after 30 mins incubation.....	71
Figure 4.12. Interaction forces between two mica surfaces in 5 ppm MF solution of different CaCl ₂ concentrations: (a) 0.01M, (b) 0.1 M, and (c) 1 M after 30 mins incubation.....	72
Figure 4.13. Schematic of the parameters used in fitting.....	75
Figure 4.14. Measured force-distance profiles between two mica surfaces in MF solutions during approaching stage (black dots) and theoretical fitting (red curves) : (a) no salt added fitted by equation (4.1); (b)(c)(d) 0.01 M to 1 M NaCl fitted by equation (4.2).....	77
Figure 4.15. Measured force-distance profile between two mica surfaces in MF solutions containing 0.01 M CaCl ₂ during approaching stage.	78
Figure 4.16. Change of frequency and energy dissipation associated with the adsorption of MF on QCM-D silica sensors in mili-Q water	80
Figure 4.17. Change of frequency and energy dissipation associated with the adsorption of MF on QCM-D silica sensors in 0.01 M NaCl solution.....	80
Figure 4.18. Change of frequency and energy dissipation associated with the adsorption of MF on QCM-D silica sensors in 0.01 M CaCl ₂ solution.....	81
Figure 4.19. Change of frequency and energy dissipation associated with the adsorption of MF on QCM-D silica sensors in 0.1 M NaCl solution.....	81
Figure 4.20. Change of frequency and energy dissipation associated with the adsorption of MF on QCM-D silica sensors in 0.1 M CaCl ₂ solution.....	82
Figure 4.21. Change of frequency and energy dissipation associated with the adsorption of MF on QCM-D silica sensors in 1 M NaCl solution.....	82

Figure 4.22. Change of frequency and energy dissipation associated with the adsorption of MF on QCM-D silica sensors in 1 M CaCl ₂ solution.....	83
Figure 4.23. Change of frequency and energy dissipation associated with the adsorption of MF on QCM-D alumina sensors in mili-Q water.....	84
Figure 4.24. Change of frequency and energy dissipation associated with the adsorption of MF on QCM-D alumina sensors in 0.01 M NaCl solution.....	84
Figure 4.25. Change of frequency and energy dissipation associated with the adsorption of MF on QCM-D alumina sensors in 0.01 M CaCl ₂ solution.....	85
Figure 4.26. Change of frequency and energy dissipation associated with the adsorption of MF on QCM-D alumina sensors in 0.1 M NaCl solution.....	85
Figure 4.27. Change of frequency and energy dissipation associated with the adsorption of MF on QCM-D alumina sensors in 0.1 M CaCl ₂ solution.....	86
Figure 4.28. Change of frequency and energy dissipation associated with the adsorption of MF on QCM-D alumina sensors in 1 M NaCl solution.....	86
Figure 4.29. Change of frequency and energy dissipation associated with the adsorption of MF on QCM-D alumina sensors in 1 M CaCl ₂ solution	87
Figure 4.30. Schematic of MF's interaction with silica and alumina surfaces in solutions.	91

List of Symbols

A	Hamaker constant, J
a	Length of a monomer unit, m
A_1, A_2	Prefactors to normalize the unknown term of s
A_{SSA}	The specific surface area of solid particles
B_1, B_2	Prefactors describe the relationship between elastic force and osmotic force
c_0	The concentration of counterions inside the brush, m^{-3}
c_s	The concentration of counterions outside the brush, m^{-3}
D	Separation distance between surfaces, m
e	The charge of one electron
$E_{Bridging}$	Energy of polymer bridging interaction, kT
E_{EDL}	Energy of electrostatic repulsions, kT
E_{vdW}	Energy of van der Waals attractions, kT
$F(D)$	Normal force measured at the distance D
F_{ela}	Elastic force of the polyelectrolytes, N
F_{osm1}	Stretching force of the polyelectrolytes in osmotic brush regime, N
F_{osm2}	Stretching force of the polyelectrolytes in salt brush regime, N
k_B	Boltzmann constant, J/K
k_{sp}	Spring constant of the double-cantilever force spring, N/m
L_c, L_0	The thickness of flocculant layer, m
m_s	The mass of solid particles in each tailings sample

N	Number of monomer segments
N_A	Avogadro constant
N_p	The total number of polymer molecules
R_1, R_2	Radius of spherical particles, m
R_H	Hydrodynamic radius, m
s	Grafting density, m
T	Temperature, K
α	Ratio of the total number of free mobile counterions to the total number of monomer segments
β	Effective bridging ratio
ΔD	Energy dissipation change of the sensor
ΔD_{abs}	Absolute distance between two surfaces measured by MBI, m
ΔD_{app}	Travel distance of the lower surface, m
ΔD_{jump}	Distance that the two surfaces jump apart from contact, m
Δf	Frequency change of the sensor
ε	Bonding energy per segment of flocculant, kT
ε_0	Permittivity of vacuum, F/m
ε_r	Relative permittivity
κ^{-1}	Debye length, nm
$\lambda_n^0, \lambda_{n-1}^0$	Wavelength of the nth and (n-1)th fringe when two mica surface contacts in air, m
μ	Refractive index of the medium
μ_{mica}	Refractive index of the mica

Ψ_0, ϕ_1, ϕ_2

Surface potential, mV

Ψ_S

Stern potential, mV

List of Acronyms

AFM	Atomic force microscope
Al-PAM	Al(OH) ₃ -polyacrylamide
DLS	Dynamic light scattering
DLVO theory	Theory developed by Derjaguin and Landau and Verwey and Overbeek
FECO	Fringes of Equal Chromatic Order
H-PAM	Hydrolyzed polyacrylamide
ICP-MS	Inductively coupled plasma mass spectrometry
ISR	Initial settling rate
MBI	Multiple beam interference
MF	Magnafloc
NTU	Nephelometric turbidity units
PAM	Polyacrylamide
PEO	Polyethylene oxide
ppm	Parts per million
PSD	Particle size distribution
QCM-D	Quartz crystal microbalance with dissipation monitoring
SFA	Surface forces apparatus
XRD	X-ray diffraction

Chapter 1 Introduction

1.1 Mineral processing in seawater and challenges in saline tailings treatment

Globally water restrictions are becoming a critical issue for many mines due to the shortage of available fresh water or government and social constraints. Therefore a great need for increased water recycling and reuse, or alternative water resource has been raised. Since seawater is the most abundant water reservoir of the earth [1], increasing attention has been paid to using seawater or diluted seawater as an alternative mineral processing medium.

Considerable efforts have been made to study the mineral flotation in seawater or recycled process water. Studies on mineral flotation in saline water were reviewed in a recently published paper [2]. It was found that 0.5 M NaCl solution was capable for the flotation of naturally hydrophobic minerals (i.e. bituminous coals) without any organic agents [3, 4]. It was found through the flotation of methylated model silica that the flotation of above mentioned minerals in concentrated salt solution was due to the decreasing of energy barrier opposing the attachment of bubble on mineral particles in salt solution [5]. Increasing electrolyte concentration was also found capable for preventing bubble coalescence [6]. Therefore fine bubbles can be generated in seawater without the addition of frother, which is beneficial for the flotation of minerals. Meanwhile the studies of Jan Miller's group [7, 8] indicated concentrated salt could change the bulk and interfacial water structure, which may affect the collector-particle or bubble-particle interaction depending on the type of salt.

The flotation in seawater or recycled process water of high salinity has been applied in several plants recently [9-11]. Due to the high cost of transportation of sea

water from the coast to the mine, it is critical to maximize the water recycling from the tailings impoundment. The quantity and quality of the recycle water are determined by the solid-liquid separation, or the dewatering of the tailings. Therefore the dewatering of the tailings is of great importance in the reuse of process water. Due to the decreasing resources of high-grade ore, lower-grade ore that generates large amounts of very fine tailings is increasingly explored [12, 13]. The fine solids in the tailings normally settle very slowly, which will not only lead to poor water quality for recycling, but also result in a negative impact on the performance of mineral processing operations. Therefore multivalent salts (coagulants) and long chain polymers (flocculants) are often used to enhance the setting of fine particles.

The most obvious difference between saline tailings and the regular mineral tailings is the high salt content in liquid phase of the tailings. The composition of natural seawater is shown in Table 1.1. The ion concentrations may be further increased due to the dissolution of minerals and the accumulation during water recycling. The high salt content in the saline tailings may change the interaction mechanism between flocculants and particles and bring unknown effects to the dewatering process. Given the success in the flotation in seawater, the dewatering of tailing of high salinity has not been given sufficient attention.

Table 1.1. Composition of natural seawater (modified from [14]).

Ion	Concentration in nature seawater (mol/kg)
Cl ⁻	0.545
Na ⁺	0.467
SO ₄ ²⁻	0.028
Mg ²⁺	0.054
Ca ²⁺	0.010
K ⁺	0.010
HCO ₃ ⁻	0.002
Br ⁻	0.001

1.2 Stability of colloidal system: coagulation and flocculation

Because the size of fine particles in tailings is usually comparable to the range of colloidal particles (1 nm to 1 μm) [15], the theories in colloidal system are often used to explain the sedimentation of fine particles in tailings. Particles of the same material exert mutual attraction forces, known as van der Waals forces, in colloidal suspensions. However agglomeration of the particles is usually prevented by the electrical double layer repulsion forces between particles in suspensions of low and medium electrolyte concentration. The balance between the van der Waals attraction and the electrical double layer repulsion will determine the stability of the colloid system.

Since mineral tailing particles commonly carry negative charges in neutral or alkaline condition, multivalent electrolytes are used as coagulants to reduce the electrical double layer repulsion. Inorganic salts containing highly charged ions, such as Al^{3+} , Fe^{3+} and Ca^{2+} have been long used for this purpose. The positively charged ions mentioned above act as counter ions or potential determining ions that can compress the range of the electrical double layer repulsive force or even neutralize the surface charge of the particles respectively.

The flocculation of the colloidal particles involves the formation of relatively open agglomerates by the 'bridging' effect of long chain polymers between separated particles [16, 17]. These polymers are so-called flocculants, which were used to be natural materials such as gelatine and glue, but now increasingly substituted by synthetic materials. Polyacrylamide (PAM) based flocculants are a widely used flocculant family in industry [18]. The majority of commercial polyacrylamide flocculants are anionic,

since they tend to be of higher molecular weight and less expensive than cationic ones. Moreover the negatively charged loops and trains dangles away from the negatively charged surfaces, providing more chance for forming bridging with other particles.

Coagulation and flocculation are sometimes simultaneously used to enhance the settling of mineral tailings [19]. Salts can not only compress the double layer and reduce the repulsion between particles but can change the conformation of some charged flocculants [20]. Multivalent ions, such as Ca^{2+} and Mg^{2+} could form flocculant-flocculant and flocculant-particle complexation, which will enhance the bridging between particles. In saline tailings, the synergic effect of salts and flocculants may lead to different flocculation behavior than that in tailings of normal salinity. Therefore the study of the flocculation of saline tailings is of both fundamental and practical importance.

1.3 Review of the effect of salt on tailings treatment using flocculants

Considerable research has been done on the polymer enhanced settling of industrial and model tailings [21-26]. Polymer type and charge property [27, 28], polymer adsorption on particle surfaces [26], solution chemistry [27, 29] and aggregates structure [30] were studied to elucidate corresponding settling behaviors. Although most of the studies regarding the effect of salt were limited to the low to medium salt concentration, they could provide valuable prediction of the impact of high salt.

Measurement of settling rates and floc size are two commonly used methods to characterize the flocculation behavior. It was found that the addition of 8 mM Mg^{2+} or Ca^{2+} could enhance the settling rate of oil sands tailings with 20 ppm anionic PAM [19]. Similar results were reported for kaolinite suspension treated by 500 g/ton of solid anionic PAM with 0.001 M Ca^{2+} at pH 10.5 and Mn^{2+} at pH 7.5 [27], and increased

kaolinite floc size and flocculation rate were also found with the addition of NaCl and MgCl₂ of concentration up to 1 M and 0.5 M respectively without flocculant treatment [31].

The mechanism of flocculation in salt solutions was studied in microscopic scale using scanning electron microscope (SEM), atomic force microscope (AFM) et al. Zbik et al. [30] used cryo-SEM technique to reveal the impact of pH and salt to the structure of kaolinite aggregates. The aggregate structure was changed from largely edge-edge (EE) orientation or separate chain aggregates in 0.01 M NaCl to less elongated and rather irregular structure with preferable edge-face (EF) orientation in 0.00025 M CaCl₂. This structure change reduced the intra-aggregate pore size but enlarged the distance between aggregates. This observation was in good correlation with the previous study shown that the addition of divalent cations can increase settling rates [17]. The addition of anionic PAM into kaolinite solution mentioned above did not change the orientation of kaolinite but caused the aggregates to associate by bridging flocculation, which increased the size of flocs. Therefore the settling rates were higher than kaolinite solution with barely correspond salt. Long et al. [32] measured the interaction between two silica surfaces in aqueous solution. They evaluated the effect of anionic PAM dosage, solution pH and the addition of Ca²⁺ and Mg²⁺ and attributed the increasing settling rates of oil sand tailings [19] to the enhanced bridging between particles and polymers by the divalent cations. Single molecule force spectroscopy (SMFS) was also applied to measure the interaction between single polyelectrolyte and surfaces [33, 34].

1.4 Intermolecular and surface forces

The polymer-aid flocculation process is essentially the process during which polymer-surface and polymer-polymer interactions take place. Therefore the

understanding intermolecular and surface forces, such as van de Waals forces, electrostatic force, polymer bridging force and steric repulsive force are of great importance to the interpretation of flocculation phenomena.

1.4.1 van der Waals forces

The van der Waals forces, named after Dutch scientist Johannes Diderik van der Waals, is the total effect of the attractive or repulsive forces between molecules or between groups within the same molecule, excluding those due to bonds formation, the hydrogen bonds or electrical interaction of ions with another ion or neutral molecular [35]. Three kinds of interactions contribute to the van der Waals forces: dipole-dipole interactions (Keesom force), dipole-induced dipole interactions (Debye force) and instantaneous induced dipole-induced dipole interactions (London dispersion force). Van der Waals forces are generally considered existing between all atoms and molecules. They play a role in many important phenomena such as surface tension & wetting, the flocculation of particles in liquids as well as the liquefaction of noble gases. However they are relatively weak compared to forces induced by covalent bonds or electrostatic interactions between ions. The magnitude of the force decays quickly with increasing distance (D) between objects. For example, the van der Waals forces between two atoms are proportional to D^{-7} . In macroscopic scale, the van der Waals forces also depend on the geometries of the interacting objects. For example, the van der Waals force between two flat surfaces can be expressed as $F = -A/6\pi D^3$ and for a sphere of radius R and a flat surface it's $F = -AR/6D^2$. A is the Hamaker constant defined as $A = \pi^2 C \rho_1 \rho_2$, where C is the coefficient in the atom-atom pair potential and ρ_1 and ρ_2 are the number of atoms per unit volume in the two bodies. The Hamaker constant A is dependent on the nature of the interacting objects.

1.4.2 Electrostatic double layer (EDL) force

Systems in which van der Waals forces alone play a determining role in the total interaction are limited to a few simple systems such as interactions in vacuum. In more complex systems, such as colloidal systems, long-range electrostatic forces are involved and are critical to the stability of the systems. When the particle surface is immersed in an aqueous environment, a structure called electrical double layer (EDL) is formed on the surface. The common mechanisms for the formation of double layer include (1) preferential (or differential) solution of surface ions, (2) direct ionization of surface groups, (3) substitution of surface ions, (4) specific ion adsorption, and (5) charges deriving from specific crystal structures [15]. A schematic of the double layer structure around a positively charged particle is shown in Figure 1.1. The particle surface carries positive or negative charge due to aforementioned reasons. The ions that carry opposite charge of the surface, namely counter-ions, are accumulated near the surface to compensate the surface charge and form so-called double layer. The first layer is composed of immobile counterions that adsorbed on the surface. Because the closest distance that a counter ion can approach to the surface is limited by the size of the counterions, the counterion charge is separated from the surface. The layer between the surface charge and the charge in the plane of the centers of the adsorbed counter ions form the first layer called Stern layer, in which the electric potential drops linearly with the distance. The potential on particle surface is Ψ_0 and that on Stern layer is Ψ_s . The second layer called diffusive layer consists of counterions that normally obey the Poisson-Boltzmann distribution:

$$d^2\Psi / dx^2 = -\sum_i (z_i e \rho_{i\infty} / \epsilon_0 \epsilon) e^{-z_i e\Psi / kT} \quad (1.1)$$

where x is the distance from the Stern plane, z is the valence of the ion, e is the charge of an electron, ρ_∞ is the counter ion density in bulk, ε_0 is the permittivity of vacuum and ε is the relative dielectric constant. If the Stern potential is relatively small (< 25 mV), $e^{-ze\Psi/kT}$ can be expanded by Taylor's series, from which a simplified solution of Ψ can be solved, known as Debye–Hückel equation:

$$\Psi_x = \Psi_s e^{-\kappa x} \quad (1.2)$$

where $\frac{1}{\kappa} = \sqrt{\sum_i \left(\frac{\varepsilon_0 \varepsilon k T}{\rho_{i\infty} e^2 z_i^2} \right)}$ is identified as the electrical double layer thickness or the 'Debye length'. When two surfaces (particles) carry the same sign of charge are brought close, the electrical double layers of the two surfaces become overlapped. The repulsive force is generated by the osmotic repulsion of the counter ions in the double layers. When the concentration or the valence of the ions increases, the thickness of the double layer (κ^{-1}) is reduced. Therefore the electrical double layer force decays faster. In other word, the range of the electrical double layer force is compressed.

There is a plane inside the diffusive layer called shear plane. The counterions inside the diffusive layer move simultaneously with the particle in the liquid due to the Coulomb attraction between counterions and the surface. The potential at this plane is the zeta potential measured by instruments. Since it's very difficult to measure the surface potential (Ψ_0) or the Stern potential (Ψ_s), zeta potential is commonly used to characterize the charge property of the colloidal system. The measurement of the zeta potential is based on the electrophoresis phenomenon: when an electric field is applied across the solution, charged particles are attracted towards the electrode of opposite charge. However the viscous force of the fluid is opposing to this movement. Therefore the particles reach a constant velocity when equilibrium of these two forces is achieved. The

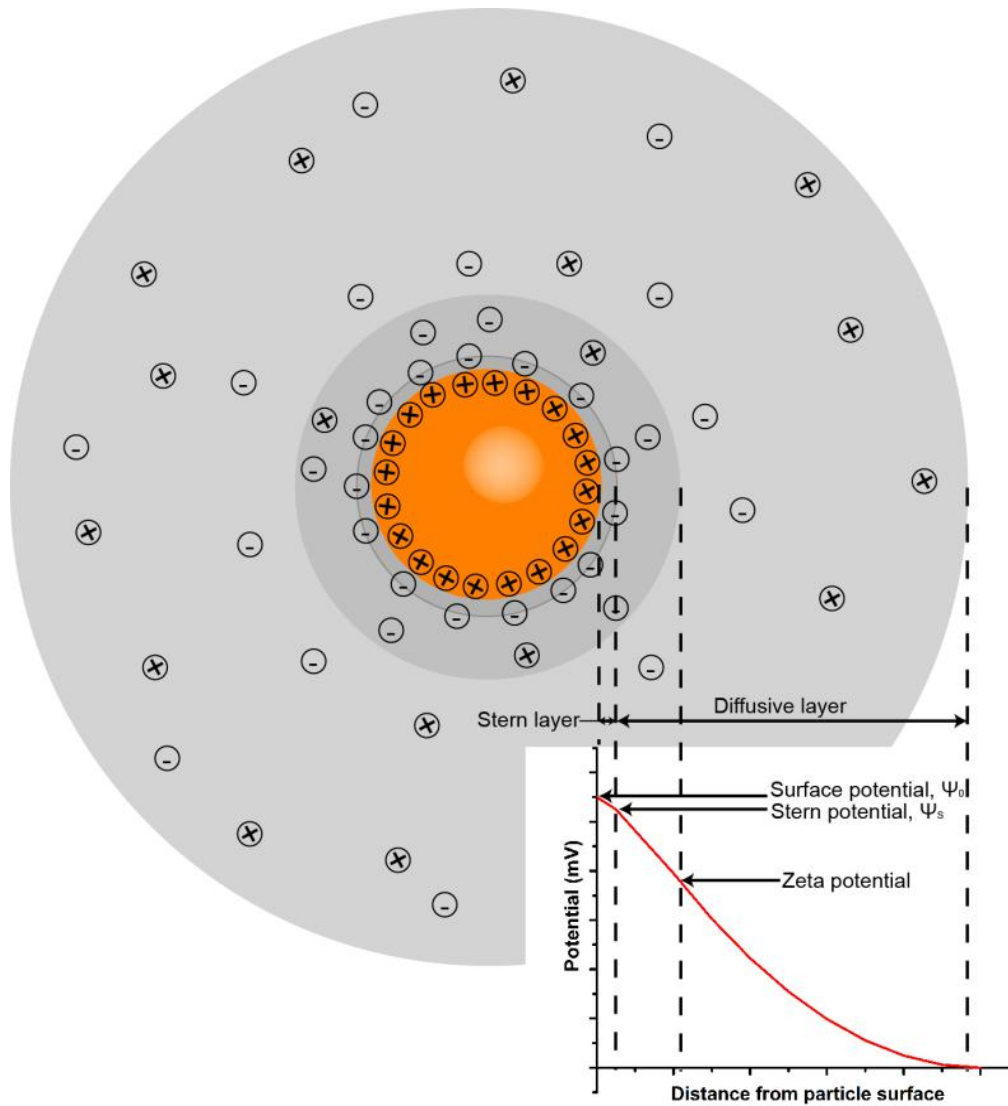


Figure 1.1. Schematic of electrical double layer structure on a positively charged particle surface.

ratio of the velocity and the electric field strength applied is defined as electrophoretic mobility μ_E . The relation between μ_E and zeta potential is described by the Smoluchowski equation as shown in Equation.(1.3):

$$\mu_E = \frac{2\varepsilon_0\varepsilon\zeta f(\kappa a)}{3\eta} \quad (1.3)$$

where ζ is the zeta potential and η is the viscosity of liquid. $f(\kappa a)$ is the so-called Henry's function. When the particles are larger than 0.2 μm , $f(\kappa a) = 1.5$ is applied, which is known as Smoluchowski approximation. For small particles in low dielectric constant media, $f(\kappa a) = 1$ is used, known as Huckel approximation.

1.4.3 Steric repulsion and bridging force

In this study, the steric repulsion and bridging force are crucial to the flocculation of colloidal particles induced by polymer flocculants. When two particles covered with polymers approach each other, the total interactions induced by polymers are polymer-polymer and polymer-surface interactions. The polymer-polymer interaction usually leads to repulsive force referred as steric repulsive force and polymer-surface interaction can either lead to repulsive force or attractive force (bridging force). These interactions are greatly dependent on the conformation of polymers, which further relies on the solvent quality and the properties of the polymer itself [36]. The ideal polymer, whose segment rotation is not perturbed by segment-segment interactions, usually presents itself as the shape of a random coil. One important length scale of such polymer is the radius of gyration:

$$R_g = \frac{l\sqrt{n}}{\sqrt{6}} = \frac{l\sqrt{M/M_0}}{\sqrt{6}} \quad (1.4)$$

where l is the length of the repeating unit, n is the total number of the repeating units in a polymer, M is the molecular weight of the polymer and M_0 is the segment molecular weight.

1.5 References

- [1] L.F. Greenlee, D.F. Lawler, B.D. Freeman, B. Marrot, P. Moulin, Reverse osmosis desalination: water sources, technology, and today's challenges, *Water Research*, 43 (2009) 2317-2348.
- [2] S. Castro, J.S. Laskowski, Froth flotation in saline water, *Kona Powder Part J*, (2011) 4-15.
- [3] V.I. Klassen, V.A. Mokrousov, *An Introduction to the Theory of Flotation*, Butterworths, 1963.
- [4] D.W. Fuerstenau, J.M. Rosenbaum, J. Laskowski, Effect of surface functional-groups on the flotation of coal, *Colloids and Surfaces*, 8 (1983) 153-174.
- [5] J. Laskowski, Z. Xu, R. Yoon, Energy barrier in particle-to-bubble attachment and its effect on flotation kinetics, in: *17th Int. Mineral Processing Congress, Dresden, 1991*, pp. 237-249.
- [6] J.S. Laskowski, Y.S. Cho, K. Ding, Effect of frothers on bubble size and foam stability in potash ore flotation systems, *The Canadian Journal of Chemical Engineering*, 81 (2003) 63-69.
- [7] M. Hancer, M.S. Celik, J.D. Miller, The significance of interfacial water structure in soluble salt flotation systems, *Journal of Colloid and Interface Science*, 235 (2001) 150-161.
- [8] O. Ozdemir, M.S. Çelik, Z.S. Nickolov, J.D. Miller, Water structure and its influence on the flotation of carbonate and bicarbonate salts, *Journal of Colloid and Interface Science*, 314 (2007) 545-551.
- [9] P.A. Moreno, H. Aral, J. Cuevas, A. Monardes, M. Adaro, T. Norgate, W. Bruckard, The use of seawater as process water at Las Luces copper-molybdenum beneficiation plant in Taltal (Chile), *Miner Eng*, 24 (2011) 852-858.
- [10] G.D. Senior, S.A. Thomas, Development and implementation of a new flowsheet for the flotation of a low grade nickel ore, *International Journal of Mineral Processing*, 78 (2005) 49-61.

- [11] J.J. Quinn, W. Kracht, C.O. Gomez, C. Gagnon, J.A. Finch, Comparing the effect of salts and frother (MIBC) on gas dispersion and froth properties, *Miner Eng*, 20 (2007) 1296-1302.
- [12] B.A. Wills, T. Napier-Munn, *Wills' Mineral Processing Technology: An Introduction to the Practical Aspects of Ore Treatment and Mineral Recovery*, Elsevier Science & Technology Books, 2006.
- [13] G. Blight, *Geotechnical Engineering for Mine Waste Storage Facilities*, 2010.
- [14] D.R. Kester, I.W. Duedall, D.N. Connors, R.M. Pytkowicz, Preparation of artificial seawater, *Limnology and Oceanography*, 12 (1967) 176-179.
- [15] D. Myers, *Surfaces, Interfaces, and Colloids*, Wiley Online Library, 1999.
- [16] T. Hunter, M. Pearse, The use of flocculants and surfactants for dewatering in the mineral processing industry, in: *CIM XIV International Mineral Processing Congress*, 1982, pp. p11.
- [17] R. Hogg, Flocculation and dewatering, *International Journal of Mineral Processing*, 58 (2000) 223-236.
- [18] D.A. Mortimer, Synthetic polyelectrolytes—a review, *Polymer international*, 25 (1991) 29-41.
- [19] A. Sworska, J.S. Laskowski, G. Cymerman, Flocculation of the Syncrude fine tailings: Part I. effect of pH, polymer dosage and Mg^{2+} and Ca^{2+} cations, *International Journal of Mineral Processing*, 60 (2000) 143-152.
- [20] N.B. Wyatt, C.M. Gunther, M.W. Liberatore, Increasing viscosity in entangled polyelectrolyte solutions by the addition of salt, *Polymer*, 52 (2011) 2437-2444.
- [21] P. Somasundaran, Y.H. Chia, R. Gorelik, Adsorption of polyacrylamides on kaolinite and its flocculation and stabilization, *Acs Symposium Series*, 240 (1984) 393-410.
- [22] C.C. Ho, K.C. Lee, The role of metallic cations on the colloidal stability of tin tailings slurries, *Colloids and Surfaces A-Physicochemical and Engineering Aspects*, 141 (1998) 19-27.
- [23] J.C.J. Boshoff, Prediction of the desiccation and sedimentation behavior of a typical platinum tailings, in: *Tailings and Mine Waste 2002*, 2002, pp. 121-125.

- [24] F.F. Peng, Z. Lu, Polymer flocculation and coagulation for sedimentation of copper flotation tailings, *Minerals & Metallurgical Processing*, 15 (1998) 14-20.
- [25] M.S. Nasser, A.E. James, Effect of polyacrylamide polymers on floc size and rheological behaviour of kaolinite suspensions, *Colloids and Surfaces A-Physicochemical and Engineering Aspects*, 301 (2007) 311-322.
- [26] M.L. Taylor, G.E. Morris, P.G. Self, R.S. Smart, Kinetics of adsorption of high molecular weight anionic polyacrylamide onto kaolinite: The flocculation process, *Journal of Colloid and Interface Science*, 250 (2002) 28-36.
- [27] P. Mpofu, J. Addai-Mensah, J. Ralston, Influence of hydrolyzable metal ions on the interfacial chemistry, particle interactions, and dewatering behavior of kaolinite dispersions, *Journal of Colloid and Interface Science*, 261 (2003) 349-359.
- [28] M.S. Nasser, A.E. James, The effect of polyacrylamide charge density and molecular weight on the flocculation and sedimentation behaviour of kaolinite suspensions, *Separation and Purification Technology*, 52 (2006) 241-252.
- [29] M.S. Nasser, A.E. James, Degree of flocculation and viscoelastic behaviour of kaolinite-sodium chloride dispersions, *Colloids and Surfaces A-Physicochemical and Engineering Aspects*, 315 (2008) 165-175.
- [30] M.S. Zbik, R.S.C. Smart, G.E. Morris, Kaolinite flocculation structure, *Journal of Colloid and Interface Science*, 328 (2008) 73-80.
- [31] F. Mietta, C. Chassagne, J.C. Winterwerp, Shear-induced flocculation of a suspension of kaolinite as function of pH and salt concentration, *Journal of Colloid and Interface Science*, 336 (2009) 134-141.
- [32] J. Long, H. Li, Z. Xu, J.H. Masliyah, Role of colloidal interactions in oil sand tailings treatment, *Aiche J*, 52 (2006) 371-383.
- [33] H. Haschke, M.J. Miles, V. Koutsos, Conformation of a single polyacrylamide molecule adsorbed onto a mica surface studied with atomic force microscopy, *Macromolecules*, 37 (2004) 3799-3803.
- [34] J. Long, Z. Xu, J.H. Masliyah, Adhesion of single polyelectrolyte molecules on silica, mica, and bitumen surfaces, *Langmuir*, 22 (2006) 1652-1659.

- [35] P. Müller, Q. Mary, Glossary of Terms Used in Physical Organic Chemistry (IUPAC Recommendations 1994), Department of Chemistry, Queen Mary and Westfield College, University of London, 1994.
- [36] M.M. Coleman, P.C. Painter, Fundamentals of Polymer Science. An Introductory Text, Technomic Publishing Company, Incorporated, 1994.

Chapter 2 Experimental Techniques

2.1 Surface forces apparatus (SFA)

2.1.1 Development of SFA

Since Tabor and Winterton described the first apparatus that can measure the forces between surfaces at the separation as low as 5-30 nm with a 3 Å resolution [1], this technique has been developed and improved for several decades [2-4].

After the development of early version SFA, the SFA Mk I was described by Israelachvili and Adams which can measure the forces between surfaces not only in air or vacuum, but in liquids [2]. A motor-driven micrometer and a piezoelectric crystal were used to control the approach and separation of two surfaces, which can achieve the range of the control from micrometer to the angstrom level.

After that, an improved model of the Mk I was developed to meet the need in interfacial phenomena studies, namely the SFA Mk II [5, 6]. Mk II replace the single cantilever spring in Mk I with a double-cantilever spring to increase strength as well as to prevent the rotation of surface during the loading of normal forces. More importantly, a ‘friction device’ was added as an attachment that allowed measurement of frictional forces-distance profiles in lateral direction.

For the requirement in increasingly complex systems, Mk III was developed by Israelachvili and McGuiggan during 1985-1989[4]. It was designed for system that needed to be totally immersed in liquid and a new attachment called bimorph slider was designed for friction measurement[7].

Although Mk III is already very stable and functional, there are still some drawbacks such as difficult to manufacture and assemble. Therefore the SFA 2000 was designed to address these drawbacks while retaining the good performance of previous models.

2.1.2 SFA 2000

A schematic of the basic SFA 2000 is shown in Figure 2.1. It is designed to have fewer parts so as to be easier to manufacture, clean and operate. The main components are the micrometers, the main stage consisting of the central single-cantilever spring, the upper and lower disk holders. Two differential micrometers, a fine micrometer driven by motor and a piezoelectric tube are used to generate the distance control between surfaces in accuracy from millimeters to angstroms.

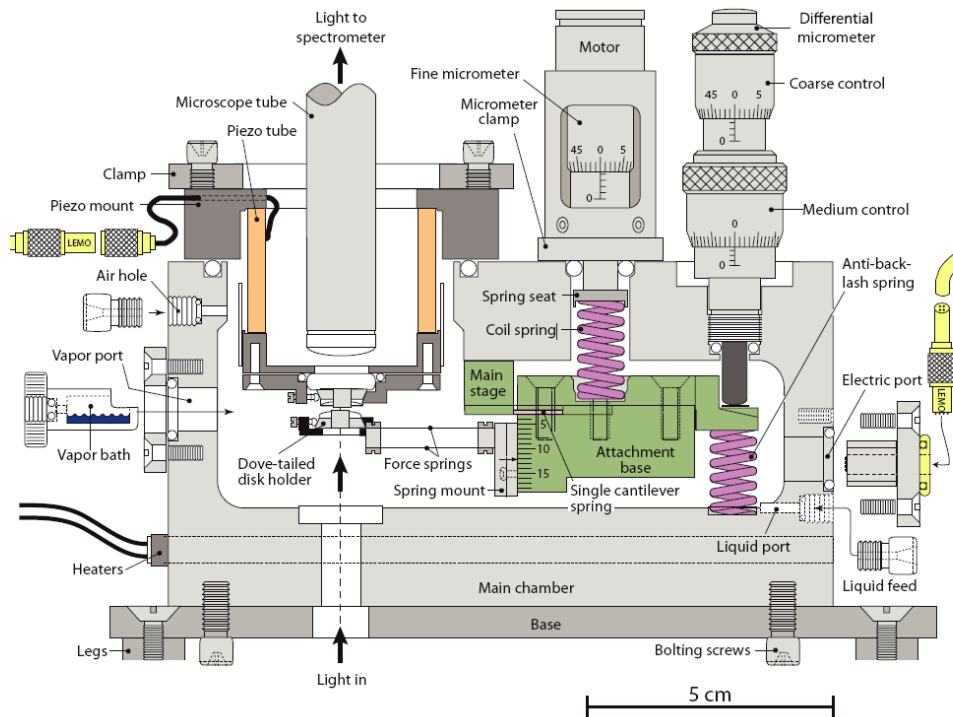


Figure 2.1. Schematic drawing of SFA 2000 [8].

The schematic of the light path in SFA is shown in Figure 2.2. When a beam of light passes through the two back silvered mica surfaces glued on two crossed cylinders with the same radius of R , the merging interference light beam is focused on a grating spectrometer which generates a series of Fringes of Equal Chromatic Order (FECO) [9, 10] shown in Figure 2.3. The absolute distance between mica surfaces is monitored through the FECO fringe pattern by using an optical technique called multiple beam interference (MBI).

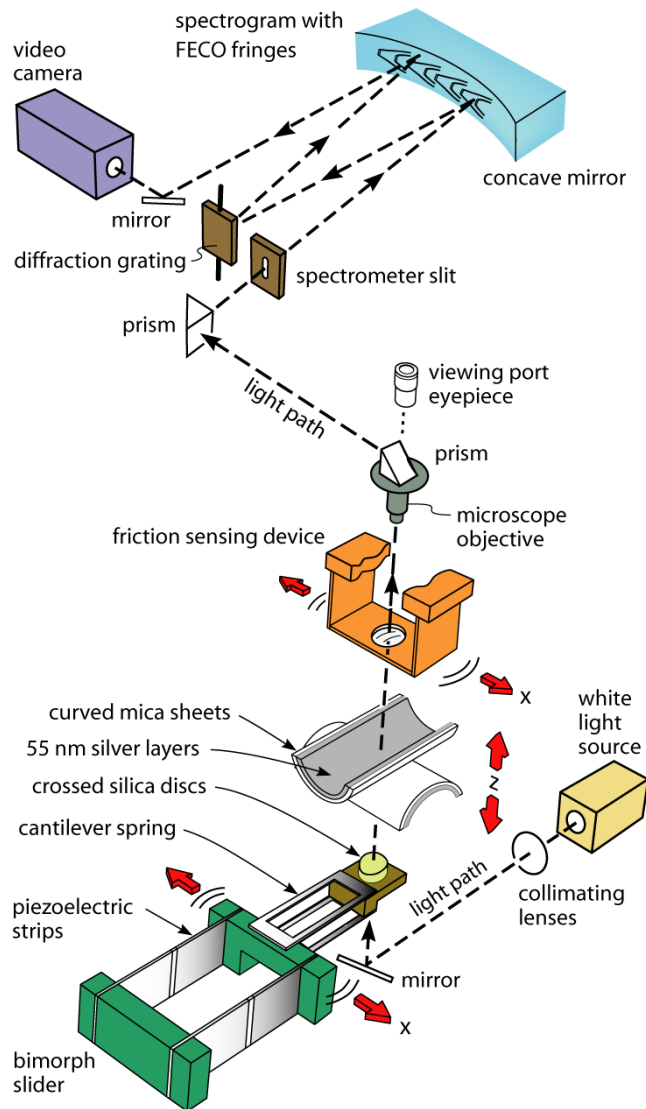


Figure 2.2. Schematic of SFA setup [8].

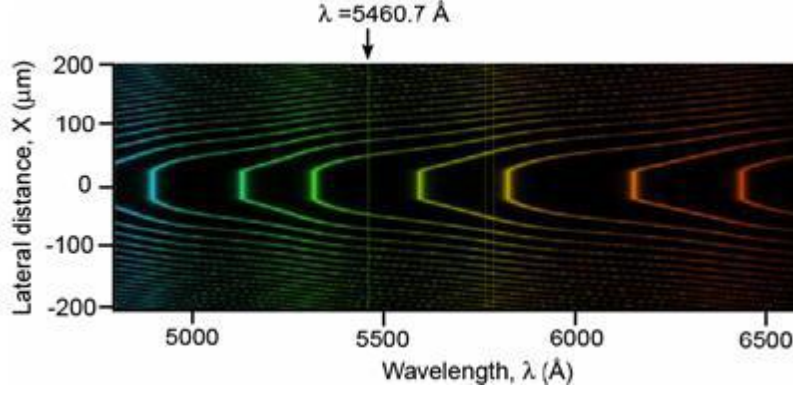


Figure 2.3. FECO fringes for two contacted mica surfaces in air.

2.1.3 Multiple beam interference (MBI)

MBI is an optical technique used in the SFA to measure the separation and the shape of the surfaces [9, 11]. As previously noted, when white light is directed normally through the two back silvered mica surfaces, Newton's rings are created by the transmitted and reflected light near the contact point of the two surfaces. The corresponded set of discrete wavelengths is visualized by a spectrometer, which are the FECO. When the two surfaces are in contact in air, the FECO are designated by λ_n^0 ($n = 1, 2, 3, \dots$). The fringe order, n , is determined by

$$n = \frac{\lambda_{n-1}^0}{\lambda_{n-1}^0 - \lambda_n^0} \quad (2.1)$$

where λ_{n-1}^0 is the next fringe at higher wavelength. When the two surfaces are separated by a distance D , the wavelength shift of n th fringe is determined by the refractive index of the medium between the surfaces and the original contact positions [12].

$$\tan(2\pi\mu D / \lambda_n^D) = \frac{2\bar{\mu} \sin[\pi(1 - \lambda_n^0 / \lambda_n^D) / (1 - \lambda_n^0 / \lambda_{n-1}^0)]}{(1 + \bar{\mu}^2) \cos[\pi(1 - \lambda_n^0 / \lambda_n^D) / (1 - \lambda_n^0 / \lambda_{n-1}^0)] \pm (\bar{\mu}^2 - 1)} \quad (2.2)$$

where the + sign is given to odd order fringes (n is odd) and the – sign refers to even order fringes. $\bar{\mu} = \mu_{mica} / \mu$, where μ_{mica} is the refractive index of mica at λ_n^D and μ is the refractive index of the medium. By using equation (2.2), the distance D can be determined by measuring the wavelengths shift of an odd fringe and an adjacent even fringe. The accuracy is about 0.1 nm when D is in the range of 0-200 nm.

2.1.4 Normal and adhesive force measurements

When the surface at the base of the double-cantilever force spring (lower surface) is driven approaching to or separating from the upper surface by the differential micrometer, motor-driven fine micrometer and/or piezo tube, the interaction forces between two surfaces are determined by Hooke's law:

$$\Delta F(D) = k_{sp} (\Delta D_{app} - \Delta D_{abs}) \quad (2.3)$$

where k_{sp} is the spring constant of the double-cantilever force spring, ΔD_{app} is the travel distance of the lower surface and ΔD_{abs} is the absolute distance between two surfaces measured by MBI as illustrated in Figure 2.4. The accuracy of force and distance are 10 nN and 0.1 nm respectively.

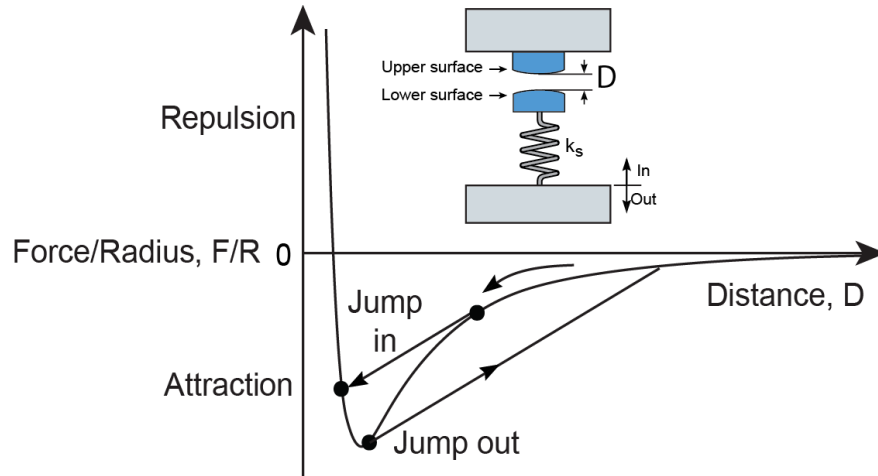


Figure 2.4. Schematic of normal and adhesive force measurement.

The adhesive forces are calculated by

$$F_{adhesive} = k_{sp} \times \Delta D_{jump} \quad (2.4)$$

where ΔD_{jump} is the distance that the two surfaces jump apart from contact.

The normal force F is usually normalized by the radius of the surface's curvature R . The measured force can be further converted to the interaction energy per unit area between two flat surfaces, $W_{flat}(D)$, by the Derjaguin approximation [10]:

$$W_{flat}(D) = \frac{F(D)}{2\pi\sqrt{R_1R_2}} = \frac{F(D)}{2\pi R} \quad (2.5)$$

2.2 Quartz crystal microbalance with dissipation monitoring (QCM-D)

2.2.1 Development of QCM-D

The history of quartz crystal microbalance (QCM) goes back to 1959 when G. Sauerbrey discovered the proportional relation between the resonance frequency change of a quartz crystal and the mass uptake on itself [13], known as Sauerbrey equation:

$$\Delta m = C \frac{\Delta f}{n} \quad (2.6)$$

where Δm and Δf is the mass and frequency change of the quartz respectively, n is the resonance number of the sensor ($n = 1, 3, 5, 7, 9, 11, 13$) and C is a constant related to the physical properties of the quartz. This relation is valid for rigid materials as there are no viscoelastic losses. However for viscoelastic materials adsorbed Equation (2.6) tends to underestimate the mass uptake. Therefore a new version of QCM was developed [14] to monitor the energy dissipation of the vibrating quartz sensor, namely The commercialized QCM-D was developed by Q-sense Company, founded in 1996 by a group of researchers at the Department of Applied physics, Chalmers University of Technology in Gothenburg. The latest model of QCM-D, Q-sense E4, was used in this thesis study to monitor the changes in resonance frequency (Δf) and energy dissipation (ΔD) of the QCM-D sensors at 7 different harmonics simultaneously and to investigate the adsorption and conformation of polymer on clay surfaces.

2.2.2 Working mechanism

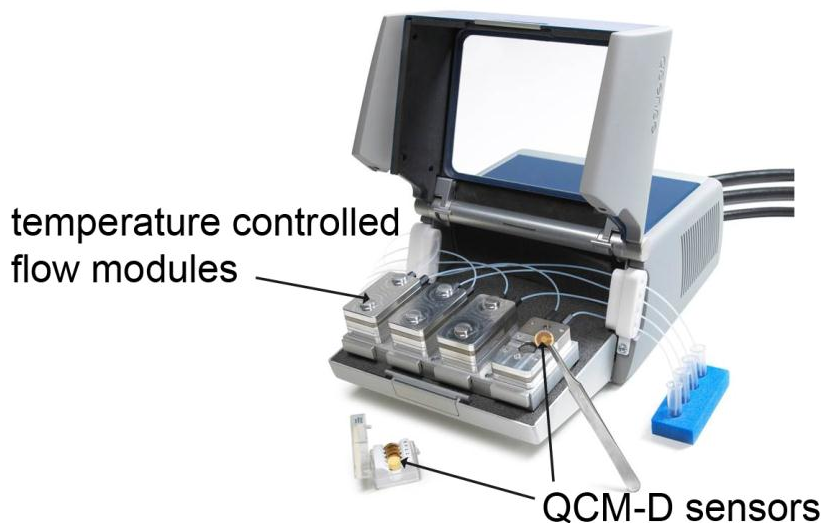


Figure 2.5. Quartz crystal microbalance with dissipation monitoring

A picture of E4 is shown in Figure 2.5. The critical part of the QCM-D is a thin quartz disk sandwiched by a pair of gold electrodes. Due to the piezoelectric properties of quartz, the crystal will oscillate when an AC voltage is applied as shown in Figure 2.6. The resonance frequency of the oscillation will decrease when a mass is added on to the sensor. When the AC voltage is disconnected from the sensor, the relaxation of the sensor is recorded. The energy dissipation change (ΔD) before and after the adsorption is calculated [15]. If the adsorbed layer is rigid, evenly disturbed and thin enough, the dissipation change is very small (Figure 2.6b). On the contrary, a large dissipation change indicates a soft viscoelastic layer adsorbed on the sensor (Figure 2.6c). The layer structures of the silicon dioxide and aluminum oxide sensors used are shown as Figure 2.7.

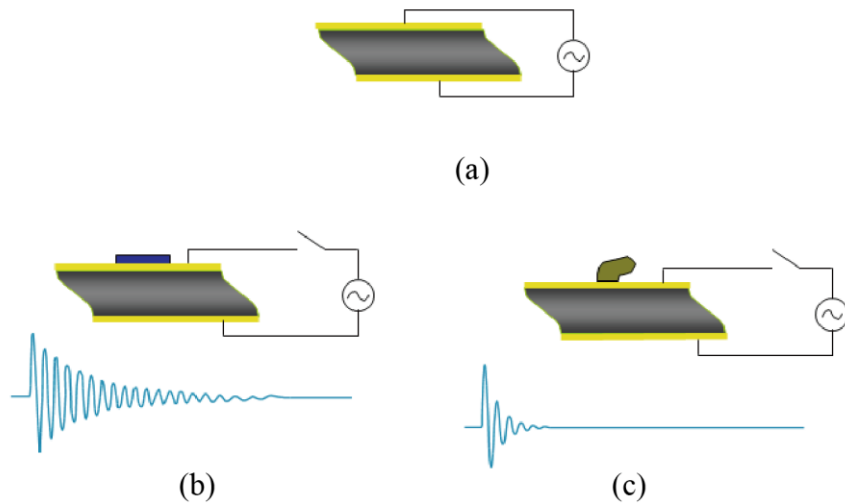


Figure 2.6. Principle of frequency and dissipation measurement: (a) sensor vibrates when an AC voltage is applied (b) slow decay-small dissipation-rigid layer (c) fast decay-large dissipation-loose layer.

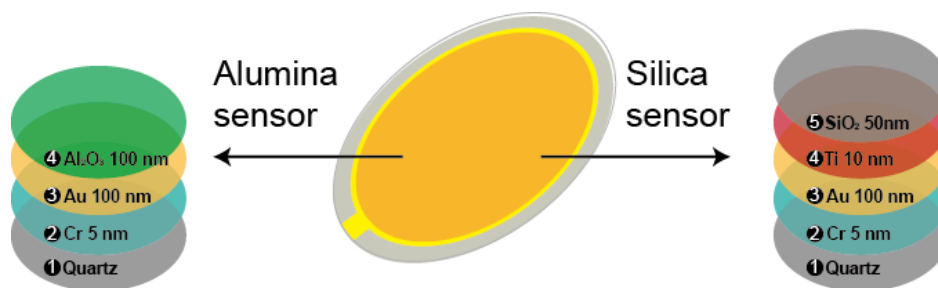


Figure 2.7. Schematic of the layer structure of silica and alumina sensors.

2.3 Other techniques

There are some other techniques used in this thesis research to characterize the ion concentration and particle size distribution in the tailings as well as the conformation of polymer in solutions, including Inductively Coupled Plasma Mass Spectrometry (ICP-MS), Dynamic Light Scattering (DLS) and Mastersizer.

2.3.1 Inductively coupled plasma mass spectrometry (ICP-MS)

ICP-MS is a type of mass spectrometry that can detect metal and some non-metal elementals at the accuracy of part per trillion. The quantification of the elemental concentration is achieved by ionizing the sample with inductively coupled plasma and then using a mass spectrometer to identify and quantify these ions. Perkin Elmer Elan6000 quadrupole ICP-MS was used in this study.

2.3.2 Dynamic light scattering (DLS)

The ALV/CGS-3 Platform based Goniometer Systems measures the hydrodynamic radius of the micro and nano particles in liquid through the DLS technique. This technique measures the time dependent fluctuations in the intensity of the light scattered by the particles because of their Brownian motion. The intensity fluctuation is correlated with the diffusion coefficients of the particles and further converted into PSD. The diffusion coefficient (D) can be calculated from the fitting of time correlation function:

$$g(\tau) = A \left[1 + B \exp(-2Dq^2\tau) \right] \quad (2.7)$$

where τ is the sample time, A is the baseline of the correlation function, B is the intercept of the correlation function, $q = [(4\pi n / \lambda_0) \sin(\theta/2)]$ is the scattering vector, n is the refractive index of solution, λ_0 is the wavelength of the laser, and θ is the scattering angle. Then the R_H is calculated from the Stokes-Einstein equation:

$$R_H = kT / (3\pi\mu D) \quad (2.8)$$

where k is the Boltzmann's constant, T is the absolute temperature and μ is the viscosity.

2.3.3 Mastersizer 2000

The Mastersizer 2000 uses the technique of laser diffraction to measure the size of particles. The laser diffraction technique measures the intensity of light scattered as a laser beam passes through a dispersed particulate sample. A large particle will give relatively smaller scattering angle than small particle (Figure 2.8). The angular scattering intensity data is used to calculate the PSD according to the Mie theory of light scattering.

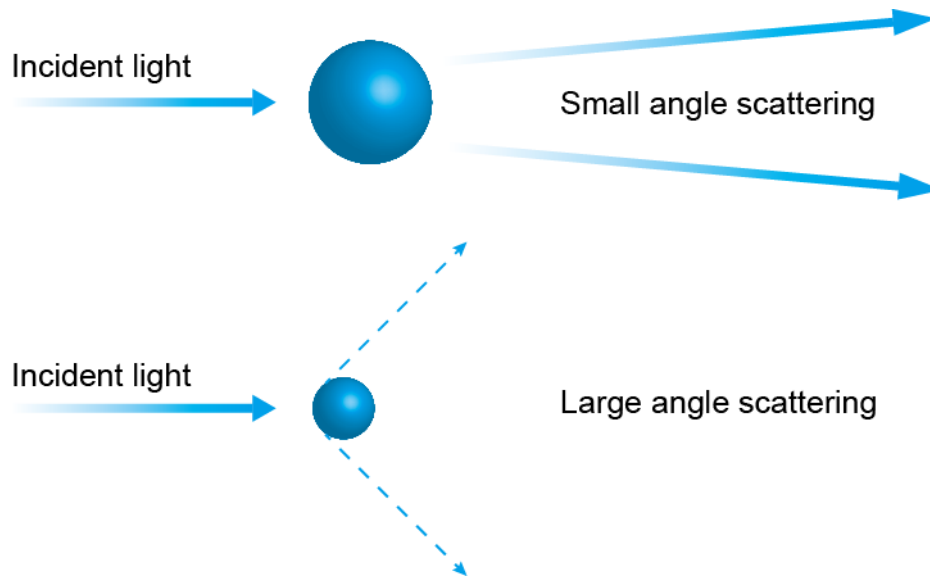


Figure 2.8. Scattering of light from small and large particles.

2.4 References

- [1] D. Tabor, R. Winterton, The direct measurement of normal and retarded van der Waals forces, Proceedings of the Royal Society of London. A. Mathematical and Physical Sciences, 312 (1969) 435-450.
- [2] J. Israelachvili, G. Adams, Direct measurement of long range forces between two mica surfaces in aqueous KNO_3 solutions, Nature, 262 (1976) 774-776.
- [3] J.N. Israelachvili, G.E. Adams, Measurement of forces between two mica surfaces in aqueous electrolyte solutions in the range 0–100 nm, Journal of the Chemical Society,

- Faraday Transactions 1: Physical Chemistry in Condensed Phases, 74 (1978) 975-1001.
- [4] J.N. Israelachvili, P.M. McGuiggan, Adhesion and short-range forces between surfaces. Part I: new apparatus for surface force measurements, *J. Mater. Res.*, 5 (1990) 2223.
- [5] J.N. Israelachvili, Techniques for direct measurements of forces between surfaces in liquids at the atomic scale, *Chemtracts Anal. Phys. Chem.*, 1 (1989).
- [6] J. Israelachvili, Direct measurements of forces between surfaces in liquids at the molecular level, *Proceedings of the National Academy of Sciences of the United States of America*, 84 (1987) 4722.
- [7] G. Luengo, F.J. Schmitt, R. Hill, J. Israelachvili, Thin film rheology and tribology of confined polymer melts: contrasts with bulk properties, *Macromolecules*, 30 (1997) 2482-2494.
- [8] J. Israelachvili, Y. Min, M. Akbulut, A. Alig, G. Carver, W. Greene, K. Kristiansen, E. Meyer, N. Pesika, K. Rosenberg, H. Zeng, Recent advances in the surface forces apparatus (SFA) technique, *Rep Prog Phys*, 73 (2010).
- [9] J. Israelachvili, Thin film studies using multiple-beam interferometry, *Journal of Colloid and Interface Science*, 44 (1973) 259-272.
- [10] J.N. Israelachvili, *Intermolecular and Surface Forces: Revised Third Edition*, Academic press, 2011.
- [11] S. Tolansky, *Multiple Beam Interferometry of Films and Surfaces*, Oxford University Press (Clarendon), London, 1948.
- [12] R.G. Horn, D.T. Smith, Analytic solution for the three-layer multiple beam interferometer, *Applied optics*, 30 (1991) 59-65.
- [13] G. Sauerbrey, Use of vibrating quartz for thin film weighing and microweighing, *Z. Phys.*, 155 (1959) 206-222.
- [14] F. Höök, M. Rodahl, P. Brzezinski, B. Kasemo, Energy dissipation kinetics for protein and antibody-antigen adsorption under shear oscillation on a quartz crystal microbalance, *Langmuir*, 14 (1998) 729-734.

- [15] M.V. Voinova, M. Rodahl, M. Jonson, B. Kasemo, Viscoelastic acoustic response of layered polymer films at fluid-solid interfaces: continuum mechanics approach, *Physica Scripta*, 59 (1999) 391-396.

Chapter 3 Effect of Solution Salinity on Settling of Mineral Tailings by Polymer Flocculants¹

3.1 Introduction

Water represents a major component in mineral processing. The mineral industry produces large amount of mine tailings which are usually in a slurry form with a mixture of fine mineral particles, water and a considerable amount of inorganic ions. Due to the shortage of available freshwater and increased environmental/social constraints for the disposal of mineral tailings, the global natural resource industries (e.g., base metals, oil sands) are facing serious water restrictions. The increasing exploitation of lower-grade ores [1] makes the situation more challenging, due to the generation of large amounts of very fine tailings [2]. Much attention has been paid to such engineering and environmental challenges of water, particularly from two aspects: (1) recycle and reuse of water by settling the mineral tailings and (2) development of mineral processing technologies by using saline water instead of freshwater (e.g., flotation using sea water).

Significant progresses have been made towards the settling of both industrial and model tailings [3-8]. Various flocculants, particularly polymers, have been developed and applied to enhance the settling of the colloidal particles in mineral tailings. Mpofo et al. [9] compared the flocculation of kaolinite suspensions by using hydrolyzed polyacrylamide (H-PAM) containing anionic acrylate segments and nonionic polyethylene oxide (PEO). Higher settling rate was found for PEO treated kaolinite suspension than for H-PAM treated one, which was proposed to be mainly due to the

¹ A version of this chapter has been submitted for publication. Y. Ji, H. Zeng, Q. Liu 2013. Colloids and Surfaces A: Physicochemical and Engineering Aspects (under review).

electrostatic repulsive interactions between carboxyl groups of H-PAM and negatively charged kaolinite surfaces leading to the formation of fragile flocs [9]. The impact of charge type (e.g., cationic, anionic) of modified polyacrylamide (PAM) polymers on kaolinite flocculation was investigated in detail [10]. It was found that kaolinite suspension treated with cationic PAMs produced a supernatant of lower turbidity, while anionic PAM treated suspension yielded a higher settling rate at the low flocculant dosage.

The interaction mechanisms of polymer flocculants and clay particles have also received considerable attention [11-17], although more work is still required for a complete understanding. The concentration of inorganic ions can be easily accumulated associated with recycling and reuse of water in mineral processing [18]. The presence of inorganic ions was found to have dramatic influence on the interaction between polymer flocculants and clay particles in the settling of tailings. It was found that the addition of 8 mM Mg^{2+} or Ca^{2+} could enhance the settling rate of oil sands tailings with 20 ppm H-PAM [19], which was attributed to the enhanced bridging between particles and polymers by the divalent cations [20]. Enhanced flocculation was reported for kaolinite suspension treated with 500 g/ton of H-PAM in the presence of 0.001 M Ca^{2+} and Mn^{2+} at pH 10.5 and 7.5 respectively [21], and increased kaolinite agglomeration was also found with the addition of NaCl and $MgCl_2$ of concentration up to 1 M and 0.5 M respectively in the absence of flocculant [22].

More recently, seawater and diluted seawater have been used directly as an alternative mineral processing medium due to its abundance on the earth [23, 24]. Flotation of some naturally hydrophobic minerals (i.e. bituminous coals) was achieved in 0.5 M NaCl solution without any organic reagents [25, 26]. The recovery of quartz in

saline water with non-thio collectors was dependent on collector concentration, and the recovery of some sulfides with thio-collectors was found to depend on solution pH [27, 28]. Nevertheless, the salinity of the sea water would affect the settling behaviors of the mineral particles in the tailings and the quality of the recycling water which would further influence the efficiency of mineral processing.

Despite the recent advances on mineral flotation in saline water [29-31], the understanding of settling of saline tailings remains limited, which is of both fundamental and practical importance. In this study, the settling behaviors of mineral tailings in both freshwater and saline solution treated by three polymers, polyacrylamide (PAM), Magnafloc 1011 (MF) and $\text{Al}(\text{OH})_3$ -polyacrylamide (Al-PAM) were investigated and compared through the measurements of initial settling rate (ISR) and turbidity of the supernatant. Zeta potential analyzer and dynamic light scattering (DLS) were applied to study the interactions between clays particles and polymer molecules. A simplified model by including the van der Waals attractions, electrostatic repulsions, and polymer bridging was proposed to help understand the interaction mechanisms. This work focuses on the settling of real mineral tailing systems. In a separate related report, the intermolecular and surface interactions of polymers and model clay surfaces (i.e. silica, mica) in freshwater and saline water have been directly measured by surface forces apparatus, quartz crystal microbalance and other techniques, which provides complementary information to the understanding of the settling behaviors of real mineral tailings reported in this work.

3.2 Materials and methods

3.2.1 Tailings

The saline tailings were provided by Teck Resources, which contain an average solid content of 33 wt%. The solids in the saline tailings were filtrated, dried and characterized by X-ray diffraction (XRD, Rigaku, Japan). The size distribution of solid particles was determined by laser diffraction (Mastersizer 2000, Malvern). The pH of tailings samples was measured by using a pH meter (Accumet Basic AB15, Fisher Scientific). In order to understand the impact of salinity on the settling of the solid particles, freshwater tailings were prepared by decanting the supernatant of saline tailings which was replaced by mili-Q water until the conductivity dropped below 400 μ S. The ions concentrations in the tailings were measured by inductively coupled plasma mass spectrometry (ICP-MS).

3.2.2 Polymer flocculants

Three different polymer flocculants were used to study the settling of the tailings, and their properties (i.e. chemical structure, molecular weight) are shown in Table 3.1. Polyacrylamide (Sigma-Aldrich) is a non-ionic flocculant widely used in water treatment. Magnafloc 1011 (MF) (Ciba, UK) is a negatively charged copolymer of acrylamide and sodium acrylate. The charge density of the MF used is 27% [32]. $\text{Al}(\text{OH})_3$ -polyacrylamide (Al-PAM) was synthesized in-house by polymerization of acrylamide monomer in a $\text{Al}(\text{OH})_3$ suspension using $(\text{NH}_4)_2\text{S}_2\text{O}_8$ and NaHSO_3 as initiator [33].

Table 3.1. Properties of the flocculants used for enhancing tailings settling.

Flocculant	Structure	Molecular weight (g/mol)	Charge
Magnafloc 1011 (MF)	$\left[\text{CH}_2 - \underset{\substack{ \\ \text{C}=\text{O} \\ \\ \text{NH}_2}}{\text{CH}} \right]_m \left[\text{CH}_2 - \underset{\substack{ \\ \text{C}=\text{O} \\ \\ \text{O}^- \text{Na}^+}}{\text{CH}} \right]_n$	1.75×10^7	Anionic
Polyacrylamide (PAM)	$\left[\text{CH}_2 - \underset{\substack{ \\ \text{C}=\text{O} \\ \\ \text{NH}_2}}{\text{CH}} \right]_n$	5.00×10^6	Nonionic
Al-PAM	$\text{Al(OH)}_3(\text{PAM})_n$	2.60×10^6	Cationic core

3.2.3 Settling test

The settling tests of tailings followed a procedure reported recently [34]. Basically, tailings sample was first homogenized in a reservoir (typically a 4-L jar) under high speed agitation using an RW 20 stand agitator (IKA Works Inc., US). The 120 g tailings were then transferred into a 250 mL standard baffled beaker on a balance and then agitated under 600 rpm for 2 min, followed by adding desired amount of 1000 ppm polymer stock solution into the slurry in 1 min under a lower agitation speed of 300 rpm to achieve a uniform mixture and avoid breaking the flocs. The agitation was stopped immediately after the addition of desired amount of polymer. Finally, the slurry was transferred into a 100 ml graduated cylinder. The cylinder was inverted for 5 times and the so-called mudline was monitored as a function of settling time. The initial settling rate (ISR) was calculated from the initial slope of the mudline height (h) versus settling time (t), as shown in Figure 3.1. The supernatant was then extracted for zeta potential and turbidity measurements using a zeta potential analyzer (Zetasizer Nano, Malvern) and a Micro-100 Turbidity Meter (Fisher, US), respectively.

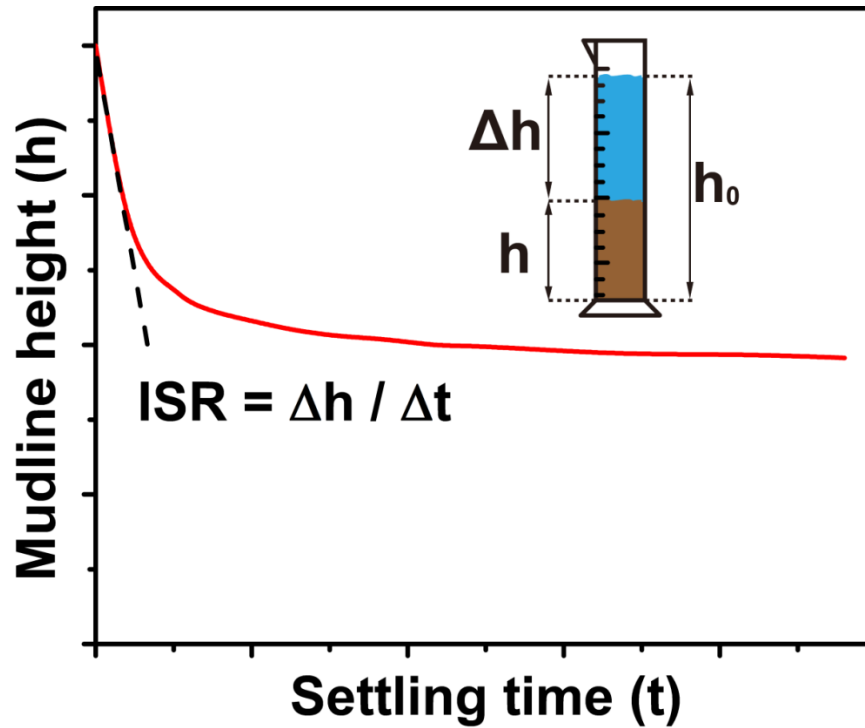


Figure 3.1. Schematic of ISR calculation based on the settling results of mudline height vs. settling time

3.2.4 Molecular conformations of polymer flocculants

The molecular conformations of polymer flocculants in bulk solutions were determined by dynamic light scattering (DLS) using an ALV/CGS-3 Platform based Goniometer System. Polymer solutions of 50 ppm were prepared and then filtrated by a Millex-AA Filter Unit with a pore size of 0.8 μm (EMD Millipore) before the DLS measurements. DLS measures the hydrodynamic radii (R_H) of polymer molecules in solution, which is defined as the radius of a hypothetical hard sphere that diffuses at the same speed as the polymer molecule under the test condition [35]. Therefore R_H can provide useful information to reveal molecular conformations (swelling or shrinking) of the polymers under different solution conditions.

3.2.5 Simplified model for polymer-particle interaction

The interactions between polymers and particles are crucial for the stabilization of colloidal systems [36]. In order to better understand the flocculation mechanism, a simplified model was developed to analyze the polymer-particle interaction during flocculation by considering interaction energy between two spherical silica particles in the presence of polymer flocculants, which was calculated as a sum of van der Waals attractions (E_{vdW}), electrostatic repulsions (E_{EDL}), and polymer bridging interaction ($E_{Bridging}$) as shown in Equations (3.1) to (3.3), respectively [37-39]. The configuration of the model and the parameters in the three equations are shown in Figure 3.2 and Table 3.2 respectively.

$$E_{vdW}(D) = -\frac{A_{131}R_1R_2}{6D(R_1 + R_2)} \quad (3.1)$$

$$E_{EDL}(D) = \frac{\pi\epsilon_r\epsilon_0R_1R_2}{R_1 + R_2} \left[2\phi_1\phi_2 \ln\left(\frac{1 + \exp(-\kappa D)}{1 - \exp(-\kappa D)}\right) + (\phi_1^2 + \phi_2^2) \ln(1 - \exp(-2\kappa D)) \right] \quad (3.2)$$

$$E_{Bridging}(D) = \beta \frac{4\pi R_1 R_2 \epsilon}{(R_1 + R_2) s^2} \frac{(L_c D - D^2 / 2 - L_c^2 / 2)}{l} \quad (3.3)$$

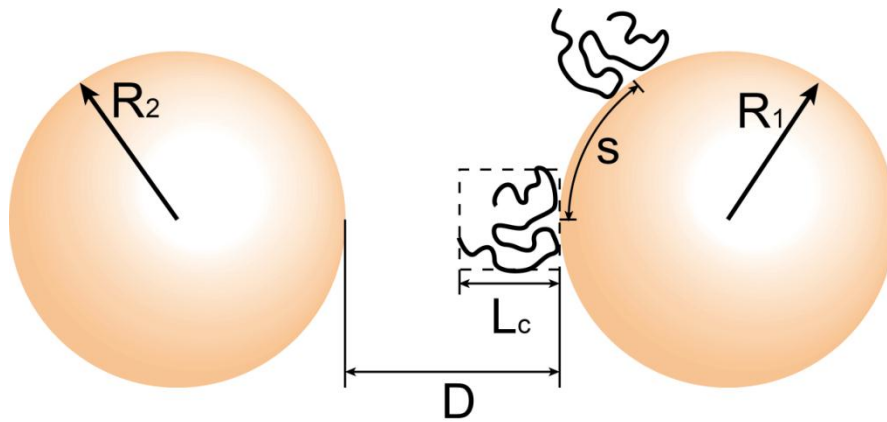


Figure 3.2 Schematic of interaction energy calculation.

Table 3.2. Parameters and constants used in equation (3.1) to (3.3).

Parameters and constants	MF		PAM and Al-PAM	
	Freshwater tailings, 15 ppm	Saline tailings, 100 ppm	Freshwater tailings, 75 ppm	Saline tailings, 75 ppm
Separation of two particles (D , nm)				
Radius of particles ($R_1 = R_2$, μm)	5			
Flocculant grafting density (s , nm)	271.3	105.1	64.9	
Flocculant contour length (L_C , nm)	135.7	52.5	32.5	
Bonding energy per segment (ϵ , kT)	3.9	15	10	
Segment length (l , nm)	0.304			
Effective bridging ratio (β)	0.01	0.05	0.02	
Temperature (T , K)	298			
Boltzmann constant (k_B , J/K)	1.38×10^{-23}			
Relative permittivity (ϵ_r)	80.4			
Vacuum permittivity (ϵ_0 , F/m)	8.85×10^{-12}			
κ^{-1} (Debye length, nm)	3.4	0.5	3.4	0.5
Surface potential of particles ($\phi_1 = \phi_2$, mV)	-35	-13	-35	-13
Hamaker constant (A_{131} , J)	3.92×10^{-21}			

Derjaguin-Landau-Verwey-Overbeek (DLVO) energy is the summation of E_{vdW} and E_{EDL} . The grafting density s was calculated from the specific surface area and the optimum flocculant dosage at the maximum ISR of each condition: $s = \sqrt{\frac{m_s}{A_{SSA} N_p}}$, where m_s is the mass of solid particles in each tailings sample, A_{SSA} is the specific surface area of solid particles and N_p is the total number of polymer molecules corresponding to the optimum flocculant dosage in each tailings sample. The shape of the polymer on particles

was simplified as a cube with the edge length of L_C . Because it was assumed that half of the particle was covered by polymer under the optimum dosage, L_C was taken as half of the s value. The bonding energy per segment ε was determined by the single molecule force measurements. The segment length l here was considered as twice the C-C bond length. It is noted that an effective bridging ratio β was introduced in the calculation of bridging energy (Equation (3.3)), which is defined as the percentage of molecules that form effective bridging among all absorbed polymer molecules. The value of β was estimated from the impact of salinity on the interaction between polymer and particles: for PAM and Al-PAM, β was not affected by the salinity due to the neutral charge property of PAM and Al-PAM; the value of β in MF treated saline tailings was larger than that in tailings treated by PAM and Al-PAM due to the present of Ca^{2+} ; the value of β in MF treated freshwater tailings was the smallest among all the situations due to the repulsion between negatively charged MF and negatively charged particles. The Debye lengths κ^{-1} corresponding to freshwater tailings and saline tailings were estimated by considering major ions (K^+ , Na^+ , Ca^{2+} , Mg^{2+} and corresponding anions) in the solution

using $\kappa = \sqrt{\frac{e^2 N_A}{\varepsilon_r \varepsilon_0 k_B T} \sum_i M_i z_i^2}$ where e is the charge of one electron, N_A is the Avogadro

constant, M_i is the concentration of ions in mol/m^3 , and z_i is the valence of ions. The zeta potential measured was used as approximation for the surface potential of silica particles.

The Hamaker constant was calculated based on $A_{131} = (\sqrt{A_{11}} - \sqrt{A_{33}})^2$, where A_{11} and A_{33} are the Hamaker constant of silica and water respectively.

3.3 Results and discussion

3.3.1 Characterization of tailings

The properties of the solid and liquid phases of saline tailings have a significant influence on their settling behavior. Therefore, the composition and size distribution of the solid particles, and the pH and ionic concentrations of the solutions were characterized. Figure 3.3(a) shows the XRD pattern of the solid particles in the saline tailings, which indicates that the main composition of the particles were quartz (SiO_2) and albite ($\text{NaAlSi}_3\text{O}_8$). The particle size distribution of solid particles is shown in Figure 3.3(b). The D_{10} , D_{50} and D_{90} of the solid particles were $6.55 \mu\text{m}$, $80.14 \mu\text{m}$ and $284.45 \mu\text{m}$ respectively. The subscript number indicates the weight percentage of the particles whose sizes are below the corresponding diameter. For example, $D_{50} = 80.14 \mu\text{m}$ means that 50 wt% particles are smaller than $80.14 \mu\text{m}$. The specific surface area of $0.114 \text{ m}^2/\text{g}$ was calculated based on the size distribution.

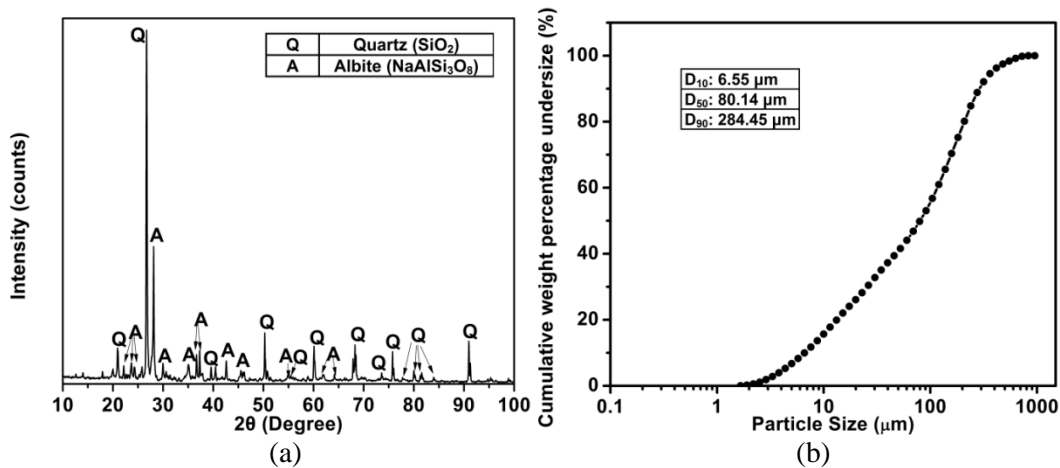


Figure 3.3. Characterization of the saline tailings: (a) XRD pattern of the solids, and (b) particle size distribution measured by Mastersizer.

The pH of the saline tailings supernatant was 7.5, while that of freshwater tailings was 8.3. The ion concentrations of saline and freshwater tailings are summarized in,

which shows that the ionic strength in saline tailings was significantly higher than that in freshwater tailings. The most abundant ions (Na^+ , Mg^{2+} , K^+ and Ca^{2+}) in seawater were detected in the saline tailings. The presence of other trace metal ions in the saline tailings could be due to the oxidation or dissolution of minerals during processing.

Table 3.3. Ion concentrations (ppm) of saline and freshwater tailings.

Tailings	Na	Mg	K	Ca	Fe
Saline	5832	701	275	679	0.100
Freshwater	141	7.87	12.5	11.4	0.0461
Tailings	Se	Sr	Mo	Ag	Sb
Saline	0.109	4.24	0.0859	0.00009	0.00151
Freshwater	0.0035	0.0604	0.0155	<DL	0.00081
Tailings	Ni	Cu	As	Au	Bi
Saline	0.0750	0.235	0.0323	0.00679	<DL
Freshwater	0.00346	0.0146	0.00137	0.00105	<DL

3.3.2 Settling test

3.3.2.1 ISR of tailings treated by polymer flocculants

Figure 3.4 (a) and (b) show the ISR of freshwater and saline tailings treated by the three different polymer flocculants, respectively. It was found that the high salinity environment increased the ISR of tailings treated by PAM and Al-PAM, and the maximum ISR located around the polymer concentration of 75 ppm for both freshwater (~2 m/hr) and saline tailings (~6 m/hr). For MF treated tailings, the maximum ISR of both freshwater (~5 m/hr) and saline tailings (~9 m/hr) were higher than that of Al-PAM and PAM treated cases, which could be due to the higher molecular weight of MF resulting in better flocculation performance than PAM and Al-PAM. For the settling of saline tailings, the ISR increases monotonically from 0 to 9 m/hr with increasing the MF dosage (0 to 100 ppm), indicating strong flocculation of particles and enhanced flocculation capacity with higher MF dosage. In contrast, the ISR of freshwater tailings shows a maximum value of 5 m/hr located at the dosage of ~15 ppm and then decreases

with further increasing the MF dosage, suggesting an overdose of MF may lead to steric stabilization. The formation of gel-like suspension for fresh tailings was observed for MF dosages above 25 ppm and there was no obvious settling. The above settling results indicate that although the maximum ISR of freshwater tailings is lower than that of saline tailings, the freshwater tailings consume less MF than saline tailings to obtain the same ISR.

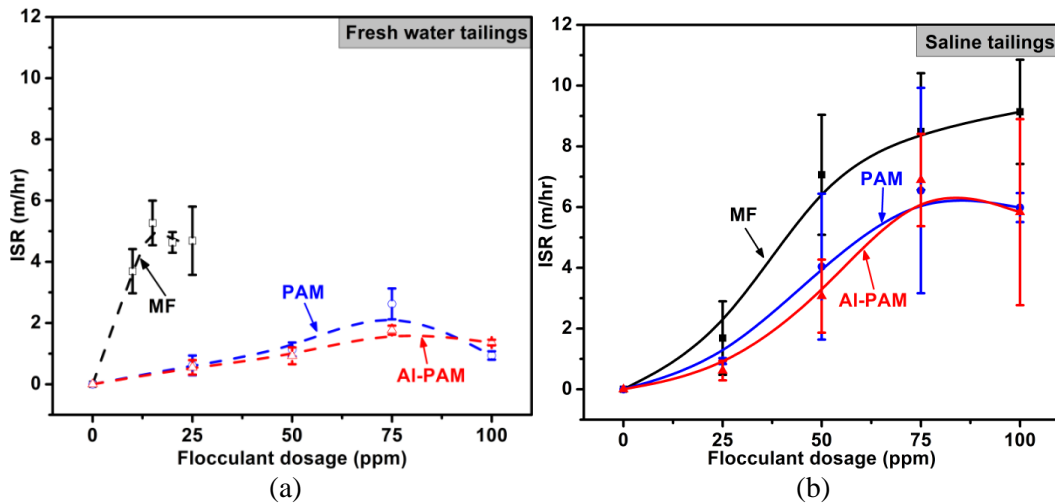


Figure 3.4. The impact of flocculant type and dosage on the initial setting rate (ISR) of tailings: (a) freshwater tailings treated by MF (black, 0- 25 ppm), PAM (blue, 0-100 ppm), and Al-PAM (red, 0-100 ppm), and; (b) saline tailings treated by MF (black, 0-100 ppm), PAM (blue, 0-100 ppm), and Al-PAM (red, 0-100 ppm).

3.3.2.2 Turbidity of supernatant

The turbidity of supernatant indicates the amount of fine particles remaining in the solution after flocculation and settling. A lower turbidity value represents a clearer supernatant and fewer particles remained. Figure 3.5 shows the turbidity of tailings supernatant after 18 hours settling. For saline tailings, the three polymers showed similar impact and trends for the turbidity which dropped from 40 to 10-18 Nephelometric Turbidity Units (NTU) with 50 ppm polymer addition and then leveled off. For freshwater tailings, the effects of three polymers were quite different. The turbidity of

PAM treated freshwater tailings gradually dropped from 55 to 30 NTU, while Al-PAM and MF showed negative impact on the clarity of supernatant when the polymer concentration increased from 0 to 100 ppm. The turbidity of MF treated freshwater tailings increased dramatically from 55 to above 300 NTU with the addition of >10 ppm MF. Therefore, when the same type and amount of polymer flocculant was used, the supernatant of saline tailings showed lower turbidity than the supernatant of freshwater tailings, which was mainly due to the different interactions among the solid particles and polymers under the different solution conditions as discussed below.

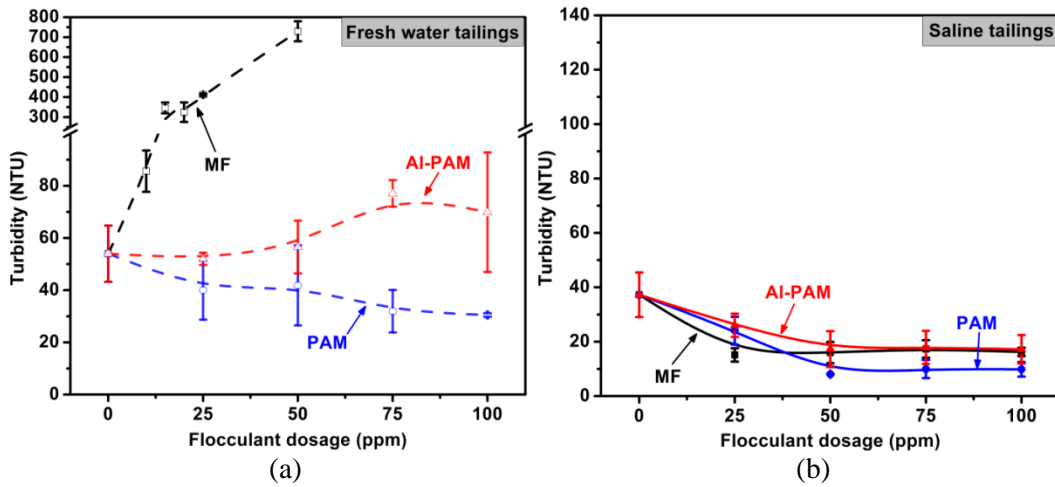


Figure 3.5. The impact of flocculant type and dosage on the supernatant turbidity of tailings: (a) freshwater tailings treated by MF (black, 0- 50 ppm), PAM (blue, 0-100 ppm), and Al-PAM (red, 0-100 ppm); (b) saline tailings treated by PAM (0-100 ppm), Al-PAM (0-100 ppm) and MF (0- 100 ppm).

3.3.2.3 Zeta potential measurements

The zeta potential of the fine particles in the supernatant of tailings treated by PAM, Al-PAM and MF of different dosages after 18 hours of settling was measured to characterize the surface charge properties of fine particles suspended in the supernatant. It should be noted that the zeta potential measurement was made mainly on the fine particles that remained in the supernatant according to Section 3.2.3 . The zeta potential

results are shown in Figure 3.6 (a) and (b) for freshwater tailings and saline tailings, respectively. The zeta potential for untreated freshwater tailings was around -35 mV. The addition of MF led the zeta potential to be slightly more negative which could be attributed to the adsorption of MF molecules with negative charged segments. The addition of PAM and Al-PAM showed negligible impact on the zeta potential values, which was most likely due to the neutral nature of PAM chains (note for Al-PAM, the aluminum hydroxide core is mostly covered by the PAM chains). For saline tailings, the zeta potential of fine particles remained around -15 mV regardless of the polymers and dosage used (see Figure 3.6(b)), which was lower than that for freshwater tailings due to the compressed electrical double layer under the high ionic strength condition in saline tailings.

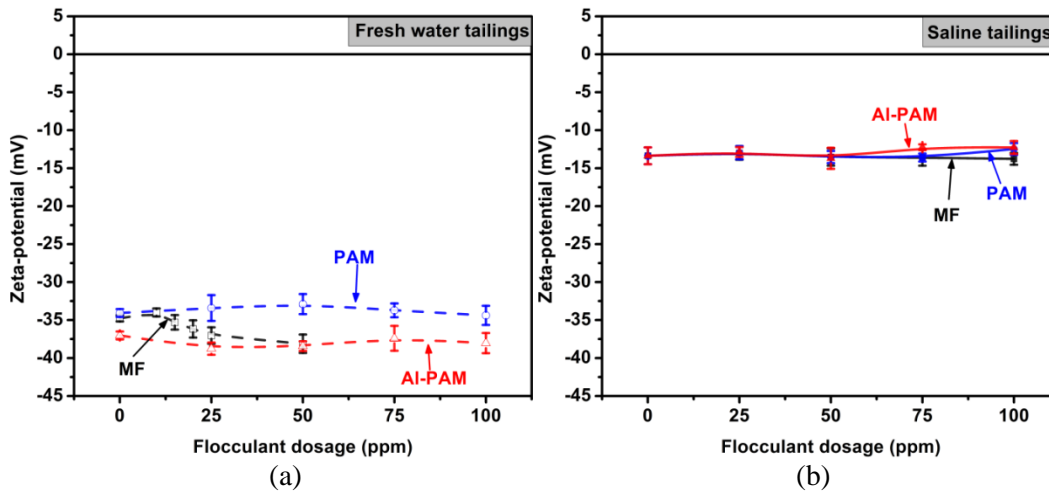


Figure 3.6. The impact of flocculant type and dosage on the supernatant zeta potential of tailings: (a) freshwater tailings treated by MF (black, 0- 50 ppm), PAM (blue, 0-100 ppm), and Al-PAM (red, 0-100 ppm); (b) saline tailings treated by MF (black, 0-100 ppm), PAM (blue, 0-100 ppm), and Al-PAM (red, 0-100 ppm).

3.3.3 Conformation of the flocculants in bulk solution

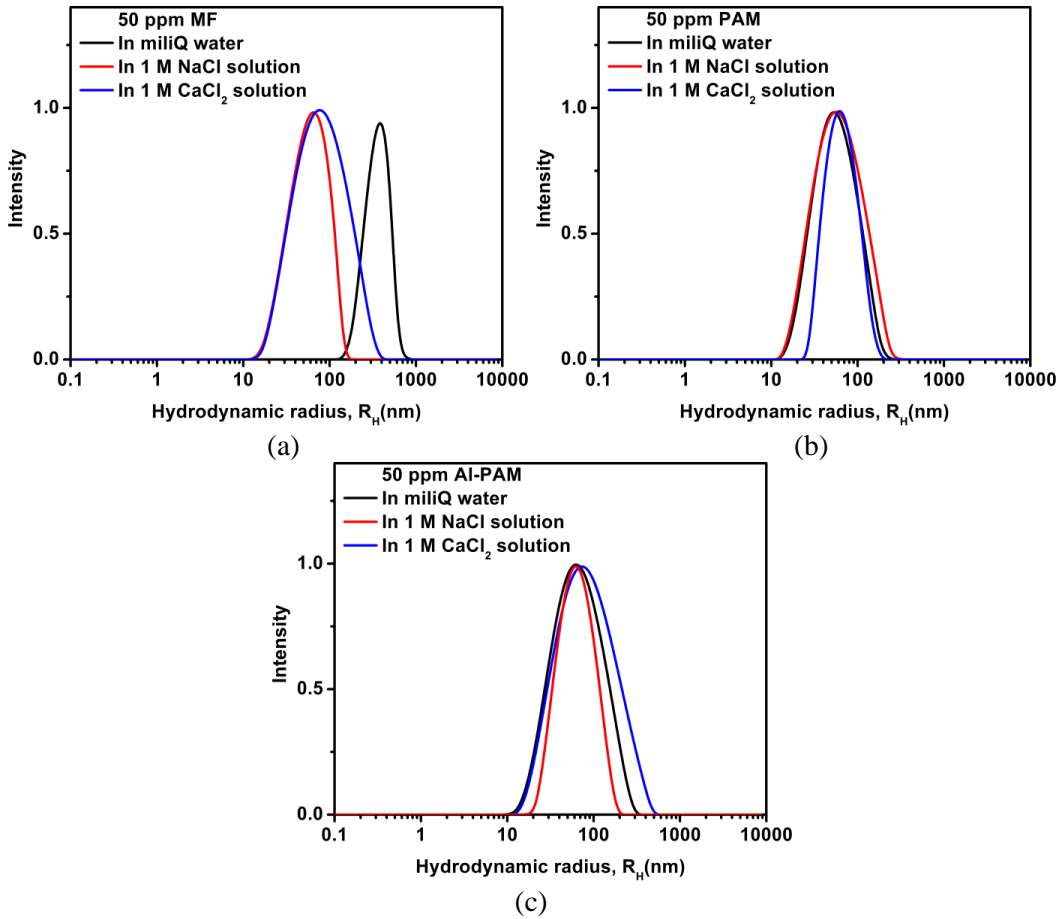


Figure 3.7. The impact of salt type and concentration on the distribution of hydrodynamic radii R_H of the flocculants: (a) 50 ppm MF, (b) PAM, and (c) Al-PAM in mili-Q water (black), 1 M NaCl solution (red), and 1 M CaCl_2 solution (blue).

The hydrodynamic radii R_H of MF, PAM and Al-PAM under various solution conditions are shown in Figure 3.7(a), (b) and (c) respectively. The R_H of 50 ppm MF dropped from 364 nm in mili-Q water to 62 nm in 1 M NaCl solution and 94 nm in 1 M CaCl_2 solution. The decrease of R_H for MF molecules under high salinity condition is mainly due to the compression of the electrical repulsion between negatively charged segments favoring the condensation of the polymer chains [40]. The larger R_H in CaCl_2 solution than that in NaCl solution may result from the interaction between $-\text{COO}^-$

groups in the MF molecules and Ca^{2+} ions [20]. The DLS results suggest that the more condensed MF molecules could form a denser adsorption layer on the particle surfaces in saline water than that in mili-Q water, thus leading to a higher consumption of polymers for saline tailings as observed in the settling tests. For PAM and Al-PAM, such a conformation change due to the salt addition was not observed. Both PAM and Al-PAM showed R_H between 65 and 100 nm regardless of salt addition.

3.3.4 Interaction mechanism between polymers and solid particles under different solution conditions

3.3.4.1 Proposed interaction mechanism

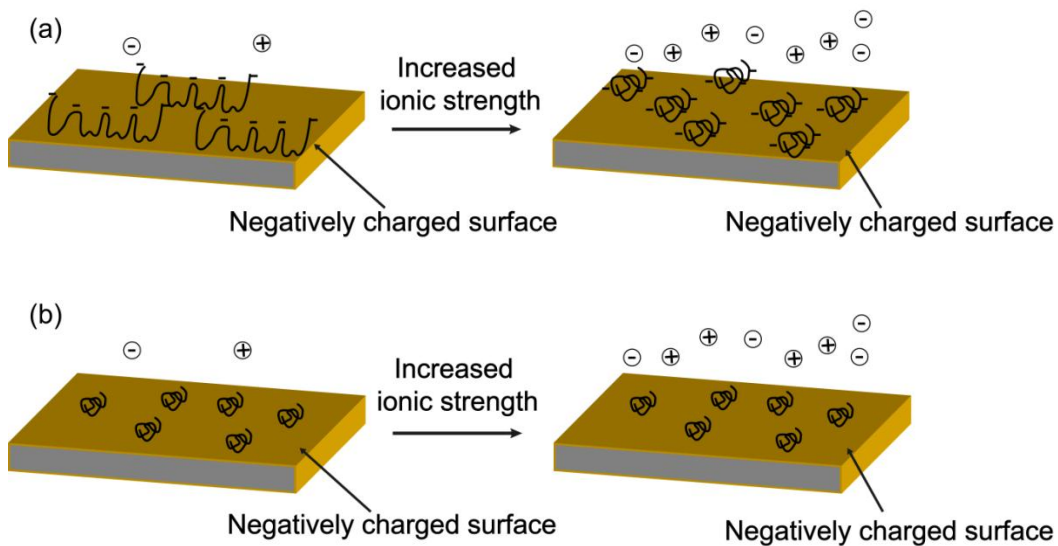


Figure 3.8. Schematic of the impact of ionic strength on the conformation and adsorption of flocculants on negatively-charged particle surfaces: (a) MF, (b) PAM and Al-PAM.

Based on the settling tests, zeta potential and dynamic light scattering measurements, it is evident that the different settling behaviors of saline and freshwater tailings are mainly driven by the differences in the interactions among fine solids and polymers as well as the polymer conformations under various solution conditions. It is

noted that the electrical double layer force, van der Waals forces and the bridging force induced by hydrogen bonding between the primary amide groups on polymers and adsorption sites on particles (i.e. silanols groups) are considered as the major driving forces that affect the flocculation process.

Figure 3.8(a) shows the illustration of the impact of increased salt concentration on the conformation and adsorption of MF on particle surfaces. The particle surfaces were considered negatively charged according to the zeta-potential measurement (Figure 3.6). In freshwater, the formation of relatively short-range hydrogen bonding between the primary amide on MF and Si-O-Si and Si-OH groups on particle surface could be inhibited by the long-range electrostatic repulsion. Therefore the adsorption and bridging of MF on particle surfaces was relatively weaker in freshwater condition. With increasing the salt concentration, the electrical double layer was much compressed, and the hydrogen bonds between the MF molecule and particle surfaces could be more easily formed to enhance the polymer bridging. It is noted that the conformations of adsorbed polymers could also change in different solution conditions. In a solution of high salinity, the suppressed intramolecular electrostatic repulsive force between negatively charged segments in MF allowed a more condensed conformation and adsorption state, and the adsorption density of MF could be significantly enhanced. The enhancement of the adsorption density and bridging of MF molecules led to the fast formation of flocs than that in freshwater with higher ISR and lower turbidity of the supernatant. For PAM and Al-PAM, the ionic strength showed negligible effect on their conformation (Figure 3.8(b)) due to their neutral charge properties.

3.3.4.2 Theoretical simulation of interaction energies

In our simplified analysis, it was assumed that half of the particle surfaces area was covered by polymers at the optimum dosage corresponding to the maximum ISR. Therefore the polymer grafting density s was calculated from the specific surface area and the optimum flocculant dosage at the maximum ISR of each condition. The bonding energy per segment ε of MF and PAM (Al-PAM) in freshwater tailings was calculated using $\varepsilon = Fl$ based on single molecule force measurements [41, 42]. The bonding energy per segment of PAM or Al-PAM ($\varepsilon \approx 10$ kT) corresponds to the energy of one hydrogen bond [39]. The low ε of MF in freshwater could be due to the electrostatic repulsion between MF molecules and particle surfaces of similar charge. In saline tailings, it was assumed that the ε of PAM and Al-PAM does not change due to their neutral charge. The ε of MF in saline tailings was assumed to be higher than the energy of one hydrogen bond due to the bridging enhancement effect of divalent ions. It should be noted that the steric repulsive interaction between polymers on particles was not considered in the total interaction energy calculation. As two particles came close enough to each other (i.e. separation distance ≈ 5 nm), the steric repulsive force would increase dramatically and make the interaction between two particles repulsive. Thus there are separation distances between two particles corresponding to the minimum interaction energy in Figure 3.9(b) and Figure 3.11(b), which are not shown. It is also noted from previous studies that a long range attractive interaction (expanded polymer conformation on particles) might lead to a large floc size [43] and a strong attractive interaction could tightly bind the particles, which further resulted in the increasing of floc density and the settling rate [20, 44].

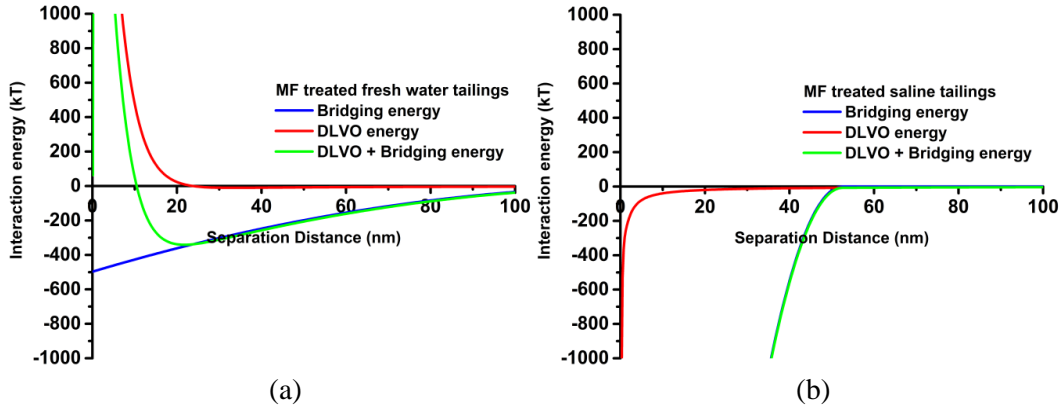


Figure 3.9. Theoretical interaction energy vs. distance profiles between two silica particles in MF treated tailings: (a) freshwater, and (b) saline tailings.

According to the theoretical interaction energy between two silica particles treated by MF (Figure 3.9), the synergic effect of conformation change and the suppression of electrostatic repulsion leads to different settling behaviors of MF treated tailings. In the calculation of bridging energy between MF treated particles, the bonding energy ϵ and effective binding ratio β in saline tailings are higher than that in freshwater tailings due to the reduced electrostatic repulsion between MF molecules and particle surfaces. In freshwater, the long-range electrostatic repulsion competes with the bridging attraction of MF. As the MF molecules show extended conformation in freshwater as confirmed by DLS measurement, the extended loops and tails of absorbed MF and free MF molecules of high molecular weight in the bulk solution could lead to a long-range bridging effect. As shown in Figure 3.9(a), the attractive interaction could initiate when two particles are at $D \approx 135.7$ nm, which is larger than $D \approx 52.5$ nm in MF treated saline tailings. Thus the floc size in freshwater tailings treated by 25 ppm MF (Figure 3.10(a)) is larger than that in saline tailings treated by 25 ppm MF (Figure 3.10(c)). Since Stokes' law predicts the terminal velocity of a settling particle $v_t \propto r^2 \Delta\rho$, where r is the radius of particle and $\Delta\rho$ is the density difference between the particle and suspending fluid (i.e. water), higher ISR could be achieved for freshwater tailings than saline tailings under the same low MF

dosage at 25 ppm (note based on the Stokes equation, although the density of flocs in saline tailings might be higher than in freshwater tailings, the size of the flocs played a more dominant role in determining the v_s). However the overall attractive interaction energy is weaker in freshwater condition due to the relatively low bonding energy ε , low effective binding ratio β and the electrostatic repulsion between the particles. Thus the high turbidity value was observed in MF treated freshwater tailings due to the weakly bound flocs. It should be also noted the particle surfaces could be easily covered by the extended MF molecules in freshwater and the attractive bridging would compete with the steric repulsion between the polymer layers. Therefore as the MF dosage was over 25 ppm the freshwater tailings became overdosed and formed gel-like suspension as shown in Figure 3.10(c). In saline tailings, on the other hand, the strong attractive interaction (Figure 3.9(b)) indicates the binding between particles was stronger than freshwater tailings. Indeed the relatively short range of bridging force (compared to the range in freshwater tailings) resulted from the MF conformation change in saline tailings led to higher consumption of MF to form effective bridging in saline tailings than in freshwater tailings; however when high ratio of MF (i.e. 100 ppm) was provided, flocs of both larger size and higher density (Figure 3.10(d)) than those in freshwater tailings treated by MF (Figure 3.10(a) and Figure 3.10(c)) could be formed. Therefore the maximum ISR in saline tailings treated by MF was higher than that in freshwater tailings treated by MF. Since the particles were more tightly bound, lower turbidity value was recorded in saline tailings than that in freshwater tailings.

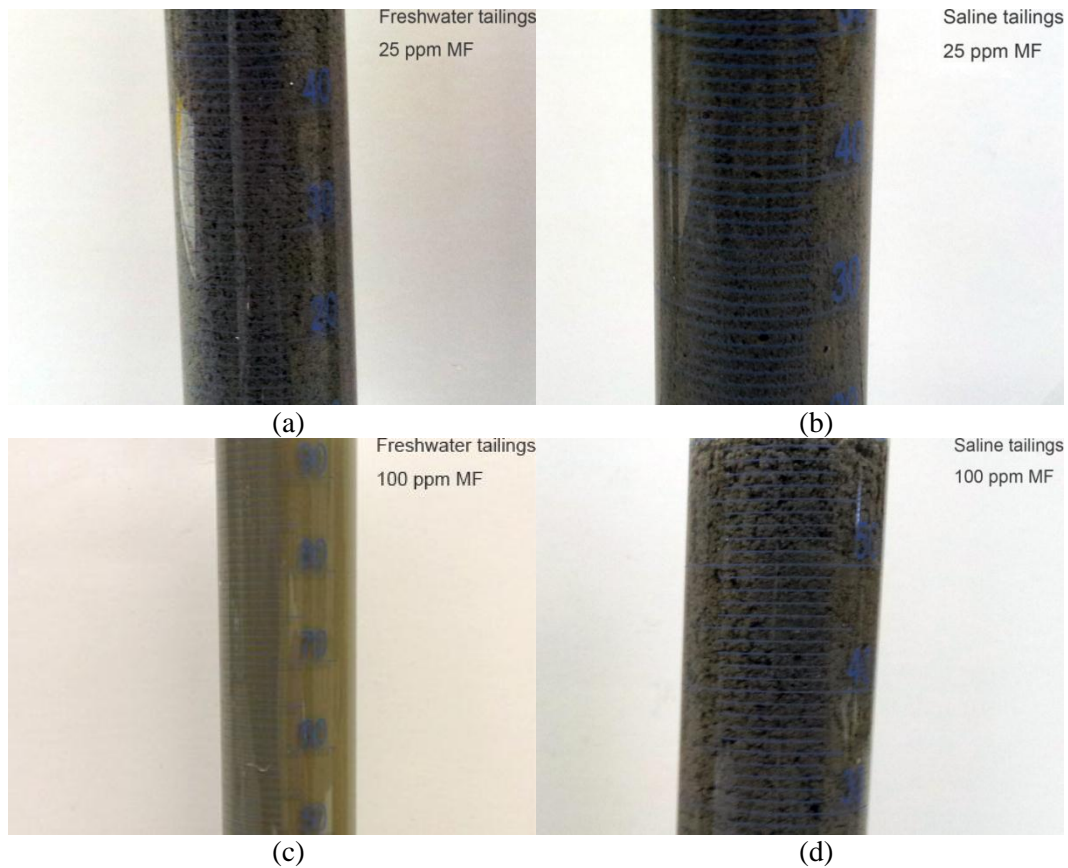


Figure 3.10. Images of the flocs after 4 mins of settling tests for: (a) freshwater tailings treated by 25 ppm MF (b) saline tailings treated by 25 ppm MF (c) gel-like suspension of freshwater tailings treated by 100 ppm MF (d) saline tailings treated by 100 ppm MF

The conformation of PAM and Al-PAM as well as their interactions with the particle surfaces are barely affected by the change of salt content because of their neutral charge properties. Therefore, the range and strength of the bridging energy between two particles treated by PAM and Al-PAM are not affected by the salt content as shown in Figure 3.11. In both freshwater and saline tailings, the attraction interaction between two silica particles treated by PAM and Al-PAM started from about 30 nm. The sizes of the flocs in freshwater (Figure 3.12(b)) and saline tailings (Figure 3.12(d)) treated by 75 ppm PAM were similar (similar results were obtained for Al-PAM treated tailings), which agrees with the above analysis. In freshwater tailings the interaction energy was determined by the competition between polymer bridging and electrical repulsion (among

clay particles). However in saline tailings the interaction is mainly determined by the polymer bridging, and the electrical repulsive interaction is negligible. The interaction difference above most likely led to different floc densities in freshwater and saline tailings treated by PAM and Al-PAM, which accounts for the higher ISR measured in saline tailings than that of fresh water tailings treated by PAM and Al-PAM.

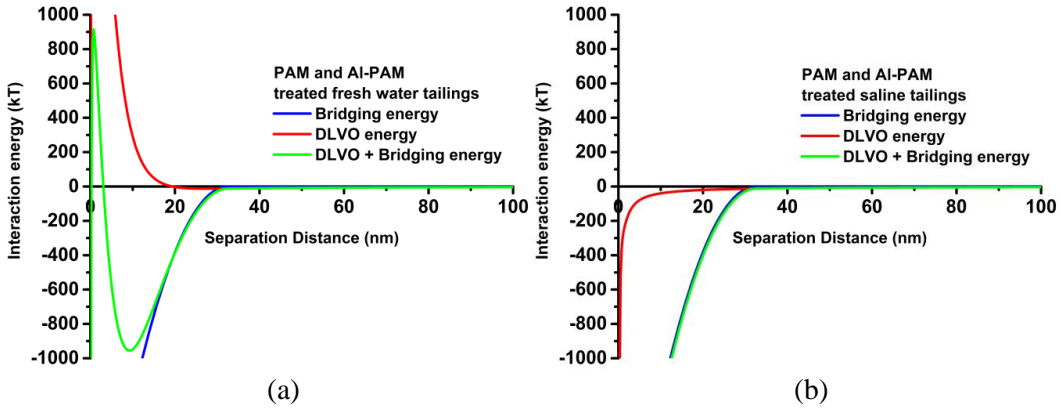


Figure 3.11. Theoretical interaction energy vs distance profiles between two silica particles in PAM and Al-PAM treated tailings: (a) freshwater tailings, and (b) saline tailings.

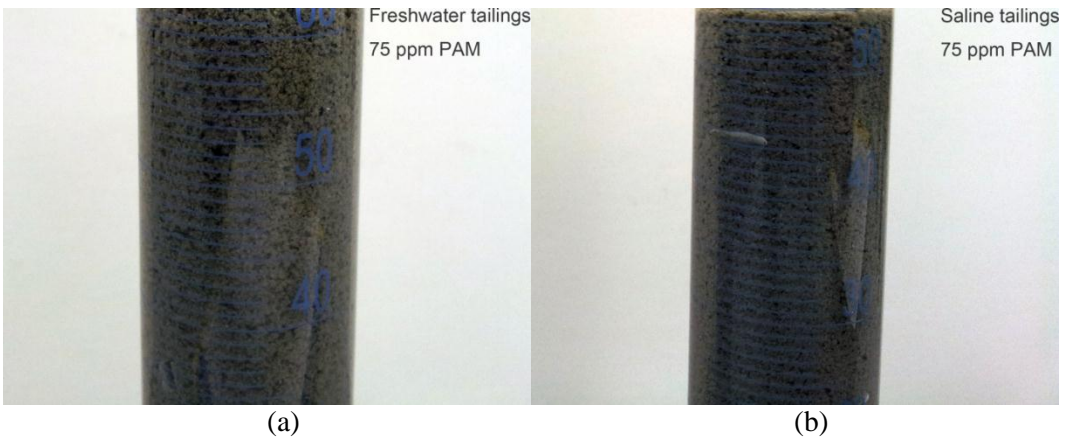


Figure 3.12. Images of the flocs after 4 mins of settling tests for: (a) freshwater tailings treated by 75 ppm PAM, and (b) saline tailings treated by 75 ppm PAM.

3.4 Conclusion

The effects of three polymers, MF, PAM and Al-PAM on the settling of mineral tailings in freshwater and in saline solution were investigated. The settling of tailings significantly depends on solution salinity, flocculant type and dosage. MF was identified as the most effective polymer flocculant for the tailings settlement among the three polymers used. The particle settling was driven by a competition of various polymer-particle and particle-particle interactions in the tailings such as electrostatic repulsion, van der Waals attraction, and polymer bridging. Ionic strength of solutions can significantly impact the electrostatic interaction between particles and the conformation of charged polymer flocculants. The settling rate and turbidity of MF treated tailings largely depend on solution salinity. The increased solution salinity can cause a more compressed molecular conformation of MF and dramatically reduce the electrostatic repulsion among the negatively charged solid particles and polymers, which enhances the settling of mineral tailings. On the other hand, the solution ionic strength has negligible effect on the molecular conformation and adsorption of PAM and Al-PAM, and the settling of tailings is mainly determined by the competition between polymer bridging and electrical repulsion among the negatively charged particles in freshwater and by polymer bridging in saline water. Our results provide some new insights into the understanding of the effects of solution salinity on the settling of mineral tailings and the selection of proper polymer flocculants.

3.5 References

[1] G. Blight, *Geotechnical Engineering for Mine Waste Storage Facilities*, 2010.

- [2] B.A. Wills, T. Napier-Munn, *Wills' Mineral Processing Technology: An Introduction to the Practical Aspects of Ore Treatment and Mineral Recovery*, Elsevier Science & Technology Books, 2006.
- [3] P. Somasundaran, Y.H. Chia, R. Gorelik, Adsorption of polyacrylamides on kaolinite and its flocculation and stabilization, *Acs Symposium Series*, 240 (1984) 393-410.
- [4] C.C. Ho, K.C. Lee, The role of metallic cations on the colloidal stability of tin tailings slurries, *Colloids and Surfaces A-Physicochemical and Engineering Aspects*, 141 (1998) 19-27.
- [5] J.C.J. Boshoff, Prediction of the desiccation and sedimentation behavior of a typical platinum tailings, in: *Tailings and Mine Waste 2002*, 2002, pp. 121-125.
- [6] F.F. Peng, Z. Lu, Polymer flocculation and coagulation for sedimentation of copper flotation tailings, *Minerals & Metallurgical Processing*, 15 (1998) 14-20.
- [7] M.S. Nasser, A.E. James, Effect of polyacrylamide polymers on floc size and rheological behaviour of kaolinite suspensions, *Colloids and Surfaces A-Physicochemical and Engineering Aspects*, 301 (2007) 311-322.
- [8] M.L. Taylor, G.E. Morris, P.G. Self, R.S. Smart, Kinetics of adsorption of high molecular weight anionic polyacrylamide onto kaolinite: The flocculation process, *Journal of Colloid and Interface Science*, 250 (2002) 28-36.
- [9] P. Mpofu, J. Addai-Mensah, J. Ralston, Investigation of the effect of polymer structure type on flocculation, rheology and dewatering behaviour of kaolinite dispersions, *International Journal of Mineral Processing*, 71 (2003) 247-268.
- [10] M.S. Nasser, A.E. James, The effect of polyacrylamide charge density and molecular weight on the flocculation and sedimentation behaviour of kaolinite suspensions, *Separation and Purification Technology*, 52 (2006) 241-252.
- [11] P. Mpofu, J. Addai-Mensah, J. Ralston, Flocculation and dewatering behaviour of smectite dispersions: effect of polymer structure type, *Miner Eng*, 17 (2004) 411-423.
- [12] G. Moody, The use of polyacrylamides in mineral processing, *Miner Eng*, 5 (1992) 479-492.

- [13] L. Nabzar, E. Pefferkorn, R. Varoqui, Polyacrylamide-sodium kaolinite interactions: flocculation behavior of polymer clay suspensions, *Journal of Colloid and Interface Science*, 102 (1984) 380-388.
- [14] L. Nabzar, E. Pefferkorn, An experimental study of kaolinite crystal edge-polyacrylamide interactions in dilute suspensions, *Journal of Colloid and Interface Science*, 108 (1985) 243-248.
- [15] L. Lee, R. Rahbari, J. Lecourtier, G. Chauveteau, Adsorption of polyacrylamides on the different faces of kaolinites, *Journal of Colloid and Interface Science*, 147 (1991) 351-357.
- [16] H. Heller, R. Keren, Anionic polyacrylamide polymer adsorption by pyrophyllite and montmorillonite, *Clays and clay minerals*, 51 (2003) 334-339.
- [17] J. Du, G. Morris, R.A. Pushkarova, R. St. C. Smart, Effect of surface structure of kaolinite on aggregation, settling rate, and bed density, *Langmuir*, 26 (2010) 13227-13235.
- [18] F. Teng, H. Zeng, Q. Liu, Understanding the deposition and surface interactions of gypsum, *The Journal of Physical Chemistry C*, 115 (2011) 17485-17494.
- [19] A. Sworska, J.S. Laskowski, G. Cymerman, Flocculation of the Syncrude fine tailings: Part I. effect of pH, polymer dosage and Mg²⁺ and Ca²⁺ cations, *International Journal of Mineral Processing*, 60 (2000) 143-152.
- [20] J. Long, H. Li, Z. Xu, J.H. Masliyah, Role of colloidal interactions in oil sand tailings treatment, *Aiche J*, 52 (2006) 371-383.
- [21] P. Mpofu, J. Addai-Mensah, J. Ralston, Influence of hydrolyzable metal ions on the interfacial chemistry, particle interactions, and dewatering behavior of kaolinite dispersions, *Journal of Colloid and Interface Science*, 261 (2003) 349-359.
- [22] F. Mietta, C. Chassagne, J.C. Winterwerp, Shear-induced flocculation of a suspension of kaolinite as function of pH and salt concentration, *Journal of Colloid and Interface Science*, 336 (2009) 134-141.
- [23] L.F. Greenlee, D.F. Lawler, B.D. Freeman, B. Marrot, P. Moulin, Reverse osmosis desalination: water sources, technology, and today's challenges, *Water Research*, 43 (2009) 2317-2348.

- [24] S. Castro, J.S. Laskowski, Froth flotation in saline water, *Kona Powder Part J*, (2011) 4-15.
- [25] V.I. Klassen, V.A. Mokrousov, *An Introduction to the Theory of Flotation*, Butterworths, 1963.
- [26] D.W. Fuerstenau, J.M. Rosenbaum, J. Laskowski, Effect of surface functional-groups on the flotation of coal, *Colloids and Surfaces*, 8 (1983) 153-174.
- [27] G.Y. Onoda, D.W. Fuerstenau, Amine flotation of quartz in the presence of inorganic electrolytes, *Proc. 7th Int. Mineral Processing Congress*, (1964) 6.
- [28] J. Alvarez, S. Castro, Flotation of chalcocite and chalcopyrite in seawater and salty water, *Proc. IV Encontro Nacional de Tratamento de Minerios, São José dos Campos, Brazil, Vol. 1* (1976) 6.
- [29] P.A. Moreno, H. Aral, J. Cuevas, A. Monardes, M. Adaro, T. Norgate, W. Bruckard, The use of seawater as process water at Las Luces copper-molybdenum beneficiation plant in Taltal (Chile), *Miner Eng*, 24 (2011) 852-858.
- [30] G.D. Senior, S.A. Thomas, Development and implementation of a new flowsheet for the flotation of a low grade nickel ore, *International Journal of Mineral Processing*, 78 (2005) 49-61.
- [31] J.J. Quinn, W. Kracht, C.O. Gomez, C. Gagnon, J.A. Finch, Comparing the effect of salts and frother (MIBC) on gas dispersion and froth properties, *Miner Eng*, 20 (2007) 1296-1302.
- [32] M. Dash, R. Dwari, S. Biswal, P. Reddy, P. Chattopadhyay, B. Mishra, Studies on the effect of flocculant adsorption on the dewatering of iron ore tailings, *Chemical Engineering Journal*, (2011).
- [33] W.Y. Yang, J.W. Qian, Z.Q. Shen, A novel flocculant of Al(OH)₃-polyacrylamide ionic hybrid, *Journal of Colloid and Interface Science*, 273 (2004) 400-405.
- [34] X.T. Wang, X. Feng, Z. Xu, J.H. Masliyah, Polymer aids for settling and filtration of oil sands tailings, *The Canadian Journal of Chemical Engineering*, 88 (2010) 403-410.
- [35] G.R. Strobl, *The Physics of Polymers : Concepts for Understanding Their Structures and Behavior*, 3rd. rev. and expanded ed., Springer, Berlin ; New York, 2007.

- [36] L. Zhang, Q. Lu, Z. Xu, Q. Liu, H. Zeng, Effect of polycarboxylate ether comb-type polymer on viscosity and interfacial properties of kaolinite clay suspensions, *Journal of Colloid and Interface Science*, 378 (2012) 222-231.
- [37] R. Hogg, T. Healy, D. Fuerstenau, Mutual coagulation of colloidal dispersions, *Trans. Faraday Soc.*, 62 (1966) 1638-1651.
- [38] J. Gregory, Approximate expressions for retarded van der Waals interaction, *Journal of Colloid and Interface Science*, 83 (1981) 138-145.
- [39] J.N. Israelachvili, *Intermolecular and Surface Forces*, 3rd ed., Academic Press, Burlington, MA, 2011.
- [40] N.B. Wyatt, C.M. Gunther, M.W. Liberatore, Increasing viscosity in entangled polyelectrolyte solutions by the addition of salt, *Polymer*, 52 (2011) 2437-2444.
- [41] J. Long, Z. Xu, J.H. Masliyah, Adhesion of single polyelectrolyte molecules on silica, mica, and bitumen surfaces, *Langmuir*, 22 (2006) 1652-1659.
- [42] H. Haschke, M.J. Miles, V. Koutsos, Conformation of a single polyacrylamide molecule adsorbed onto a mica surface studied with atomic force microscopy, *Macromolecules*, 37 (2004) 3799-3803.
- [43] A.J. McFarlane, K.E. Bremmell, J. Addai-Mensah, Optimising the dewatering behaviour of clay tailings through interfacial chemistry, orthokinetic flocculation and controlled shear, *Powder technology*, 160 (2005) 27-34.
- [44] H. Li, J. Long, Z. Xu, J. Masliyah, Synergetic role of polymer flocculant in low-temperature bitumen extraction and tailings treatment, *Energy & fuels*, 19 (2005) 936-943.

Chapter 4 Molecular and Surface Interactions between Polymer Flocculants and Clay Particles: Effect of Salinity

4.1 Introduction

Colloid science is of great importance in daily life, such as medicines, paints and inks, as well as in industrial application, such as food processing and environmental protection [1]. For example, the major components of industrial wastes in mineral processing and oil sands extraction tailings are clays. Sedimentation, filtration and thermal drying are three dewatering methods commonly used in mineral processing as combination. Up to 80% of the water can be separated in the sedimentation stage [2]. Because mineral wastes are usually charged particles with small size (i.e. clay), the Brownian motion and the electrostatic repulsion between those particles can hinder the settling process. Therefore electrolytes or long chain polymers, known as coagulants and flocculants respectively, are used to enhance the sedimentation. The theory developed by Derjaguin and Landau [3] and Verwey and Overbeek [4], known as the DLVO theory, where the stability of the charged fine particle suspension is determined by the competition of electrostatic and van der Waals forces, are often used to interpret the enhanced sedimentation by coagulants (electrolytes). However when flocculants is introduced, the non-DLVO forces such as steric force between flocculant molecules and bridging forces between flocculant and particle surfaces, make the system rather complicated. Previous studies [5-7] suggested that the flocculant enhanced settling is achieved through the bridging between suspended particles by long chain polymers and the formation of flocs of multiple particles by such bridging.

Extensive attention has been given to the flocculation of kaolinite-based mineral tailings treated by polyacrylamide (PAM) and its derivatives or copolymers to achieve better understanding of the flocculation mechanism and to improve the flocculation efficiency. Parameters such as the pH and ionic strength of the tailings, flocculant types, charge and dosage, as well as adsorption and conformation of the flocculants were studied by many researchers [8-12]. Hydrolyzed PAM (H-PAM) that carry negative charge are the most widely used and studied polymer flocculants in PAM family because they tend to be of higher molecular weight than cationic PAM and are less expensive [2].

Because of the charge property of the H-PAM, addition of salt into tailings or clay suspension treated by H-PAM not only affects the interaction between particles as described by DLVO theory but impacts the particle-flocculant interactions. Therefore the effect of salt on the flocculation of H-PAM has been paid considerable attention. Sworska et al. [13] found the settling rate of oil sands tailings treated by 20 ppm H-PAM was enhanced when 8 mM Mg^{2+} or Ca^{2+} were introduced into the system and Long et al. [14] attributed the increasing of settling rate to the enhanced bridging between particles and flocculants by the divalent cations. The flocculation of kaolinite treated by an anionic polyacrylamide–acrylate flocculant was reported enhanced by 0.001 M Ca^{2+} and Mn^{2+} at pH 10.5 and 7.5 respectively [8] and the optimum flocculant dosage and metal ions concentrations was found corresponding with the partial coverage of particle surface by both metal ions and anionic PAM.

Despite the studies on macroscopic settling and flocculation behaviors, the impact of salt on the flocculation enhanced by H-PAM has not been elucidated in microscopic scale. However previous studies on the influence of adsorption and conformation of polymer flocculants on the flocculation behaviors can help interpret the flocculation

mechanism in this study. McFarlane et al. [15] compared the flocculation of anionic PAM, nonionic PAM and PEO treated kaolinite. It was found the settling rates of anionic PAM and PEO treated slurries were higher than that of nonionic PAM treated slurry, which was attributed to the more expanded interfacial conformation of anionic PAM and PEO. Besra et al. [16] investigated the flocculation and dewatering behaviors of kaolinite suspension treated by high molecular weight polyacrylamide flocculants of different ionic nature in the absence and the presence of some surfactants. They found ionic flocculants with high hydrodynamic radii or adsorbed layer thickness was detrimental to flocculation due to the hindrance of particle approaching to each other. They also attributed the increasing settling rate of surfactant pre-treated kaolin to the conformation change of the adsorbed flocculants induced by the pre-adsorbed surfactant. The seemingly controversial results indicate the flocculation is not a process that can be explained by solely the conformation of polymer flocculants but a synergic effect of polymer conformation and polymer-particle interaction. The addition of salts may simultaneously change the factors mentioned above and significantly affect the settling behavior of clay suspensions.

Therefore the impact of salt on the adsorption and conformation of Magnafloc 1011 (a kind of H-PAM) on clay particles as well as the consequential sedimentation behavior were investigated in this study. Settling tests were conducted to evaluate the flocculation efficiency of MF under different salt concentrations. Interaction between two mica surfaces in MF solutions with salt was measured by a SFA [17, 18], which provides new insights into the flocculation mechanism in salt solutions. Quartz crystal microbalance with dissipation monitoring (QCM-D) and dynamic light scattering (DLS) technique were used to investigate the effect of salts on the adsorption and conformation of MF on clay particles. The direct probing of polymer flocculant molecules on model

clay particles provided systematic explanations towards the polymer enhanced clay flocculation in salt solution.

4.2 Experimental

4.2.1 Materials

Pure kaolinite (Acros Organics) was used in this work to prepare model tailings. The particle density and BET surface area are 2.60 kg/dm³ and 11.14 m²/g respectively. The particle size distribution of kaolinite was determined by Mastersizer 2000 (Malvern). The D₁₀, D₅₀ and D₉₀ of the kaolinite particles were measured to be 1.45 μm, 5.75 μm and 22.9 μm respectively. The subscript of the diameter indicates the weight percentage of the particles whose size is below that diameter. For example, D₅₀ = 5.75 μm means the mean diameter of 50 wt% particles are below 5.75 μm. An anionic polymer flocculant MF 1011 (Percol 727) purchased from Ciba Specialty Chemicals Basel, Switzerland, was used in this study. The structure and properties of the polymer are shown in Table 4.1. A stock solution of 1000 ppm was prepared and used within 2 days. NaCl and CaCl₂ (Certified ACS, Fisher Scientific) were used to adjust the salt content in model tailings. All reagents were analytical grade, unless stated otherwise. Mili-Q water (resistivity = 18.2 MΩ·cm) was used for sample preparation and chemical dissolving. Potassium hydroxide and nitric acid (Fisher Scientific) were used to control the pH.

Table 4.1. Properties of MF 1011.

Polymer	Structure	Molecular weight	Charge
Magnafloc 1011	$\left[\text{CH}_2 - \underset{\substack{ \\ \text{C}=\text{O} \\ \\ \text{NH}_2}}{\text{CH}} \right]_m \left[\text{CH}_2 - \underset{\substack{ \\ \text{C}=\text{O} \\ \\ \text{O}^- \text{Na}^+}}{\text{CH}} \right]_n$	1.75 × 10 ⁷	27 % anionic

4.2.2 Settling test

The settling test procedure in this study was modified based on a recent report [19]. The procedure is shown in Figure 4.1. NaCl and CaCl₂ solutions of certain salt content were prepared in 1 L volumetric flasks. 50 g kaolinite and 950 g mili-Q water or salt solution were mixed and conditioned in a 2 L beaker stirring at 350 rpm overnight to make a 5 wt% kaolinite suspension (Figure 4.1(a)). 90 mL of slurry was collected by a pipet (Eppendorf Easypet Motorized Pipet, Fisher, US) from six sampling point (Figure 4.1(b)) and was decanted into a 250 mL standard baffled beaker under high speed agitation using an RW 20 stand agitator (IKA Works Inc., US) and an four-blades impeller (Fisher, US). The mass of the slurry in each beaker was monitored by a balance for polymer dosage calculation. The collected tailings were agitated under 600 rpm for 2 min followed by adding desired amount of 1000 ppm polymer stock solution into the slurry under 300 rpm in 1 min (Figure 4.1(c)). The agitation was stopped immediately after the polymer addition to avoid breaking the flocs. The slurry was then transferred into a 100 mL graduated cylinder (Fisher Class B Mixing Cylinders, Fisher, US). Those cylinders were inverted for 5 times and the mudlines were monitored as a function of settling time (Figure 4.1(d)). The initial settling rate (ISR) was calculated from the initial slope of the instant mudline height vs. settling time as shown in Figure 4.2. The ISR difference brought by the slurry volume change during the addition of polymer stock solution was neglected according to the study of Pearse et al. [20]. The supernatant of each cylinder was extracted 18 hours after the beginning of the test and was used for zeta potential and turbidity measurements using a zeta potential analyzer (Nano ZS, Malvern) and a Micro-100 Turbidity Meter (Fisher, US) respectively.

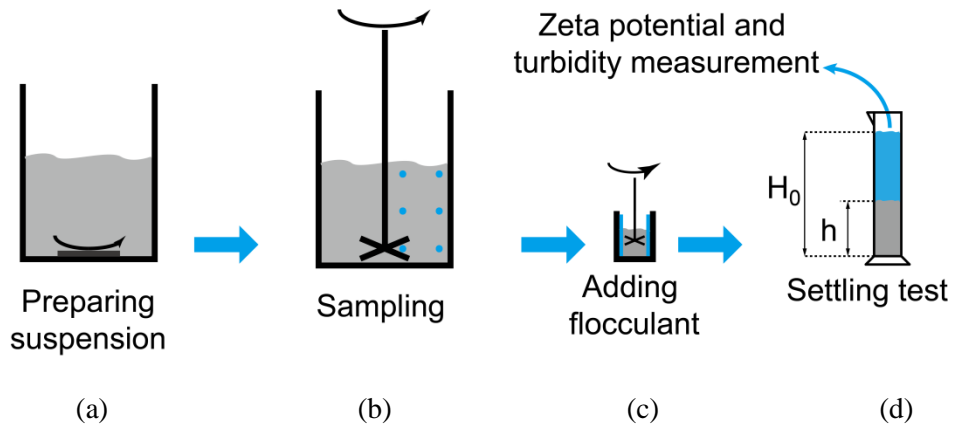


Figure 4.1. Schematic of settling test procedure.

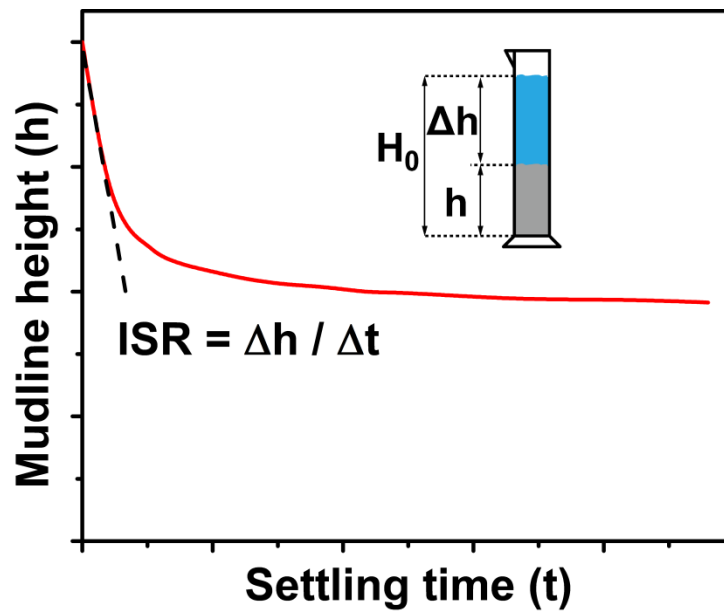


Figure 4.2. Schematic of ISR calculation

4.2.3 Surface force measurement

The interaction force-distance profiles between two model clay (mica) surfaces in the presence of polymer flocculants were measured using a surface forces apparatus (SFA) coupled with Multiple-Beam Interferometry (MBI) technique. A detailed setup for SFA experiments can be found in previous reports [21-24]. Briefly, the back surface of a thin

mica sheet (1-5 μm thick) was coated with an about 50 nm thick semi reflective layer of silver, required to obtain multiple beam interference fringes of equal chromatic order (FECO). The FECO was used to determine the surface separation, surface geometry, deformations and the contact area *in situ* and in real time. The silver coated mica sheet was glued onto a cylindrical silica disk (radius $R = 2$ cm). The prepared silica disks were then mounted into the SFA chamber in a cross-cylinder geometry, which roughly corresponds to a sphere of radius R approaching a flat surface locally. With this arrangement, the measured force $F(D)$ was converted to interaction energy per unit area between two flat surfaces $W(D)$ using the Derjaguin approximation: $F(D) = 2\pi RW(D)$. A schematic of the SFA experimental setup for measuring the interactions between two mica surfaces in MF solutions of different salt concentration is shown in Figure 4.3. In each set of measurements, the reference distance ($D = 0$) was determined at the adhesive contact between the two bare mica surfaces in air prior to introducing the solutions between the surfaces. Normal forces between the two surfaces were measured by moving the lower surface supported on a double-cantilever ‘force springs’ towards the upper surface by a distance $\Delta D_{\text{applied}}$. The actual distance that the surfaces moved to each other, ΔD_{meas} , was measured by multiple beam interferometry in real time. The change in the force ΔF between the surfaces, when they came to rest at a separation distance D , was calculated from the deflection of the cantilever spring by, $\Delta F(D) = k (\Delta D_{\text{applied}} - \Delta D_{\text{meas}})$, where k is the spring constant. When $\partial F(D)/\partial D > k$, there would be a mechanical instability that causes the lower surface to jump either towards or away from the upper surface during approaching or separation process, respectively. Since the silica layers were exposed when mica was cleaved and glued on the silica disks of SFA [25], the experiments were designed to study the interaction between silica surfaces covered by MF. During a typical force measurement, the polymer salt solution filtrated by a Millex-

AA Filter Unit with a pore size of $0.8\ \mu\text{m}$ (EMD Millipore) was incubated between the mica surfaces for 30 mins. The normal force-distance (F vs. D) profiles were then obtained by an initial approach to a “confined polymer thickness” followed by separation of the two surfaces. The confined polymer thickness in this study is defined as the mica-mica separation distance or thickness of confined polymers which barely changed with increasing the normal load or pressure.

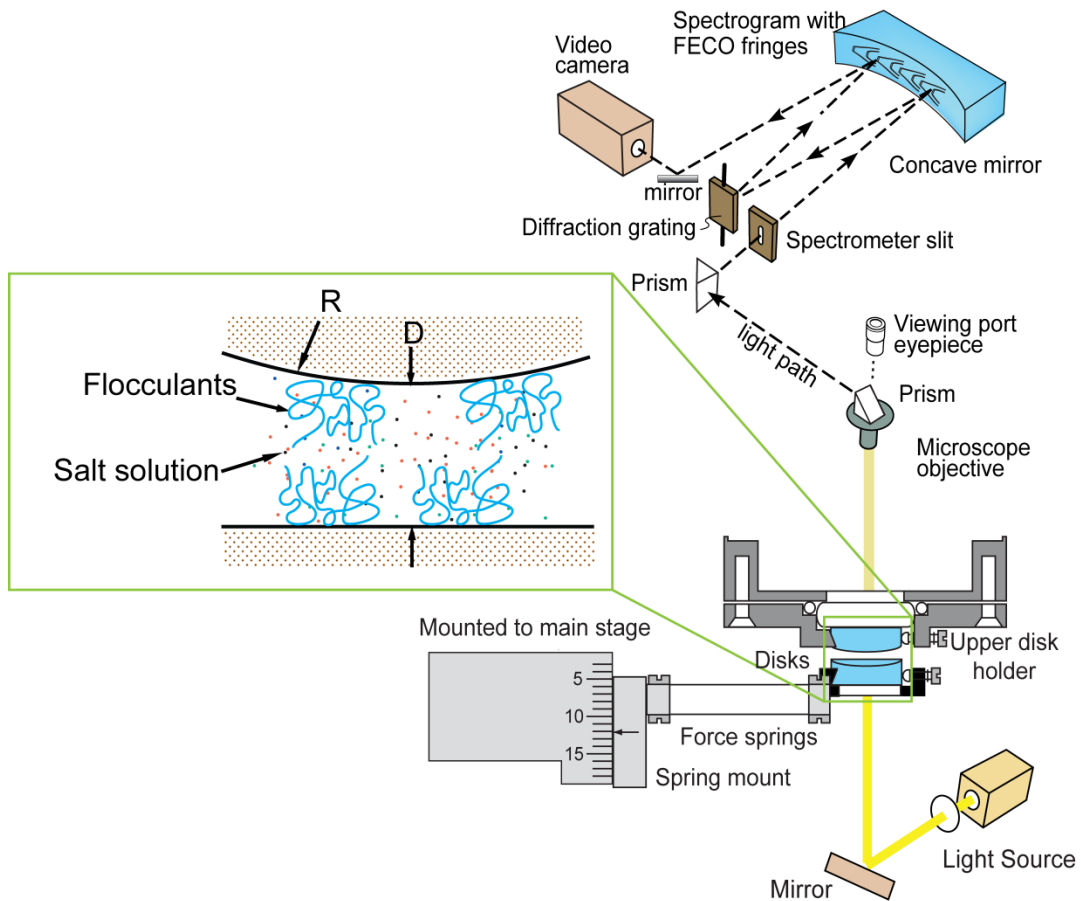


Figure 4.3. Schematic of the SFA experimental setup for measuring the interactions between two mica surfaces in MF solutions of different salt concentration.

4.2.4 Measurement of hydrodynamic radii of polymer flocculants

The molecular conformations of MF in bulk solutions were determined by dynamic light scattering (DLS) technique. An ALV/CGS-3 Platform based Goniometer System was used to measure the hydrodynamic radius (R_H) of MF molecules in solution, which is defined as the radius of a hypothetical hard sphere that diffuses with the same speed as the polymer molecule under the test condition [26]. The solution with 50 ppm MF and NaCl or CaCl₂ of various concentrations was filtrated by a Millex-AA Filter Unit with a pore size of 0.8 μm (EMD Millipore) to remove possible impurities.

4.2.5 Measurement of adsorption of MF on model clay surfaces using quartz crystal microbalance with dissipation monitoring (QCM-D)

QCM-D was used to monitor the adsorption of MF on sensors in solutions of different salt concentrations. Silica and alumina sensors were used in this study to mimic the Si and Al compositions on the clay particle surfaces [27]. The detailed principle of the technique has been described previously [28, 29]. Generally, the instrument can simultaneously monitor the change in resonance frequency (Δf) and energy dissipation (ΔD) of QCM-D sensors in 8 harmonics. The decrease of frequency indicates the accumulating of polymer layer on the sensor surface. The dissipation value represents the rigidity of adsorbed polymer layer. A rigid adsorbed layer gives little change in dissipation while a viscoelastic layer that incorporates solvent molecules leads to a large dissipation. The typical procedures for QCM-D measurement and typical curves of changes in frequency (Δf) and dissipation (ΔD) vs. time are described as following. All the solutions in this study were adjusted to pH \approx 7.5 before the experiment. The resonance frequency of sensor was first recorded in a background solution (identical salt concentration to the polymer solution) to obtain a baseline where Δf and ΔD is defined as

zero. Then the polymer solution was pumped over the QCM-D sensor and the changes in frequency and dissipation during the polymer adsorption was recorded in real time. After the Δf and ΔD reached equilibrium, the sensor was rinsed by pure background solution to remove any unbound polymers. The final Δf and ΔD values and the associated kinetics could help elucidate the adsorption behaviors and conformations of polymers on sensor surfaces under different solution conditions. For the convenience of comparison, only the third harmonic is shown in the results.

4.3 Results and discussion

4.3.1 Effect of NaCl and CaCl₂ on the settling of kaolinite

4.3.1.1 Initial settling rate

The initial settling rate (ISR) of 5 wt% solid kaolinite suspension of various NaCl and CaCl₂ concentration at pH 7.5 are shown in Figure 4.4 and Figure 4.5 respectively. Very low settling rates (from almost 0 to 0.27 m/hr) were observed for sedimentation of kaolinite suspension without MF treatment regardless of salt concentration. In mili-Q water, the ISR increased to a maximum of 33 m/hr at 15 ppm and then declined back to almost 0 at 25 ppm due to the formation of gel suspension. Similar result has been reported by Somasundaran et al. [30]. The maximum ISR was dramatically increased when 0.01 M and 0.1 M salt were added in to the suspension. The maximum ISR of suspension in NaCl increased to about 134 m/hr while that of suspension in CaCl₂ was between 143 m/hr to 154 m/hr. The ISRs obtained in suspensions containing 0.01 M and 0.1 M salts were higher than those in references [8, 13], which is most likely due to the optimized orthokinetic flocculation conducted [15]. Interestingly, the dosage corresponding to the maximum ISR shifted to higher dosage when higher salt

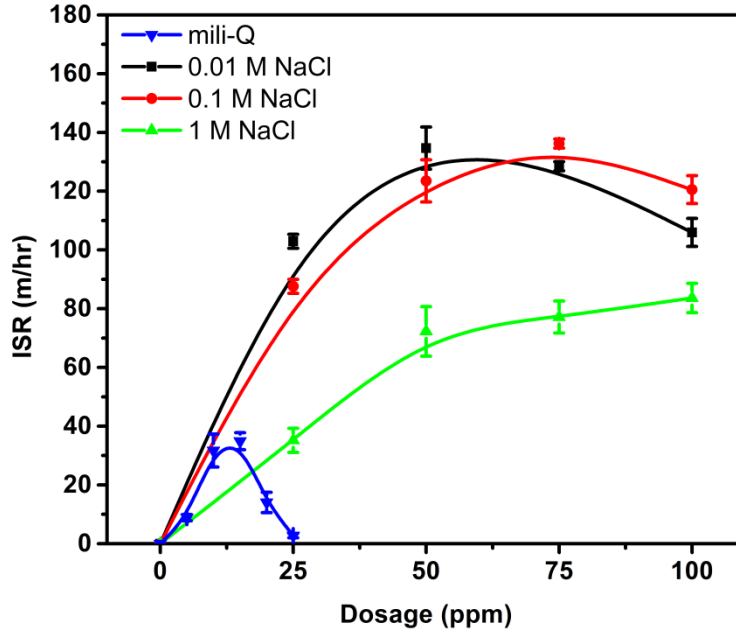


Figure 4.4. The initial settling rate of 5 wt% solid kaolinite suspension versus MF dosage at pH 7.5 in mili-Q (\blacktriangledown) and in the presence of 0.01 M (\blacksquare), 0.1 M (\bullet) and 1 M (\blacktriangle) Na (I) ions.

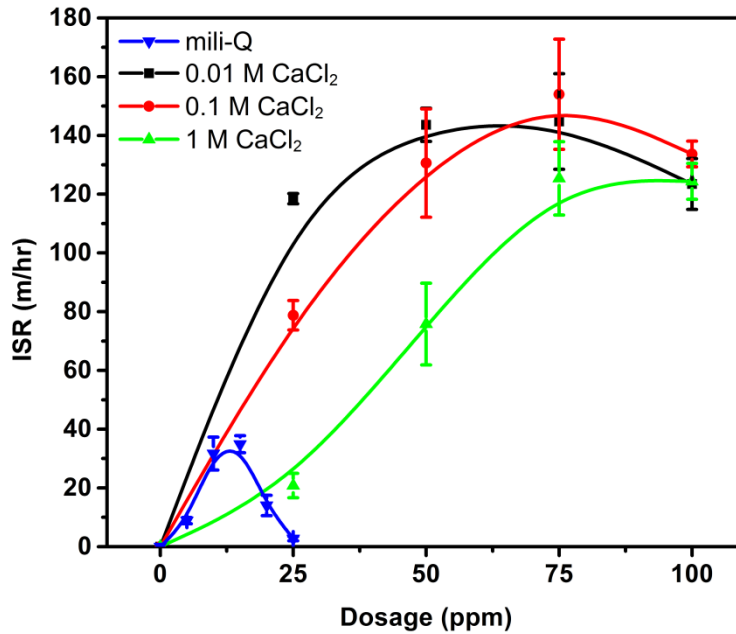


Figure 4.5. The initial settling rate of 5 wt% solid kaolinite suspension versus MF dosage at pH 7.5 in mili-Q (\blacktriangledown) and in the presence of 0.01 M (\blacksquare), 0.1 M (\bullet) and 1 M (\blacktriangle) Ca (II) ions.

concentration was introduced to the system. When 1 M salt was added to the suspension, the ISR was found increasing monotonically with the polymer dosage. Meanwhile the settling rate of the suspension in 1 M salt was reduced comparing to those of the suspensions in 0.01 M and 0.1 M salts. When the effect of different salt type was compared, the maximum settling rate of kaolinite in CaCl_2 suspension was found higher than that of kaolinite in NaCl suspension when the same amount of salt was added.

4.3.1.2 Turbidity of the supernatant

The turbidity values of the supernatants of suspension in NaCl and CaCl_2 after 18 hours above settling tests are shown in Figure 4.6 and Figure 4.7 respectively. The turbidity of kaolinite in mili-Q suspension was above the range of the turbidity meter and therefore not shown in the figures. It was found both NaCl and CaCl_2 could reduce the turbidity in the supernatant while the magnitude of the reduction was different. The turbidity of kaolinite in NaCl suspension gradually decreased with the increasing salt concentration. In the suspension of 0.01 M NaCl the turbidity increased from ~50 to ~190 Nephelometric Turbidity Units (NTU) with the addition of MF. While this trend diminished in the suspension of 0.1 M NaCl, in which the a lower turbidity of untreated suspension (~16.9 NTU) comparing to that in 0.01 M NaCl suspension was found slightly increased to ~33.8 NTU when 100 ppm MF was dosed. When the NaCl concentration was further increased to 1 M, the turbidity decreased from ~15 to ~7.3 NTU when 25 ppm MF was added and then leveled off. For kaolinite in CaCl_2 , on the other hand, the turbidity trends in all three concentrations were similar to that of 1 M NaCl suspension, which show negligible dependence on the CaCl_2 content.

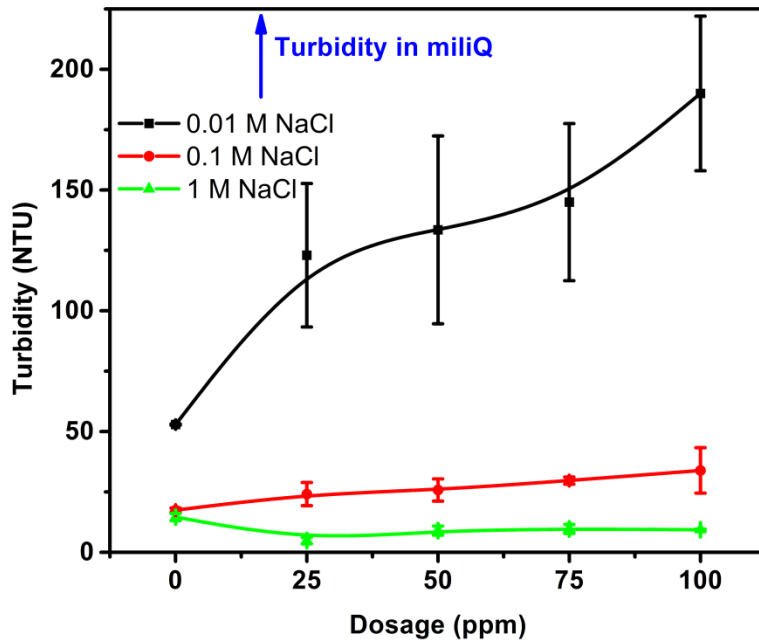


Figure 4.6. The supernatant turbidity values of 5 wt% solid kaolinite suspension after 18 hours settling versus MF dosage at pH 7.5 in mili-Q (not shown) and in the presence of 0.01 M (■), 0.1 M (●) and 1 M (▲) Na (I) ions.

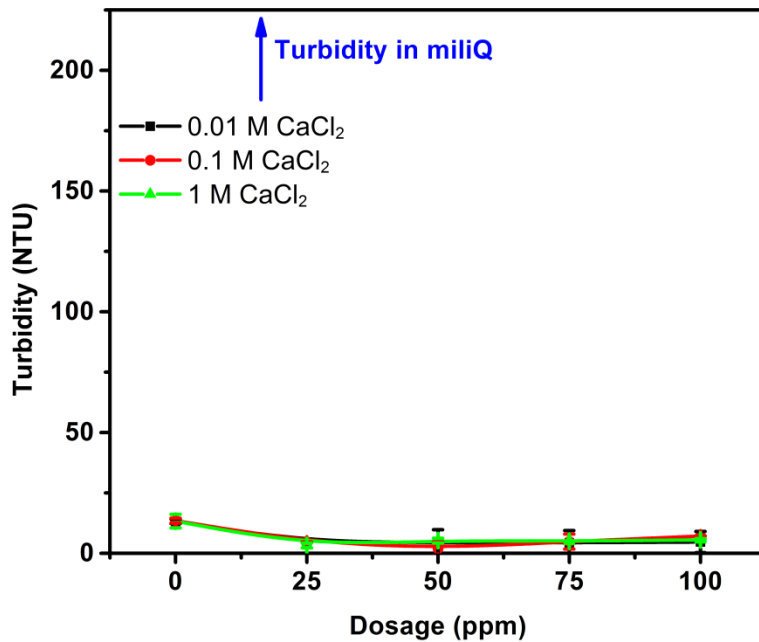


Figure 4.7. The supernatant turbidity values of 5 wt% solid kaolinite suspension after 18 hours settling versus MF dosage at pH 7.5 in mili-Q (not shown) and in the presence of 0.01 M (■), 0.1 M (●) and 1 M (▲) Ca (II) ions.

4.3.1.3 Zeta potential

Figure 4.8 and Figure 4.9 show the zeta potential of the supernatants of suspension in NaCl and CaCl₂ after 18 hours above settling tests respectively. The zeta potential of the supernatant of kaolinite in mili-Q was not measured due to the effects of anomalous surface conductance on the zeta potential under electrolyte concentration below 5 mM [31]. It was found that the magnitude of zeta potential was significantly reduced by adding salt. The zeta potential was decreased from around -40 mV to -13 mV when the concentration of NaCl was increased from 0.01 M to 1 M. By adding 0.01 M and 0.1 M CaCl₂ the zeta potential was reduced to between -13 mV and -5 mV, which was in accordance with the study of Mpofo et al. [8]. Further increasing the CaCl₂ concentration to 1 M can reverse the sign of zeta potential. The treatment of MF was found to have little effect on the zeta potential value.

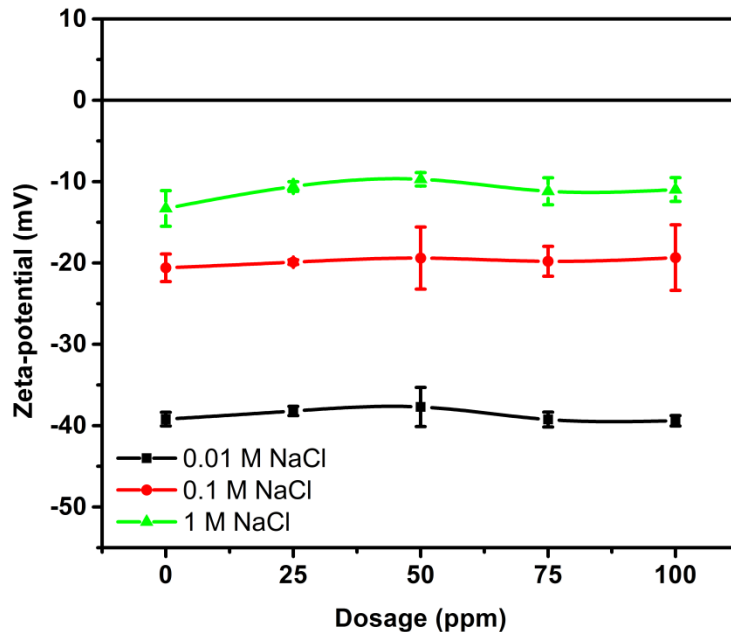


Figure 4.8. The zeta potential values of kaolinite particles in the supernatant of 5 wt% solid kaolinite suspension after 18 hours settling at pH 7.5 in the presence of 0.01 M (■), 0.1 M (●) and 1 M (▲) Na (I) ions.

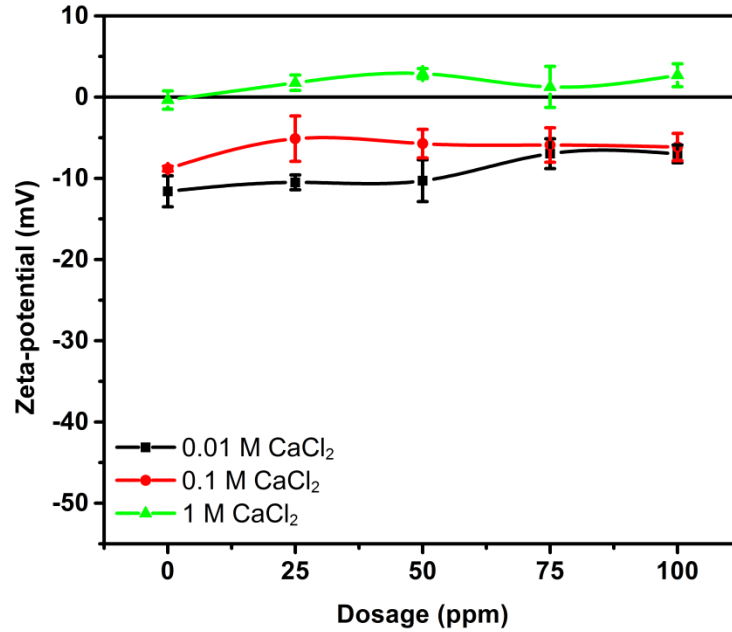


Figure 4.9. The zeta potential values of kaolinite particles in the supernatant of 5 wt% solid kaolinite suspension after 18 hours settling at pH 7.5 in the presence of 0.01 M (■), 0.1 M (●) and 1 M (▲) Ca (II) ions.

4.3.2 Mica-mica interaction in polymer solution with salt

Table 4.2. Key parameters in force measurement.

Solution	Confined polymer thickness (nm)	Distance of obvious force observed (nm)	Adhesive force (mN/m)
No salt	7.8±0.9	60.0±4.9	N/A
0.01 M NaCl	7.7±0.4	30.2±4.8	N/A
0.1 M NaCl	7.3±0.8	20.2±3.8	N/A
1 M NaCl	3.7±0.6	19.4±3.2	-2.8±0.4
0.01 M CaCl ₂	4.5±0.5	17.4±2.5	-0.6±0.1
0.1 M CaCl ₂	3.7±0.9	15.2±3.0	-3.0±0.5
1 M CaCl ₂	3.6±0.8	14.6±2.6	-6.5±0.2

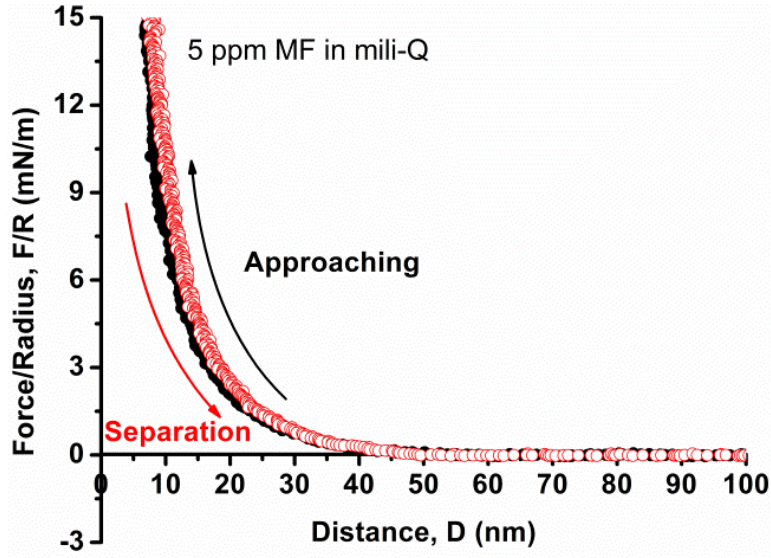
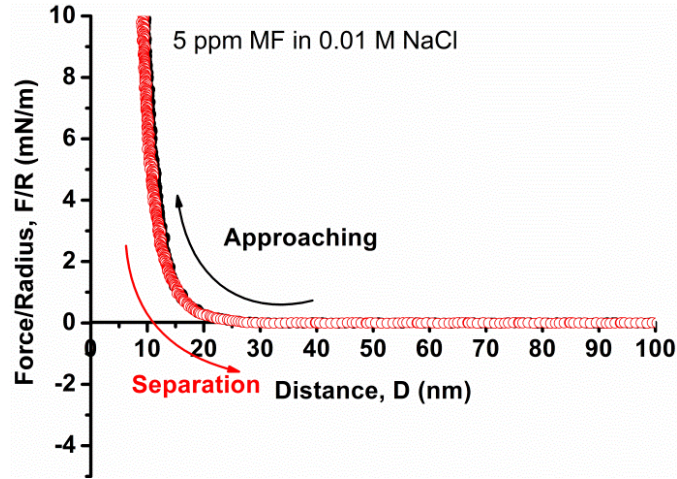
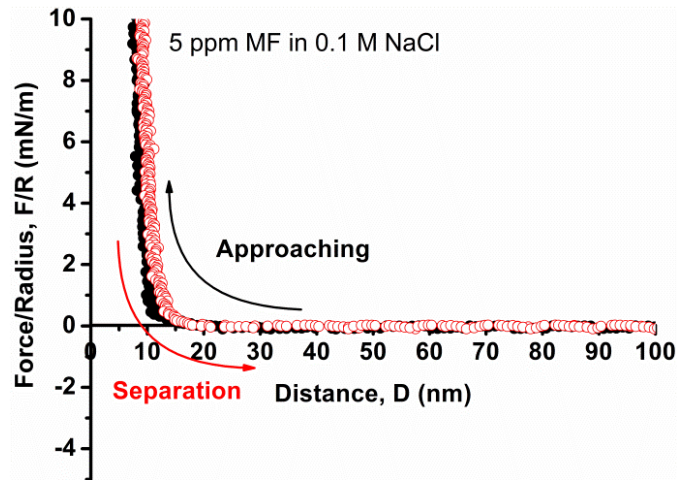


Figure 4.10. Interaction forces between two mica surfaces in 5 ppm MF solution without salt at 30 mins incubation.

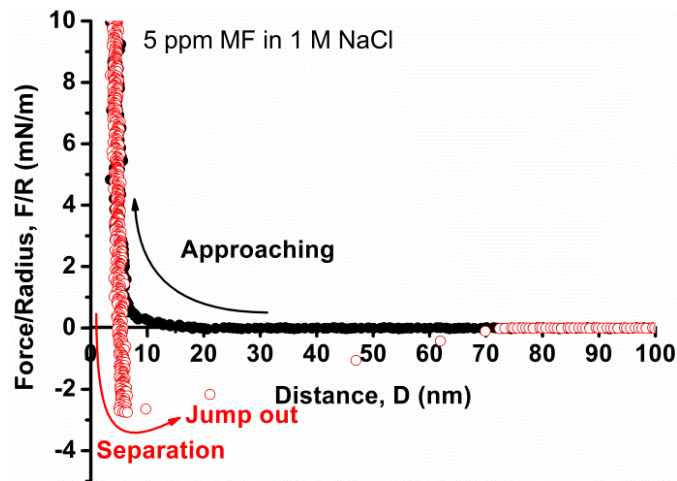
The interaction forces between two mica surfaces in 5 ppm MF solution with various salt concentrations and types at 30 mins incubation are shown in Figure 4.10 to Figure 4.12. The key parameters in these measurements are presented in Table 4.2. Purely repulsive forces were measured between mica surfaces in 5 ppm MF solution without salt during both approaching and separation stages, which may be due to the steric repulsion between the absorbed MF chains on mica (Figure 4.10). Obvious repulsive force in the approaching stage was observed at the distance of 60.0 nm. A confined polymer thickness of 7.8 nm was recorded. Figure 4.11 and Figure 4.12 indicate that the addition of salts has profound influence to the interaction of two surfaces. By increasing the NaCl concentration from 0.01 M to 1 M the repulsion forces during approaching stages were gradually reduced as well as the distance of obvious force observed and the confined polymer thickness (Figure 4.11). An adhesive force of ~ 2.8 mN/m was observed during the separation stages in MF solution with 1 M NaCl (Figure 4.11(c)). In MF with CaCl_2 solutions (Figure 4.12) the repulsion during approaching



(a)

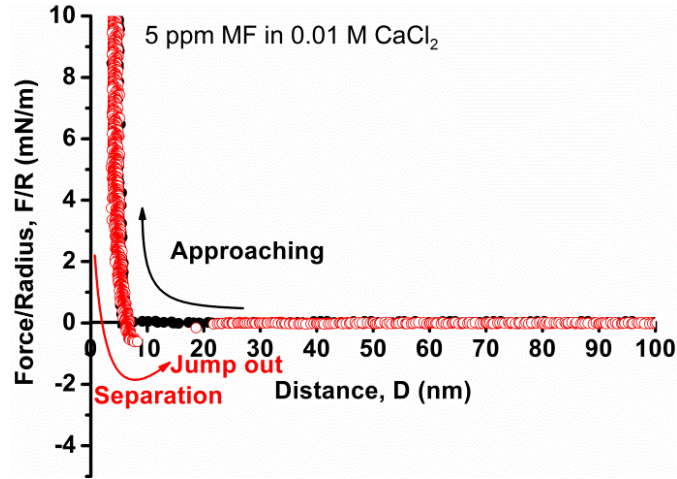


(b)

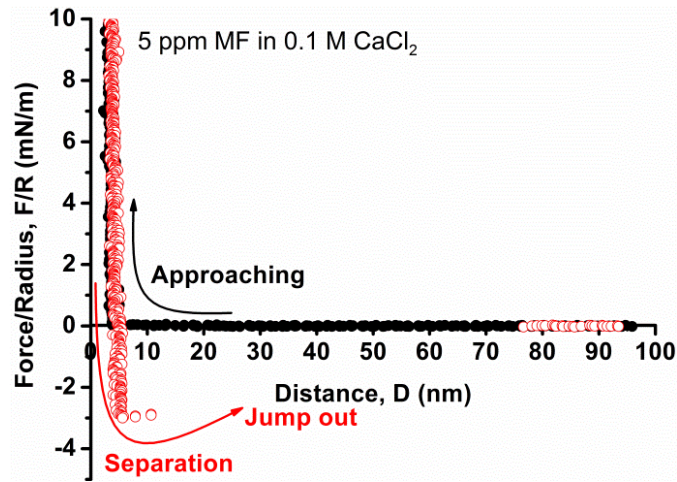


(c)

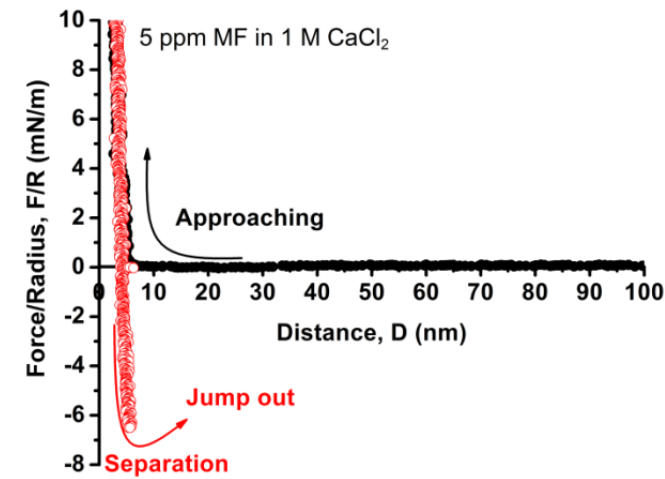
Figure 4.11. Interaction forces between two mica surfaces in 5 ppm MF solution of different NaCl concentrations: (a) 0.01M, (b) 0.1 M and (c) 1 M after 30 mins incubation.



(a)



(b)



(c)

Figure 4.12. Interaction forces between two mica surfaces in 5 ppm MF solution of different CaCl_2 concentrations: (a) 0.01M, (b) 0.1 M, and (c) 1 M after 30 mins incubation.

stages was extensively reduced. The adhesive interactions increasing with CaCl_2 concentration were measured in all MF with CaCl_2 solutions. It is noted that the adhesive force observed correlated very well with the trend of turbidity curve in Figure 4.8 and Figure 4.9: if adhesive force was measured under certain solution condition (salt type and concentration), the turbidity of kaolinite suspension of the same solution condition would decrease with the addition of MF. Otherwise the turbidity increased with the addition of MF.

In order to understand the nature of the interaction between two mica surfaces covered by MF, the force-distance profiles during approaching stage were fitted using the scaling theory originally developed by Alexander and de Gennes and modified by Pincus [32], which describes the steric forces between surfaces grafted with polyelectrolytes in solution of various salt concentrations. It was assumed that all of the counterions are trapped within the polyelectrolyte brush as suggested by most previous theories [32-35]. For polyelectrolytes that are end-grafted to the solid surfaces, the mean-field scaling theories distinguish two regimes depending on the concentration of the counterions confined in the brush and the ionic strength in the solution, namely osmotic brush regime and ‘salt brush’ regime. The concentrations of the counterions in brush can be calculated from the neutrality condition of the brush, i.e. $c_0 = \alpha N / (L_0 s^2)$, where α is the ratio of the total number of free mobile counterions to the total number of monomer segments N , L_0 is the thickness of unperturbed polyelectrolyte layer and s is the grafting density of the brush. When the concentration of counterions inside the brush (c_0) is greater than external salt concentration in bulk solution (c_s), the stretching of the polyelectrolytes is induced by the osmotic pressure of the counterions confined in the brush ($F_{osm1} \approx \alpha N k T / L_0$ where k is the Boltzmann constant and T is the temperature). This regime is named osmotic brush regime. When the external salt concentration is higher than the concentration of the

confined counterions inside the brush, this regime is named ‘salt brush’ regime. In this regime the electrostatic interaction between chain segments is screened. The brush is still stretched by the exclude-volume repulsion where chain may still be swollen within a Debye length. The stretching force can be modeled as $F_{osm2} \approx kTN^2\alpha^2 / (c_s L_0^2 s^2)$. The thickness of the brush layer L_0 is determined by the balance of stretching force and elastic force of the brush ($F_{ela} \approx 3L_0 kT / (Na^2)$ where a is the length of a monomer unit) and can be expressed by $L_{0(osm)} \approx \alpha^{1/2} Na$ and $L_{0(salt)} \approx \alpha^{2/3} Na^{2/3} \sigma^{-1/3} c_s^{-1/3}$ for osmotic brush and salt brush regimes respectively. Equation (4.1) and equation (4.2) modified from Balastre et al. [17] are used to model the approaching force-distance profiles obtained in this study:

$$\frac{F(D)_{osm}}{R} = \frac{2\pi\alpha NkTA_1}{s^2} \left\{ \left[\left(\frac{D}{2L_0} \right)^2 - 1 \right] - B_1 \ln \left(\frac{D}{2L_0} \right) \right\} \quad (c_0 > c_s) \quad (4.1)$$

$$\frac{F(D)_{salt}}{R} = \frac{2\pi kT \alpha^{4/3} N A_2}{a^{2/3} c_s^{2/3} s^{10/3}} \left\{ \left[\left(\frac{D}{2L_0} \right)^2 - 1 \right] - B_2 \left[\frac{2L_0}{D} - 1 \right] \right\} \quad (c_0 < c_s) \quad (4.2)$$

where R is the radius of the curved surfaces in SFA, D is the separation between two mica surfaces, A_1 and A_2 are the prefactors to normalize the unknown term of s , and B_1 and B_2 are the prefactors that describe the relationship between elastic force and osmotic force.

Since the Na-acrylate groups on MF (pKa = 4.5) is fully dissociated at pH = 7.5, α can be considered equal to the charge density of MF, which equals to 0.27. The length of the monomer unit is considered as twice of the C-C bond, i.e. $a = 0.308$ nm. Since MF is a long chain polyelectrolyte, the definitions of L_0 and s are different from traditional brush polymers. As shown in Figure 4.13, L_0 is the length of the most extended loop or

tail of the MF adsorbing on the mica surface (measured by the SFA) and s is the distance between two anchors, which is normalized by A_1 and A_2 .

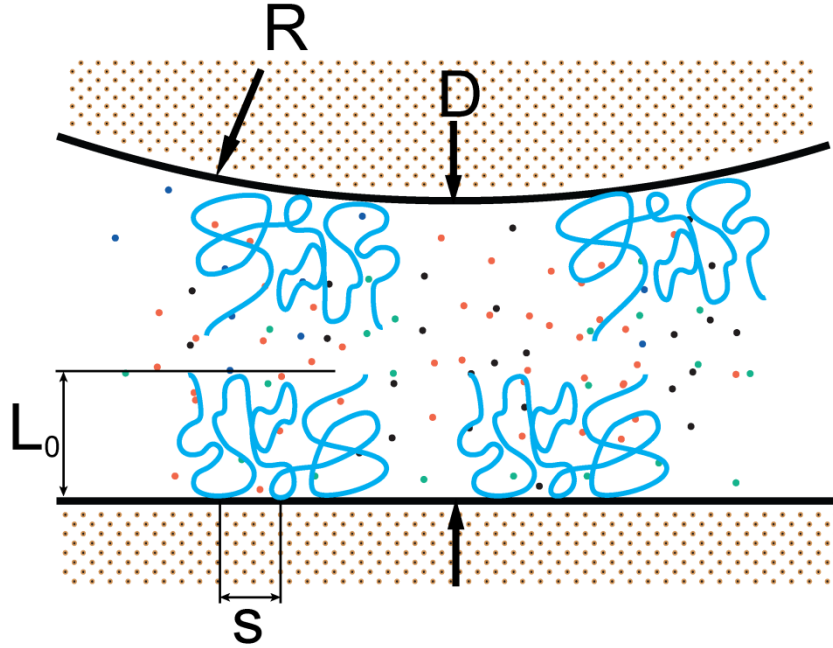


Figure 4.13. Schematic of the parameters used in fitting.

Table 4.3. Fitting parameters for measured force-distance profiles shown in Figure 4.14.

Parameters	No salt	0.01 M NaCl	0.1 M NaCl	1 M NaCl
L_0 (nm)	30.0	15.1	10.9	9.7
A_1/s^2 (nm ⁻²)	6.2×10^{-4}	N/A	N/A	N/A
B_1	2.20	N/A	N/A	N/A
$A_2/s^{(10/3)}$ (nm ^{-10/3})	N/A	3.9×10^{-5}	5.6×10^{-5}	5.7×10^{-5}
B_2	N/A	2.00	2.25	2.55

The parameters used in the fitting are shown in Table 4.3. Data of MF in mili-Q water was found well fitted by equation (4.1) while data of MF solution with NaCl from 0.01 M to 1 M was found well fitted by equation (4.2). As shown in Figure 4.14, none of the measured force curves exhibited exponential tail of the double layer force, which indicates the steric interactions occurred before the overlapping of counterions clouds of

the two MF layers. Therefore the assumption that all the counterions are trapped inside the MF brush is correct. The thickness of the MF layer decreased with the increasing of salt content indicating the collapse of the conformation of MF on mica surface. The increasing of $A_2/s^{(10/3)}$ indicates that as NaCl became concentrated the MF on mica surface formed more small loops in solution. In all the fittings B_1 or B_2 is between 2.00 and 2.55, which indicates the osmotic repulsion overwhelmed the elastic force in both regimes. The deviation of the fitting at the distance where the MF layer was highly compressed could be resulted from the interactions between MF molecules under the outmost MF layer. Similar results have been reported in the study of the interaction between two polystyrene layers [36]. It was found the force distance profiles obtained in MF solutions with CaCl_2 could not be fitted by aforementioned model. The most likely reason is that Ca^{2+} formed complexation between acrylate groups and deprotonated silanol groups, which led to the further collapse of MF layer and additional attractive forces other than the elastic force and osmotic repulsive force.

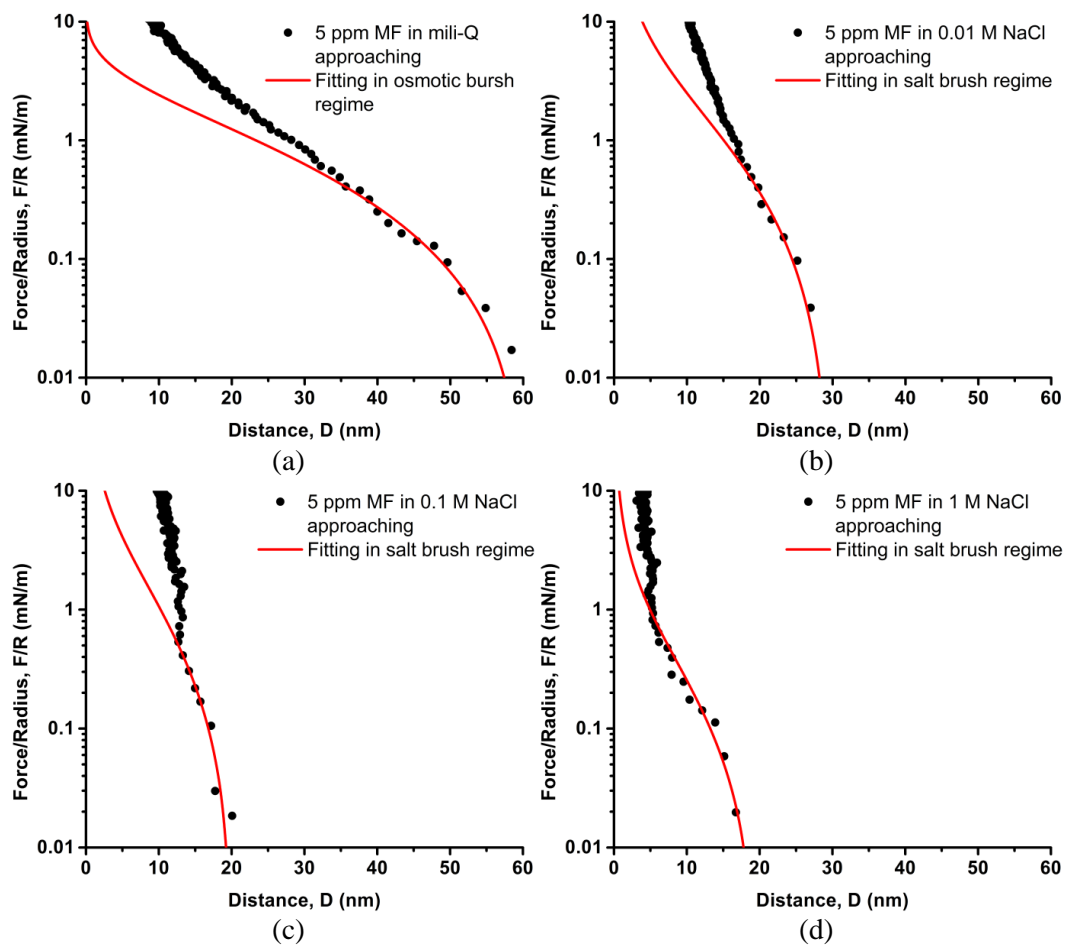


Figure 4.14. Measured force-distance profiles between two mica surfaces in MF solutions during approaching stage (black dots) and theoretical fitting (red curves) : (a) no salt added fitted by equation (4.1); (b)(c)(d) 0.01 M to 1 M NaCl fitted by equation (4.2).

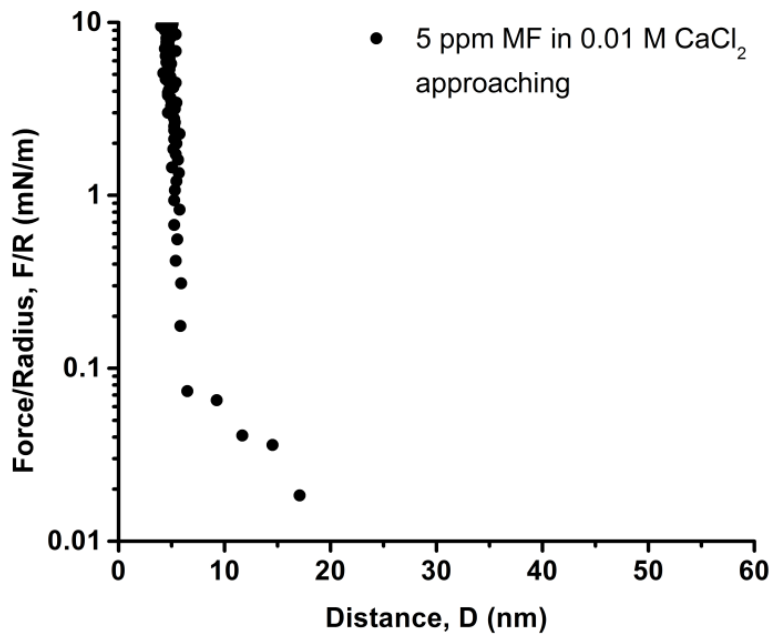


Figure 4.15. Measured force-distance profile between two mica surfaces in MF solutions containing 0.01 M CaCl_2 during approaching stage.

4.3.3 Conformation of MF molecules in solution of different salt concentrations

Table 4.4. Hydrodynamic radii of MF in solution of different salt concentration.

Salt concentration	Hydrodynamic radii (R_H , nm)	
	NaCl	CaCl_2
No salt	364.0	
0.01 M	69.9	83.7
0.1 M	81.3	102.8
1 M	91.9	109.4

The hydrodynamic radii (R_H) of MF molecules in salt solution are shown in Table 4.4. It was found by adding 0.01 M salts the R_H was reduced from 364 nm to less than 84 nm. The larger R_H in 0.01 M CaCl_2 solution than that in 0.01 M NaCl solution could be due to the interaction between the $-\text{COO}^-$ groups in the MF molecules and Ca^{2+} ions [14], which led to the aggregation of MF molecules. Further increasing the salt concentration led to a growth of R_H . It is speculated that the inter-molecular hydrogen bonding was

revealed by the compression of electrostatic repulsion force, which also led to the aggregation of MF and the increasing of R_H measured.

4.3.4 Adsorption of MF molecules on model clay surfaces

The frequency and dissipation change of silica sensors induced by MF adsorption are shown in Figure 4.16 to Figure 4.22. The adsorption on silica sensor in MF mili-Q solution was negligible due to the electrostatic repulsion between the negatively charged segments and the silica surface. The effect of adding 0.01 M and 0.1 M of NaCl was insignificant. However when 1 M of NaCl was introduced into the system a frequency drop of 22.32 Hz was observed after the removal of unbonded MF. In MF in CaCl_2 solutions, the adsorption was immediately observed ($\Delta f \approx -5.58$ Hz) when 0.01 M CaCl_2 was added. Further increase the CaCl_2 content led to a higher adsorption amount on the silica sensor than in lower CaCl_2 content. Again, the adsorption of MF on silica surfaces was correlated well with the turbidity change in kaolinite suspensions and the force measurements of mica surfaces between two mica surfaces in MF solutions in a similar way discussed in Section 4.3.2. When considering the effect of salt type, CaCl_2 was found to have a more significant effect on the adsorption than NaCl when the same amount of salt was added, which could be due to CaCl_2 can more efficiently compress the double layer and also form metal complex within MF molecules as well as between MF molecules and surface functional groups.

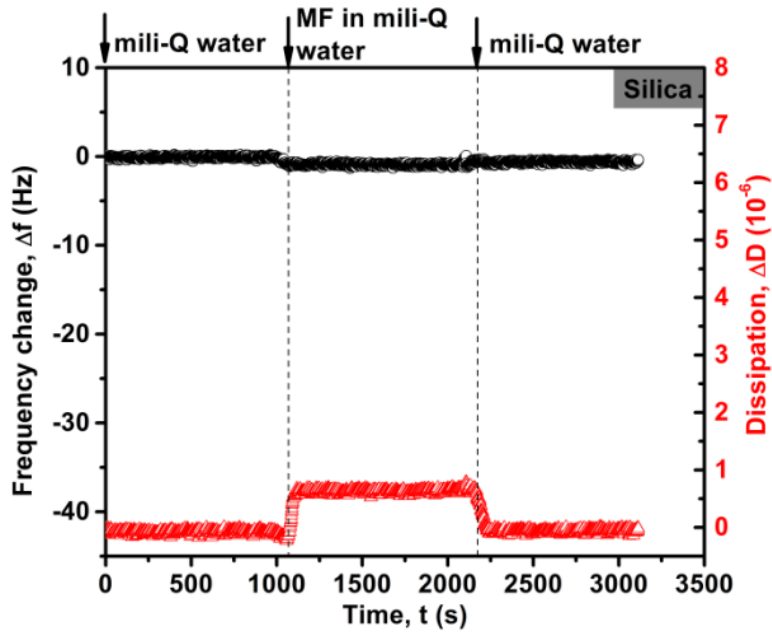


Figure 4.16. Change of frequency and energy dissipation associated with the adsorption of MF on QCM-D silica sensors in mili-Q water

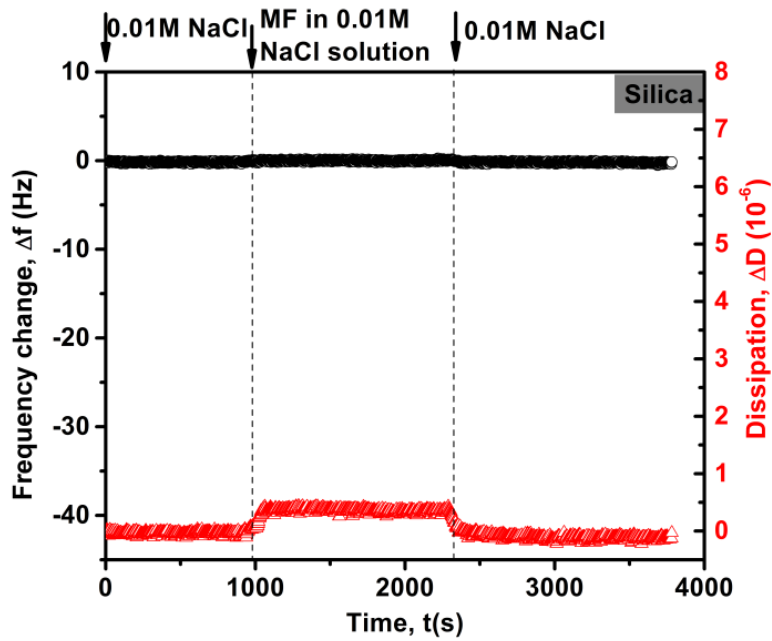


Figure 4.17. Change of frequency and energy dissipation associated with the adsorption of MF on QCM-D silica sensors in 0.01 M NaCl solution

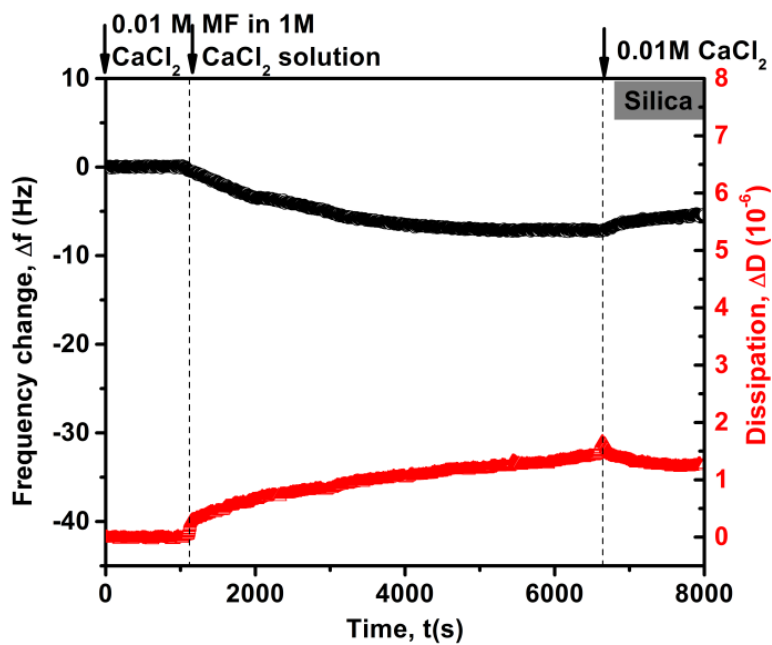


Figure 4.18. Change of frequency and energy dissipation associated with the adsorption of MF on QCM-D silica sensors in 0.01 M CaCl_2 solution

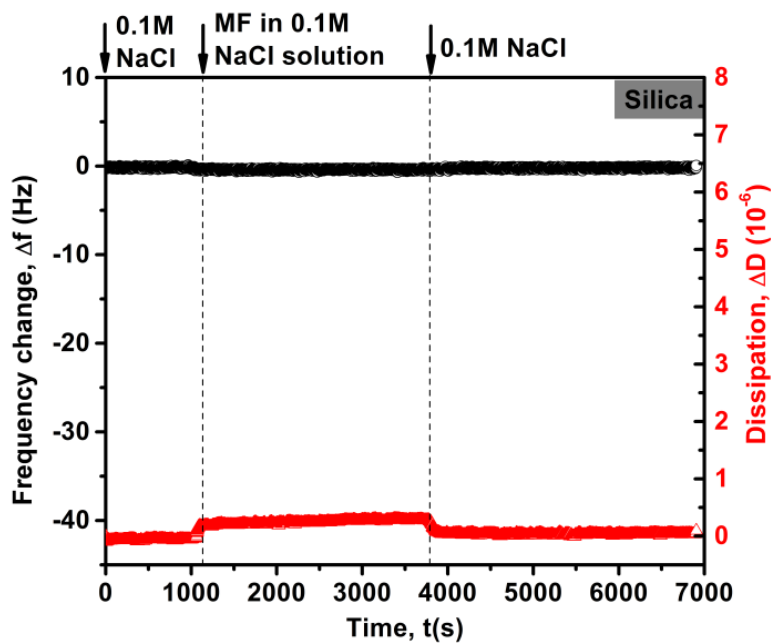


Figure 4.19. Change of frequency and energy dissipation associated with the adsorption of MF on QCM-D silica sensors in 0.1 M NaCl solution

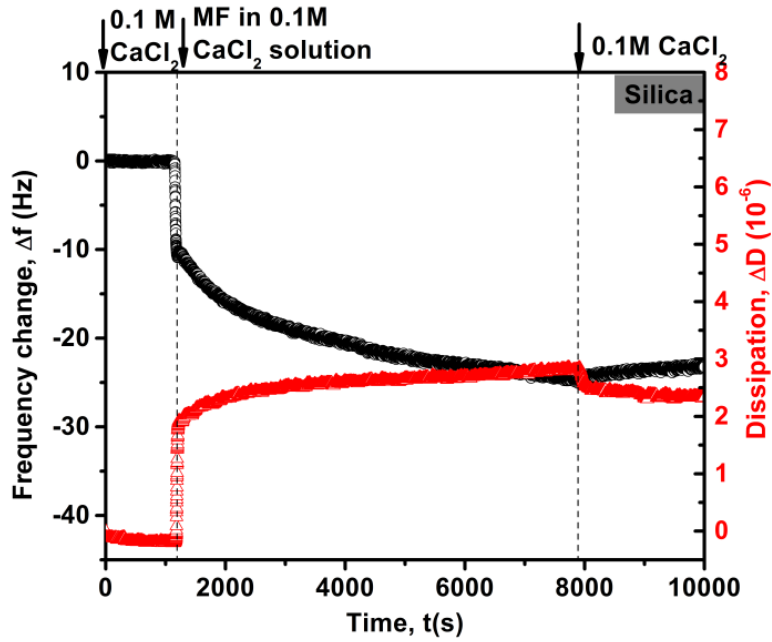


Figure 4.20. Change of frequency and energy dissipation associated with the adsorption of MF on QCM-D silica sensors in 0.1 M CaCl_2 solution

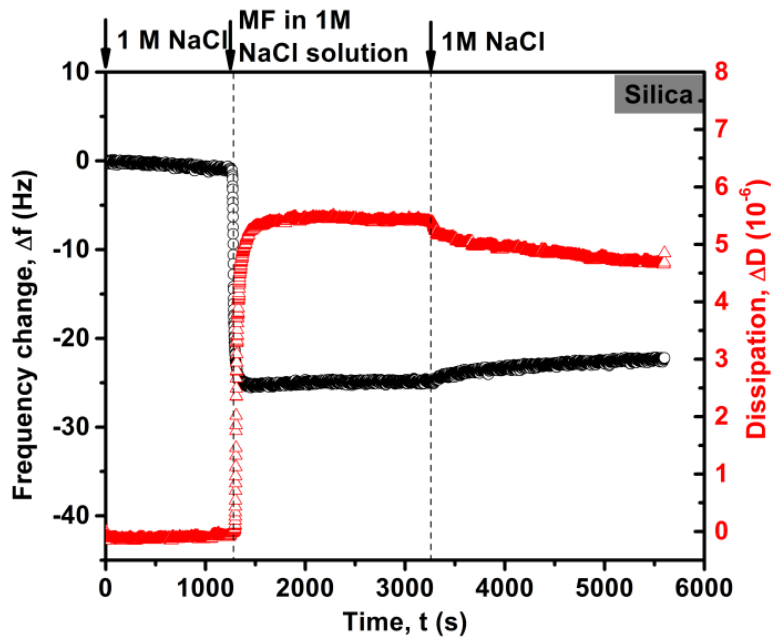


Figure 4.21. Change of frequency and energy dissipation associated with the adsorption of MF on QCM-D silica sensors in 1 M NaCl solution

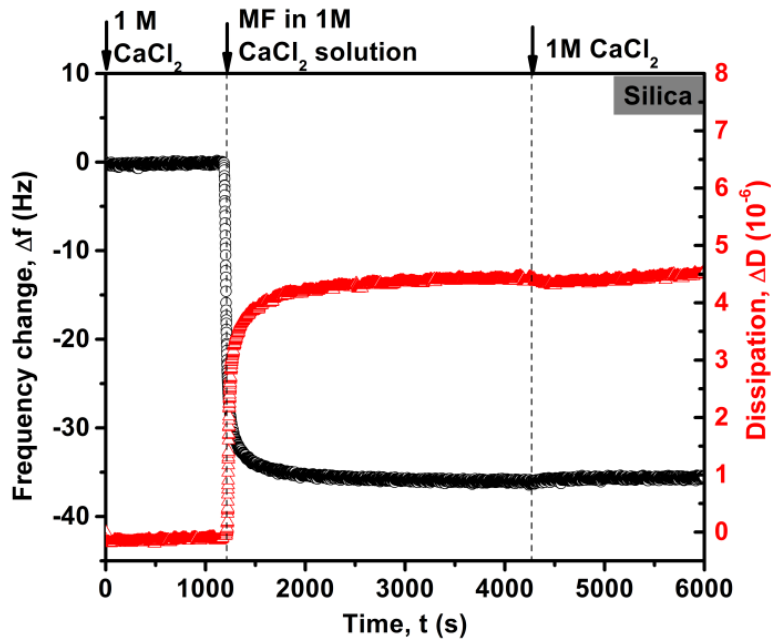


Figure 4.22. Change of frequency and energy dissipation associated with the adsorption of MF on QCM-D silica sensors in 1 M CaCl_2 solution

The frequency and dissipation change of alumina sensors induced by MF adsorption are shown in Figure 4.23 to Figure 4.29. The frequency changes of alumina sensors in milli-Q water and 0.01 M salt (NaCl or CaCl_2) solutions were higher than that of silica sensors under the same condition, which indicates a higher mass uptake of negatively charged MF on positively charged alumina sensors than negatively charged silica sensors. In MF with 0.1 M NaCl solution, such a difference was still observed. However in solutions of MF with 0.1 M CaCl_2 or 1 M salts (both NaCl and CaCl_2), the difference between silica and alumina sensors diminished. It could be due to the double layer force between MF and the surfaces was screened in concentrated salt solution, the adsorption was less determined by the charge properties of the surfaces.

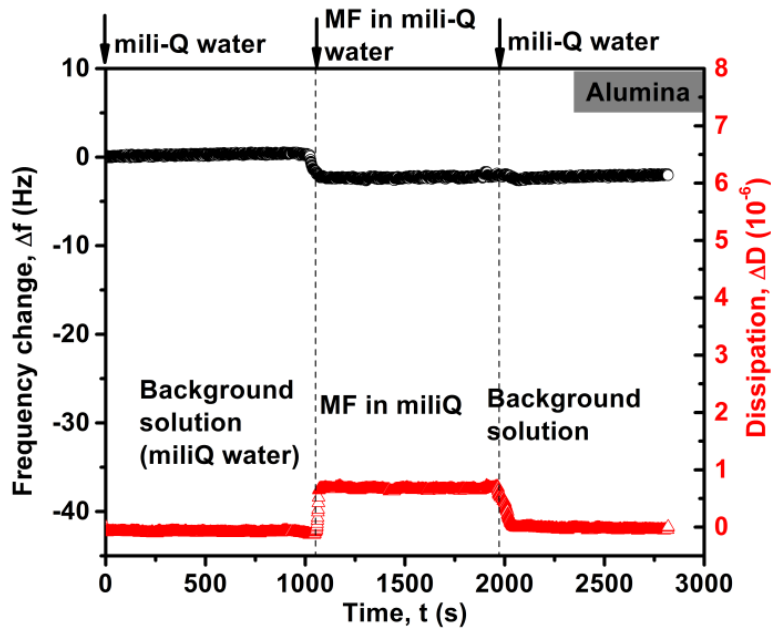


Figure 4.23. Change of frequency and energy dissipation associated with the adsorption of MF on QCM-D alumina sensors in milli-Q water

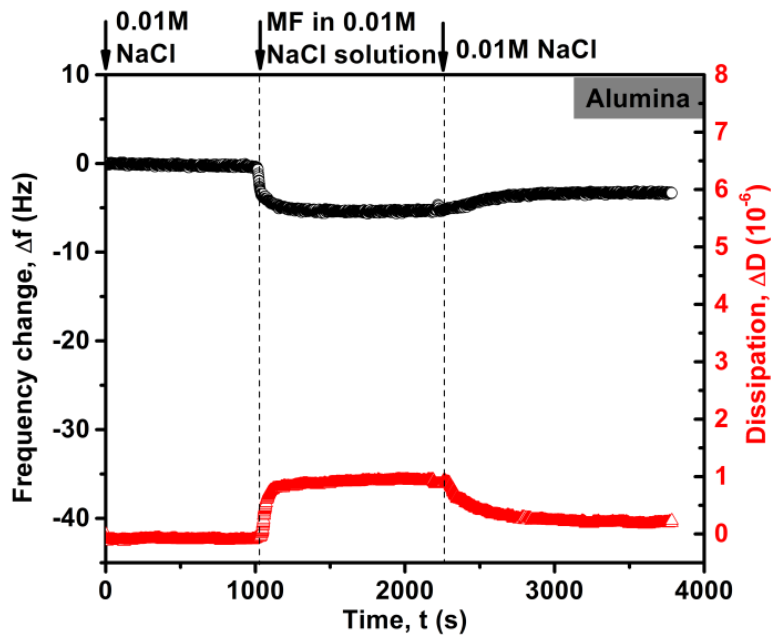


Figure 4.24. Change of frequency and energy dissipation associated with the adsorption of MF on QCM-D alumina sensors in 0.01 M NaCl solution

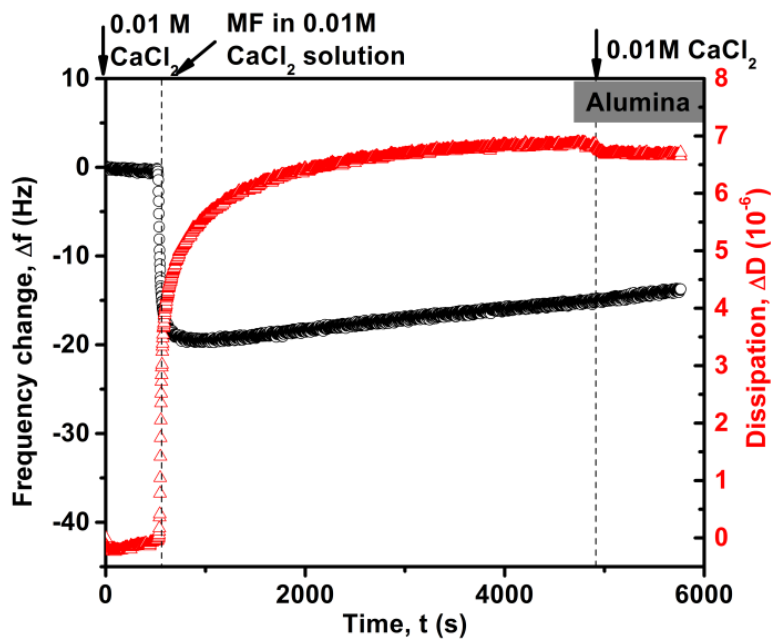


Figure 4.25. Change of frequency and energy dissipation associated with the adsorption of MF on QCM-D alumina sensors in 0.01 M CaCl₂ solution

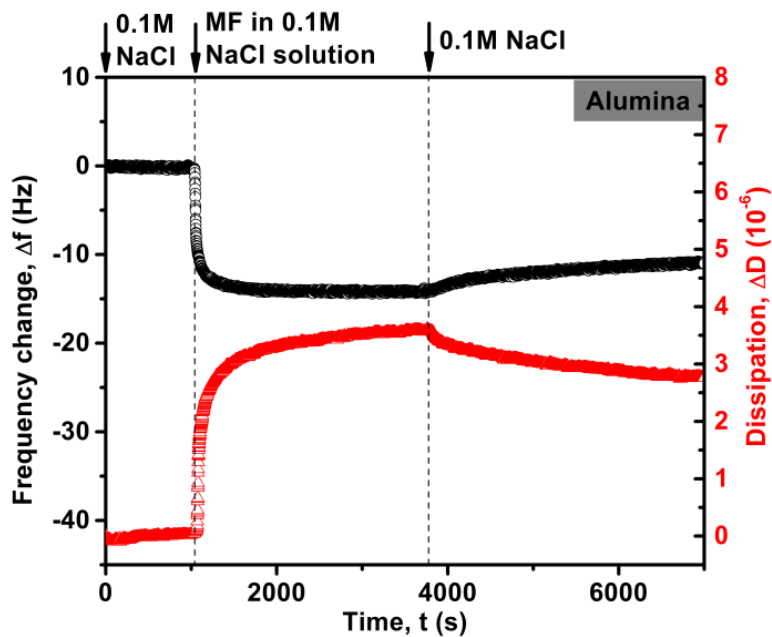


Figure 4.26. Change of frequency and energy dissipation associated with the adsorption of MF on QCM-D alumina sensors in 0.1 M NaCl solution

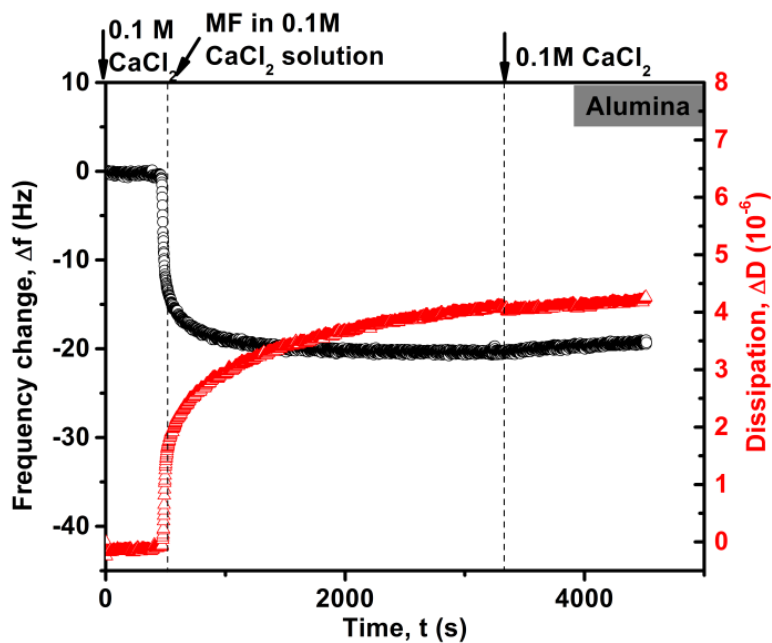


Figure 4.27. Change of frequency and energy dissipation associated with the adsorption of MF on QCM-D alumina sensors in 0.1 M CaCl_2 solution

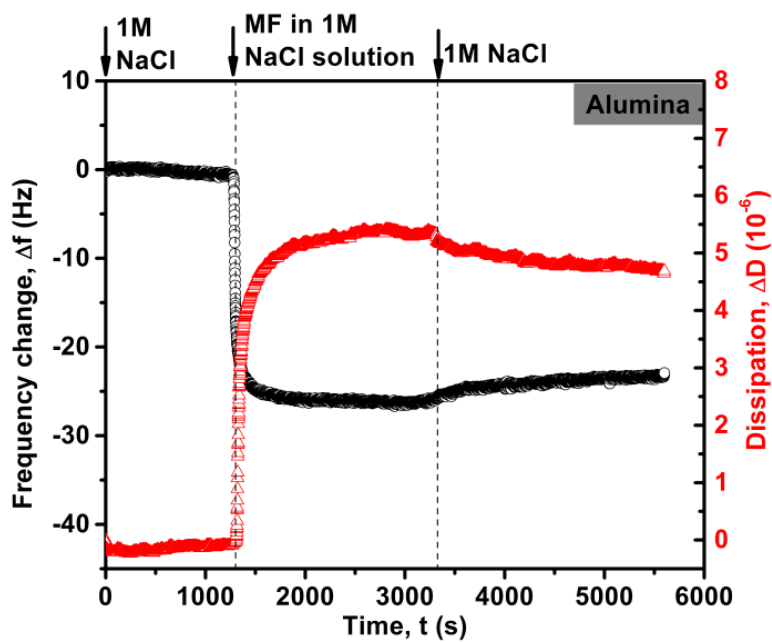


Figure 4.28. Change of frequency and energy dissipation associated with the adsorption of MF on QCM-D alumina sensors in 1 M NaCl solution

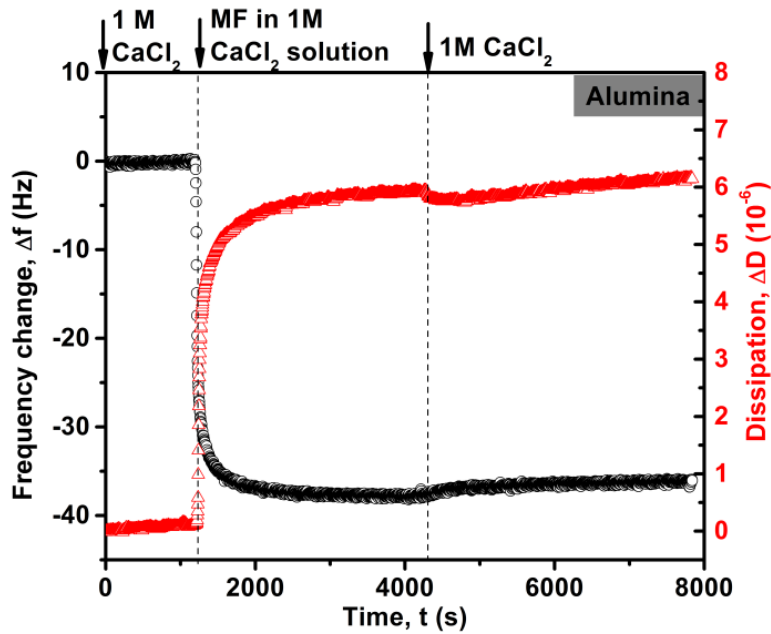


Figure 4.29. Change of frequency and energy dissipation associated with the adsorption of MF on QCM-D alumina sensors in 1 M CaCl_2 solution

4.3.5 Interaction between MF and clay particles surfaces

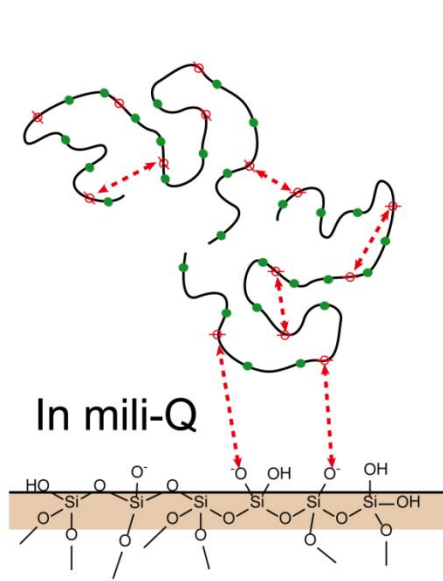
Based on the settling tests, zeta potential measurements, force measurements, adsorption measurement using QCM-D and the hydrodynamic radii determined in different salt solutions, the different settling behaviors of kaolinite suspensions are proposed to be mainly caused by the differences in the interaction forces among kaolinite surfaces and polymer flocculants as well as molecular conformations of flocculants under various solution conditions.

Figure 4.30(a) and (b) shows the schematic of MF's interaction with silica and alumina surfaces respectively when salt is not added into the solution. The conformation of MF in the salt free solution was expanded due to the intra-molecular steric and electrical repulsions, as measured by DLS. The isoelectric points of silica and alumina are 1.7-3.5 and 8-9 respectively [37]. Therefore at the $\text{pH} = 7.5$, silica surfaces were negatively charged while alumina surfaces were slightly positively charged. The

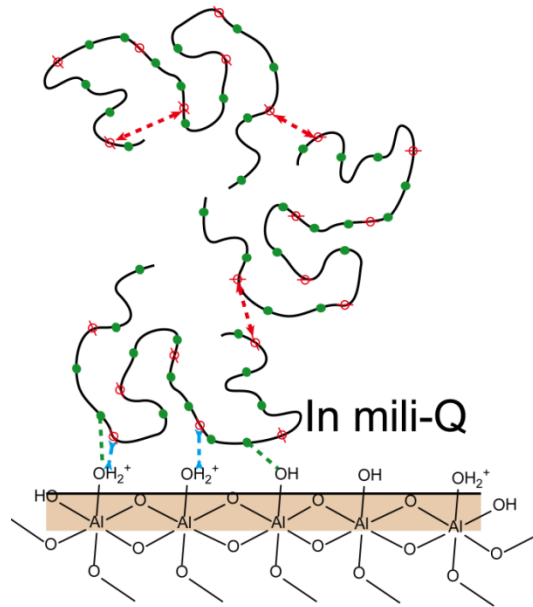
adsorption of MF on silica surface was negligible (Figure 4.30(a)) due to the electrostatic repulsion between MF's negatively charged segments and the silica surface. As measured by SFA the interaction between two mica surfaces in solution without salt (Figure 4.10) was purely repulsive and obvious repulsive force was observed at $D \approx 60.0$ nm, which suggests the force between MF molecules and mica surfaces was repulsive and the molecules on mica surfaces were in expanded conformation. The negligible frequency change in Figure 4.16 also indicates that the adsorption was very weak. The MF adsorption on alumina surface (Figure 4.23) was stronger than that on silica surface due to the electrostatic attraction and hydrogen bonding that possibly existed between molecules and alumina surfaces. However the expanded conformation and the intermolecular repulsion prevented further adsorption of MF (Figure 4.30(b)).

When salts of high concentration were introduced into the system, the electrostatic forces in the system were suppressed, which led to the screening of inter/intra-molecular repulsion as well as the electrostatic interaction between molecules and particles. Therefore the collapsed conformation was preferable for the MF molecules. The collapsed molecules could aggregate with each other due to the hydrogen bonding formed between molecules. Meanwhile the impact of charge properties of different surfaces to the polymer adsorption was diminished. Thus the frequency changes on silica and alumina sensors were almost identical in the concentrated solution of the same type salt, which were shown in Figure 4.21 and Figure 4.28, Figure 4.22 and Figure 4.29 respectively. The absence of electrostatic repulsion (either intermolecular or between molecule and surfaces) and the collapsed conformation allowed MF molecules to form more hydrogen bonds with the surface and to form a denser packed polymer layer on the surface. Therefore adhesive forces were observed under high salt concentration by SFA and the frequency drops on both sensors were higher in concentrated salt solution than in

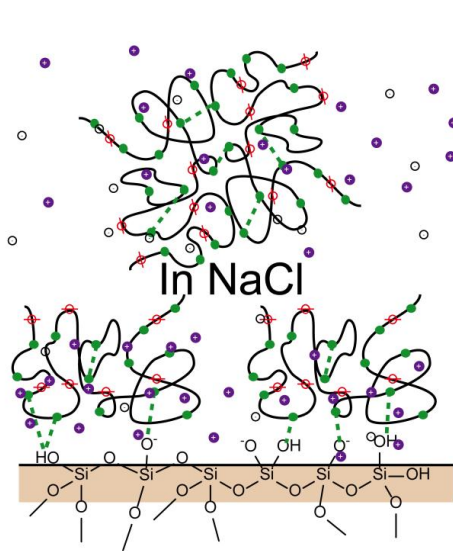
mili-Q water. The effect of CaCl_2 was more profound than that of NaCl . The reason could be that CaCl_2 can more effectively compress the double layer than NaCl . The metal complexation formed by Ca^{2+} between carboxyl groups could turn MF molecules into more condensed conformation and form aggregation between more molecules, which may also contribute to the more effective adhesion and adsorption enhancement observed.



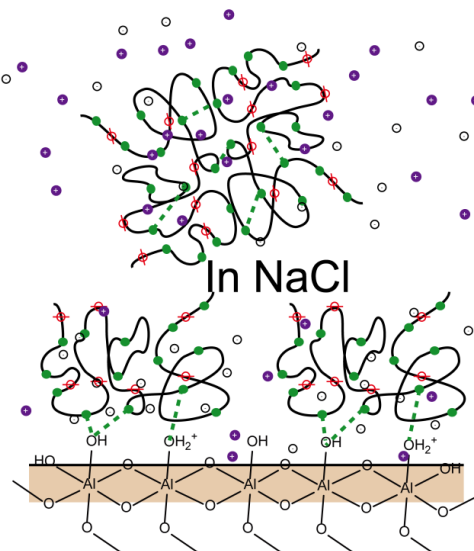
(a)



(b)



(c)



(d)

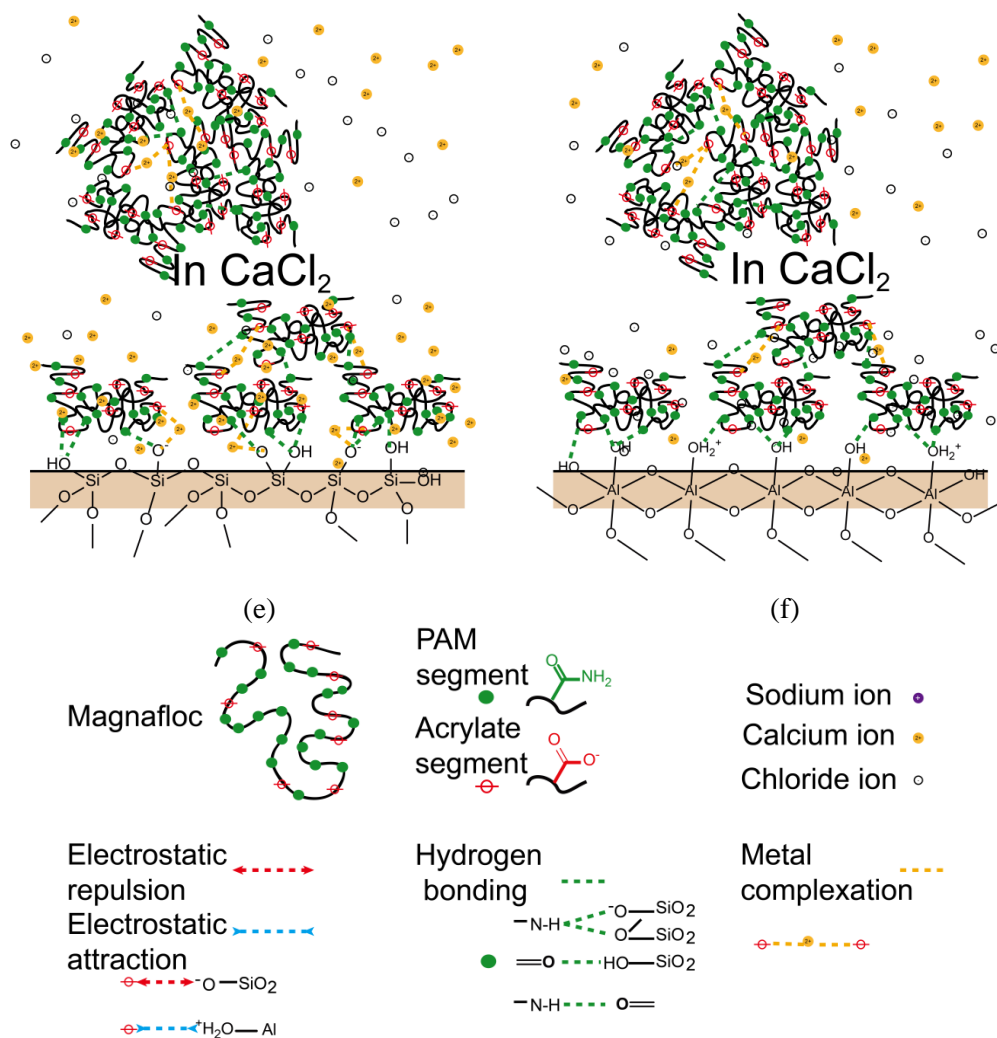


Figure 4.30. Schematic of MF's interaction with silica and alumina surfaces in solutions.

4.4 Conclusions

The effect of NaCl and CaCl₂ on the settling of MF treated kaolinite, conformation of MF and the interaction between MF and silica & alumina surfaces were investigated in this study. The following conclusions can be drawn from this study:

- (1) Both NaCl and CaCl₂ can increase the maximum ISR of MF treated kaolinite at the salt concentration of 0.01 M and 0.1 M. Adding 1 M salts reduce the maximum ISR,

which could be due to the shrink of MF on particle surface reduced the bridging chance between particles. Adding salts also increased the MF consumption.

(2) The effect of CaCl_2 was more significant than that of NaCl , which could be due to CaCl_2 can more efficiently compress the double layer and can also form metal complex within MF molecules as well as between MF molecules and surface functional groups.

(3) Introducing NaCl and CaCl_2 into system reduced the repulsion force between two mica surfaces bearing MF and induced hydrogen bonding when more than 1 M NaCl and 0.01 M CaCl_2 were added.

(4) The addition of salts changed the conformation of MF and facilitated the formation of hydrogen bonding with silica and alumina surfaces, which led to the adsorption enhancement.

4.5 References

- [1] R.J. Hunter, Foundations of Colloid Science, Oxford University Press, New York, 2000.
- [2] B.A. Wills, T. Napier-Munn, Wills' Mineral Processing Technology: An Introduction to the Practical Aspects of Ore Treatment and Mineral Recovery, Elsevier Science & Technology Books, 2006.
- [3] B. Derjaguin, Theory of the stability of strongly charged lyophobic sols and the adhesion of strongly charged particles in solutions of electrolytes, Acta Physicochim. USSR, 14 (1941) 633-662.
- [4] E.J.W. Verwey, J.T.G. Overbeek, K. Van Nes, Theory of the Stability of Lyophobic Colloids: the Interaction of Sol Particles Having an Electric Double Layer, Elsevier New York, 1948.

- [5] T. Hunter, M. Pearse, The use of flocculants and surfactants for dewatering in the mineral processing industry, in: CIM XIV International Mineral Processing Congress, 1982, pp. p11.
- [6] R. Hogg, Flocculation and dewatering, International Journal of Mineral Processing, 58 (2000) 223-236.
- [7] H. Haschke, M. Miles, S. Sheppard, Adsorption of individual polyacrylamide molecules studied by atomic force microscopy, Single Molecules, 3 (2002) 171-172.
- [8] P. Mpofu, J. Addai-Mensah, J. Ralston, Influence of hydrolyzable metal ions on the interfacial chemistry, particle interactions, and dewatering behavior of kaolinite dispersions, Journal of Colloid and Interface Science, 261 (2003) 349-359.
- [9] M.S. Nasser, A.E. James, The effect of polyacrylamide charge density and molecular weight on the flocculation and sedimentation behaviour of kaolinite suspensions, Separation and Purification Technology, 52 (2006) 241-252.
- [10] M.L. Taylor, G.E. Morris, P.G. Self, R.S. Smart, Kinetics of adsorption of high molecular weight anionic polyacrylamide onto kaolinite: The flocculation process, Journal of Colloid and Interface Science, 250 (2002) 28-36.
- [11] M.S. Nasser, A.E. James, Degree of flocculation and viscoelastic behaviour of kaolinite-sodium chloride dispersions, Colloids and Surfaces A-Physicochemical and Engineering Aspects, 315 (2008) 165-175.
- [12] M.S. Zbik, R.S.C. Smart, G.E. Morris, Kaolinite flocculation structure, Journal of Colloid and Interface Science, 328 (2008) 73-80.
- [13] A. Sworska, J.S. Laskowski, G. Cymerman, Flocculation of the Syncrude fine tailings: Part I. effect of pH, polymer dosage and Mg^{2+} and Ca^{2+} cations, International Journal of Mineral Processing, 60 (2000) 143-152.
- [14] J. Long, H. Li, Z. Xu, J.H. Masliyah, Role of colloidal interactions in oil sand tailings treatment, Aiche J, 52 (2006) 371-383.
- [15] A.J. McFarlane, K.E. Bremmell, J. Addai-Mensah, Optimising the dewatering behaviour of clay tailings through interfacial chemistry, orthokinetic flocculation and controlled shear, Powder technology, 160 (2005) 27-34.

- [16] L. Besra, D. Sengupta, S. Roy, P. Ay, Influence of polymer adsorption and conformation on flocculation and dewatering of kaolin suspension, *Separation and Purification Technology*, 37 (2004) 231-246.
- [17] M. Balastre, F. Li, P. Schorr, J. Yang, J.W. Mays, M.V. Tirrell, A study of polyelectrolyte brushes formed from adsorption of amphiphilic diblock copolymers using the surface forces apparatus, *Macromolecules*, 35 (2002) 9480-9486.
- [18] U. Raviv, S. Giasson, N. Kampf, J.F. Gohy, R. Jérôme, J. Klein, Normal and frictional forces between surfaces bearing polyelectrolyte brushes, *Langmuir*, 24 (2008) 8678-8687.
- [19] X.Y. Wang, X.H. Feng, Z.H. Xu, J.H. Masliyah, Polymer aids for settling and filtration of oil sands tailings, *Can J Chem Eng*, 88 (2010) 403-410.
- [20] M. Pearse, P. Somasundaran, Factors affecting the laboratory sizing of thickeners, in: *Int. Symp. on Fine Particle Processing*, Las Vegas, Nevada, USA, 1980, pp. 1619-1642.
- [21] J. Israelachvili, Y. Min, M. Akbulut, A. Alig, G. Carver, W. Greene, K. Kristiansen, E. Meyer, N. Pesika, K. Rosenberg, H. Zeng, Recent advances in the surface forces apparatus (SFA) technique, *Rep Prog Phys*, 73 (2010).
- [22] J.N. Israelachvili, *Intermolecular and Surface Forces*, 3rd ed., Academic Press, Burlington, MA, 2011.
- [23] J.N. Israelachvili, G.E. Adams, Measurement of forces between two mica surfaces in aqueous electrolyte solutions in the range 0–100 nm, *Journal of the Chemical Society, Faraday Transactions 1: Physical Chemistry in Condensed Phases*, 74 (1978) 975-1001.
- [24] J. Israelachvili, G. Adams, Direct measurement of long range forces between two mica surfaces in aqueous KNO₃ solutions, *Nature*, 262 (1976) 774-776.
- [25] J. Helt, J. Batteas, Mica surfaces: charge nucleation and wear, *Encyclopedia of Nanoscience and Nanotechnology*, edited by JA Schwarz, C. Contescu, and K. Putyera (Marcel Dekker, New York, 2004), 3 (2004) 1947-1966.
- [26] G.R. Strobl, *The Physics of Polymers : Concepts for Understanding Their Structures and Behavior*, 3rd. rev. and expanded ed., Springer, Berlin ; New York, 2007.

- [27] L. Alagha, S. Wang, Z. Xu, J. Masliyah, Adsorption kinetics of a novel organic–inorganic hybrid polymer on silica and alumina studied by quartz crystal microbalance, *The Journal of Physical Chemistry C*, 115 (2011) 15390-15402.
- [28] M. Rodahl, F. Hook, A. Krozer, P. Brzezinski, B. Kasemo, Quartz crystal microbalance setup for frequency and Q - factor measurements in gaseous and liquid environments, *Review of Scientific Instruments*, 66 (1995) 3924-3930.
- [29] F. Höök, B. Kasemo, T. Nylander, C. Fant, K. Sott, H. Elwing, Variations in coupled water, viscoelastic properties, and film thickness of a Mefp-1 protein film during adsorption and cross-linking: a quartz crystal microbalance with dissipation monitoring, ellipsometry, and surface plasmon resonance study, *Analytical chemistry*, 73 (2001) 5796-5804.
- [30] P. Somasundaran, Y. Chia, R. Gorelik, Adsorption of polyacrylamides on kaolinite and its flocculation and stabilization, in: *ACS Symp. Ser*, ACS Publications, 1984, pp. 393-410.
- [31] W.N. Rowlands, R.W. O'Brien, The Dynamic Mobility and Dielectric Response of Kaolinite Particles, *Journal of Colloid and Interface Science*, 175 (1995) 190-200.
- [32] P. Pincus, Colloid stabilization with grafted polyelectrolytes, *Macromolecules*, 24 (1991) 2912-2919.
- [33] O. Borisov, E. Zhulina, T. Birshstein, Diagram of the states of a grafted polyelectrolyte layer, *Macromolecules*, 27 (1994) 4795-4803.
- [34] R. Israels, F. Leermakers, G. Fleer, E. Zhulina, Charged polymeric brushes: structure and scaling relations, *Macromolecules*, 27 (1994) 3249-3261.
- [35] S. Misra, M. Tirrell, W. Mattice, Interaction between polyelectrolyte brushes in poor solvents, *Macromolecules*, 29 (1996) 6056-6060.
- [36] L. Zhang, H. Zeng, Q. Liu, Probing molecular and surface interactions of comb-type polymer polystyrene-graft-polyethylene oxide (PS-g-PEO) with an SFA, *The Journal of Physical Chemistry C*, (2012).
- [37] M. Kosmulski, *Chemical Properties of Material Surfaces*, CRC, 2001.

Chapter 5 Conclusions and Future Work

5.1 Major conclusions

Multiple techniques were applied in this work to study the effect of salinity on the flocculation of tailings or clays treated by polymeric flocculants. Settling test associated with turbidity and zeta potential measurements were used in both real tailings and kaolinite suspension to evaluate the efficiency of each flocculant. Dynamic light scattering was used to monitor the conformation of the flocculants in bulk solutions. The flocculation mechanism of MF was specifically studied by SFA and QCM-D. The major findings and conclusions of this thesis work are summarized as follows:

- 1) In real tailings, the maximum ISR of MF treated tailings (both freshwater and saline tailings) were higher than that of tailings treated by PAM and Al-PAM. However the turbidity of MF treated freshwater tailings was significantly higher than freshwater tailings treated by the other two flocculants.
- 2) The increasing of salinity could increase the maximum ISR and reduce the turbidity of real tailings treated by all three flocculants. However the consumption of MF was higher in saline tailings than in freshwater tailings.
- 3) The different settling behaviors of MF treated freshwater and saline tailings are attributed to the change of the conformation of MF and the interaction between MF and surfaces under different salinity. In freshwater tailings, the formation of relatively short range hydrogen bonding between the primary amide on MF and the sites on particle surface was inhibited by the long-range EDL repulsion. The expanded conformation and weak bridging force resulted the formation of large loose flocs in MF treated freshwater tailings and turbid supernatant. In saline

tailings, the hydrogen bonds between MF molecule and particles could be formed and the bridging effect was enhanced because of the compression of the EDL repulsion range. Therefore large flocs were tightly formed at high dosage of MF and higher maximum ISR was achieved in saline tailings.

- 4) The conformation PAM and Al-PAM and their interaction with particles were not affected by the change of salinity. Therefore the settling behaviors of the real tailings treated by PAM and Al-PAM were determined by the competing of EDL repulsive force, attractive van der Waals forces and bridging forces between particles.
- 5) Both NaCl and CaCl₂ can increase the maximum ISR of MF treated kaolinite at the salt concentration of 0.01 M and 0.1 M. Adding 1 M salts reduce the maximum ISR, which could due to the shrink of MF on particle surface reduced the bridging chance between particles. Meanwhile adding salts also increased the MF consumption.
- 6) The effect of CaCl₂ was more significant than that of NaCl, which could be due to CaCl₂ can more efficiently compress the double layer and can also form metal complex within MF molecules as well as between MF molecules and surface functional groups.
- 7) Introducing NaCl and CaCl₂ into system reduced the repulsion force between two mica surfaces bearing MF and induced hydrogen bonding when more than 1 M NaCl and 0.01 M CaCl₂ were added.
- 8) The addition of salts changed the conformation of MF and facilitated the formation of hydrogen bonding with silica and alumina surfaces, which led to the adsorption enhancement.

5.2 Contributions to the original knowledge

The effect of salt on mineral tailings flocculation has been studied by previous studies in terms of the salt type and concentration. However this study is the first of its kind to investigate the settling of mineral particles in high salinity environment, which is beneficial for using seawater as substitution of freshwater in mineral processing. The probing of molecular conformation of the polymer flocculants and the measurement of forces between surfaces with polymer absorbed under corresponding condition elucidated the flocculation mechanism in microscopic scale, which makes it possible to improve the saline tailings treatment by developing new polymer flocculants.

5.3 Future work

5.3.1 Enhancement of settling

In present study MF was identified as the most effective flocculant to treat saline tailings. However a lot of questions remain unanswered before it being applied to practical application.

- 1) The salinity of the real tailings provided by Teck is lower than real seawater due to the dilution by freshwater rivers. Therefore it would be necessary to investigate the sedimentation in tailings prepared according to seawater recipe.
- 2) According to the settling results of kaolinite with different concentration of NaCl and CaCl₂, the optimum salt concentration could be located between 0.01 M and 0.1 M salt. It can be speculated that higher maximum ISR could be achieved if the saline tailings were diluted by freshwater. Therefore the optimum level of dilution needs to be determined by experiment.

- 3) From present study it is speculated that a long chain anionic flocculant is favorable for the settling of saline tailings. It would be interesting to study the influence of chain length (molecular weight) to the ISR and turbidity.

5.3.2 Flocculation mechanism

The settling test of model kaolinite suspension with various salt concentrations and the interaction between flocculant and particle surfaces were studied to illuminate the flocculation mechanism under high salinity. In present study the effect of NaCl and CaCl₂ concentrations on the flocculation was studied. Following studies would help gain a more comprehensive picture of the flocculation in saline tailings:

- 1) Since Mg²⁺ is the second richest ion in seawater, the effect of Mg²⁺ is worth investigating even though it could have similar behavior as Ca²⁺.
- 2) In present study mica surface was used to mimic the silica basal plane in kaolinite to study the interaction between flocculant and the basal plane of kaolinite in SFA. It is desirable to coat alumina on mica and study the interaction between flocculant and alumina component.
- 3) Zeta potential measurement was used to characterize the charge property of kaolinite. However this characterization is quite rough due to the heterogeneous structure of kaolinite. The measurement of stream potential on mica and alumina surfaces will provide more accurate information of the particular surfaces.
- 4) After the study of MF, the flocculation mechanism of nonionic PAM could be a valuable complement to the current study.